BIO-SYNTHESIS OF ZINC OXIDE NANOPARTICLES AND ZINC OXIDE-BENTONITE NANOCOMPOSITE USING KOSSO (*Hagenia abyssinica*) AQUEOUS LEAF EXTRACT AND INVESTIGATION OF ITS ANTI-BACTERIAL ACTIVITIES

By: JEMAL ADEM

A THESIS SUBMITTED TO DEPARTMENT OF APPLIED CHEMISTRY

SCHOOL OF APPLIED NATURAL SCIENCE

PRESENTED IN PARTIAL FULFILLMENT OF THE REQUIREMENT FOR THE MASTER OF SCIENCE DEGREE IN APPLIED CHEMISTRY (INORGANIC CHEMISTRY)

OFFICE OF GRADUATE STUDIES

ADAMA SCIENCE AND TECHNOLOGY UNIVERSITY

ASTU

August, 2021

Adama, Ethiopia

BIO-SYNTHESIS OF ZINC OXIDE NANOPARTICLES AND ZINC OXIDE-BENTONITE NANOCOMPOSITE USING KOSSO (*Hagenia abyssinica*) AQUEOUS LEAF EXTRACT AND INVESTIGATION OF ITS ANTI-BACTERIAL ACTIVITIES

By: JEMAL ADEM

ADVISOR: Enyew Amare (PhD)

CO-ADVISOR: Neeraj Kumar Gupta (PhD)

A THESIS SUBMITTED TO DEPARTMENT OF APPLIED CHEMISTRY

SCHOOL OF APPLIED NATURAL SCIENCE

PRESENTED IN PARTIAL FULFILLMENT OF THE REQUIREMENT FOR THE MASTER OF SCIENCE DEGREE IN APPLIED CHEMISTRY (INORGANIC CHEMISTRY)

OFFICE OF GRADUATE STUDIES

ADAMA SCIENCE AND TECHNOLOGY UNIVERSITY

ASTU

August, 2021

Adama, Ethiopia

DECLARATION

I do hereby declare that the Master Thesis entitled **"Bio-Synthesis of Zinc Oxide nanoparticles and Zinc Oxide-Bentonite Nanocomposite Using Kosso (*Hagenia Abyssinica*) Aqueous Leaf Extract and Investigation of Its Anti-Bacterial Activities"**, is my original work. It has not been submitted for the award of any academic degree, diploma or certificate in any other university. It is a faithful record of bonafide and original research work carried out by me under the guidance and supervision of Enyew Amare (PhD) and Professor Neeraj Kumar Gupta, Department of Applied Chemistry, Adama Science and Technology University (ASTU), Adama. All sources of materials that are used for this thesis have been duly acknowledged through citation.

_____	_____	_____
Name of student	Signature	Date

RECOMMENDATION

We, the advisors of this thesis, hereby certify that we have read the revised version of the thesis entitled **"Bio-Synthesis of Zinc Oxide nanoparticles and Zinc Oxide-Bentonite Nanocomposite Using Kosso (*Hagenia Abyssinica*) Aqueous Leaf Extract and Investigation of Its Anti-Bacterial Activities"**; prepared under our guidance by Jemal Adem submitted in partial fulfilment of the requirements for the degree of Master of Science in Inorganic Chemistry. Therefore, we recommend that the submission of revised version of the thesis to the department following the applicable procedures.

_____	_____	_____
Advisor	Signature	Date
_____	_____	_____
Co-advisor	Signature	Date

Approval Page

We, the advisors of the thesis entitled **"Bio-Synthesis of Zinc Oxide nanoparticles and Zinc Oxide-Bentonite Nanocomposite Using Kosso (*Hagenia Abyssinica*) Aqueous Leaf Extract and Investigation of Its Anti-Bacterial Activities"** developed by Jemal Adem; hereby certify that the recommendation and suggestion made by the board of examiners are appropriately incorporated into the final version of the thesis.

Major Advisor	Signature	Date
Co-advisor	Signature	Date

We, the undersigned, members of the Board of Examiners of the thesis by Jemal Adem have read and evaluated the thesis entitled **"Bio-Synthesis of Zinc Oxide nanoparticles and Zinc Oxide-Bentonite Nanocomposite Using Kosso (*Hagenia Abyssinica*) Aqueous Leaf Extract and Investigation of Its Anti-Bacterial Activities"** and examined the candidate during open defence. We certify that the thesis is accepted for partial fulfilment of the requirement of the degree of Master of Science in Inorganic Chemistry.

Chairperson	Signature	Date
Internal Examiner	Signature	Date
External Examiner	Signature	Date

Final approval and acceptance of the thesis is contingent upon submission of its final copy to the Office of Postgraduate Studies through the Department Graduate committee and School Graduate Committee.

Department Head	Signature	Date
School Dean	Signature	Date
Office of Postgraduate Studies, Dean	Signature	Date

ACKNOWLEDGEMENT

First I give all glory and honour to the God of all ages, the source of all wisdom, knowledge and understanding. I thank Him and praise Him for giving me life and wisdom to achieve this feat. To Him alone we give all the glory. Then I would like to give my honourable thanks to my advisor, **Enyew Amare (PhD)**, for all his help and guidance that he has given me over the past eight months; in proper way and contributing of ideas as well as sharing of his precious time to direct me in every step. I'm very grateful to have your helpful suggestions and advise during my work. I would also thank my Co-advisor **professor Neeraj Kumar Gupta** for all his appreciable comments and guidance that he has given for me throughout my work. I would also like to acknowledge Adama Science and Technology University Research Office for the financial support and for providing material support during practice time. Finally, I would like to thank my family who help me in all direction for my success.

CONTENTS

LIST OF TABLES

LIST OF FIGURES

LIST OF ABBREVATIONS

AAS.....Atomic absorption spectroscopy

AFM……..Atomic force microscopy

ASTM……According to standard test method

ASTU……Adama science and technology university

CEC.....Cation exchange capacity

CFU.....Colony forming unit

DMSO.....Dimethylsulfoxide

DNA.....Deoxyribonucleic acid

DRS.....…Diffuse reflectance spectroscopy

DTA……..Differential thermal analysis

FTIR.....Fourier transforms infrared spectroscopy

FWHM.....Full width half maximum

JPCDS.....The Joint Committee on Powder Diffraction Standards

LSIE.....Liquid phase ion exchange

MMT.....Montmorillonite

NCs.....…Nanocomposites

NIR……Near infrared radiation

NPs.....…Nanoparticles

RNA.....Ribonucleic acid

ROS.....Reactive oxygen species

SEM.....Scanning electron microscopy

SSIE.....Solid state ion exchange

TEM…….Transmission electron microscopy

TGA.....….Termo-gravimetric analysis

TOT……..Tetrahedral octahedral tetrahedral

UV- Vis.....Ultraviolet-visible spectroscopy

USA……..United states of america

XRD.....….X-ray diffraction

H.AP……..Hagenia abyssinica plant

ZB1……ZnO-bentonite nanocoposite (4.4:2.2)

ZB2……ZnO-bentonite nanocoposite (2.2:2.2)

ZB3……ZnO-bentonite nanocoposite (1.1:2.2)

ZOA……Calcinated Zinc oxide nanoparticles (1:1)

ZOB……Uncalcinated Zinc oxide nanoparticles (1:1)

ZOC……Calcinated Zinc oxide nanoparticles (1:2)

ZOD……Calcinated Zinc oxide nanoparticles (0:100)

AB……..Activated bentonite

PB……Purified bentonite

MB……..Methylene blue

ABSTRACT

The increment of bacterial infectious diseases and antibacterial drug resistance enhance the development of an appropriate antibacterial agent by different methods from different precursors. The purpose of this study was to synthesize a novel and environmental friendly zinc oxide-bentonite nanocomposites (ZnO-bentonite NCs) from Zinc acetate [Zn $(CH_3COO)_2$•$2H_2O$ using bentonite as solid support and Hagenia abyssinica (H. abyssinica) plant leaf extract as capping agents and used for antibacterial application. The reaction of Zn $(CH_3COO)_2$•$2H_2O$ with Na-bentonite and Aqueous leaf extract was effected at 80 ^{0}C, pH 12 and reaction time of 30 min. ZnO NPs were also synthesized using H. abyssinica leaf extract at 60 ^{0}C and pH of 12 for comparison of its antibacterial activity with the ZnO-bentonite NCs. Thermal analysis (TGA/DTA), X-ray diffraction (XRD), UV-Visible spectroscopy (UV-Vis), UV-Visible-Diffuse reflectance spectroscopy (UV-Vis-DRS), Atomic absorption spectroscopy(AAS), Scanning electron microscopy (SEM) and Fourier transforms infrared spectroscopy (FTIR) were used for the characterizations of thermal stability, crystalline structure, Optical properties, chemical composition, morphology and functional group of synthesized ZnO NPs and ZnO-bentonite NCs. TGA/DTA analysis result of ZnO NPs (1:2) and ZnO-bentonite NCs (1:1) confirmed that the synthesized NPs and NCs are stable above 450 ^{0}Cand 550 ^{0}C. XRD analysis result indicated that the synthesized ZnO NPs and ZnO phase in NCs have hexagonal Quartzite structure with an average crystalline size between 21-28 nm and 8- 22 nm respectively; except the ZnO impregnated in ZnO-bentonite (1:2) NCs with cubic structure. UV-Vis studies of ZnO NPs and ZnO-bentonite NCs revealed the characteristic peak in wavelength range 374-377 nm and 379 nm. UV-Vis-DRS characterization shows that the band gab of ZnO (1:1) and ZnO NPs (1:2) are 3.12 eV and 3.06 eV. It also confirms that ZnO-bentonite NCs (1:1 and 2:1) has band gab of 2.8eV and 3.1eV. FTIR spectra showed the presence of hydroxyl, carbonyl, alkyl, amide and other functional group in NPs and NCs. Antibacterial activity of uncalcined ZnO NPs-1:1 (ZOB) in all concentration ranges showed a greater zone of inhibition against both bacterial strains compared to claimed ZnO NPs. ZB2 (1:1) shows the better antibacterial efficacy against both bacterial strains than ZB1 (2:1) due to the high dispersion of ZnO NPs in composite;

***Keywords*:** Capping agents, Hagenia abyssinica, Zinc oxide-bentonite nanocomposites, antibacterial activity.

CHAPTER ONE

1. INTRODUCTION

Nanotechnology is the art and science of manipulating matter at the nanoscale to create new and unique materials and products with enormous potential to change society. In nanotechnology, day-to-day incredible growth has unbolted up innovative applied and fundamental frontiers in a new branch of research, i.e., materials science and engineering, Nanobiotechnology, quantum dots, and applied microbiology. Among the most rapidly growing research area, Nanobiotechnology is playing a great role in biotechnology. Bio-nanotechnology is the integration between biotechnology and nanotechnology for developing biosynthetic and environmental friendly technologies for the synthesis of nanomaterial. Nanotechnology can be useful in diagnostic techniques, drug delivery, cosmetics, antimicrobial, disinfectants and as catalysts for greater efficiency via nanoscale structure (Meruvu *et al*., 2011).

Overuse of antibiotics by humans and animals has caused the rapid mutation of pathogenic bacteria that are immune to multiple drugs. The bacteria such as *Escherichia coli (E. coli), Staphylococcus aureus* (*S. aureus*) and *Bacillus subtilis (B. subtilis)* are known to be harmful to public health as well as to the environment. Nanoscale materials have emerged as novel antimicrobial agents owing to the high surface area to volume ratio, which is the current interest of researchers due to the growing microbial resistances against metal ions, antibiotics and the evolving resistance of microbial strains (Pouraboulghasem *et al*., 2016).

Among the known nanoscale materials used for the antibacterial activities, metal and metal oxide NPs have attracted extensive interest. These structures are of interest because of their high reactivity due to the large open area-to-mass ratio and different properties at nanometer sizes compared to the properties of the same materials in bulk conditions. According to the Appendini and Hotchkiss, (2002) reports; Ag, ZnO, TiO_2, SnO_2, W_2O, CuO etc. are some well-studied NPs. Ag, CuO and ZnO NPs have attracted extensive interest among antibacterial nanoparticles. Among metal oxide nanoparticles, ZnO NPs have drawn the attention of many researchers for their unique optical and chemical behaviours which can be easily tuned. ZnO belongs to the class of semiconductor metal oxides with wide band gap of 3.37 eV and a large excitonic binding energy of 60 meV,

which is characterized by photo-catalytic and photo-oxidizing capacity against chemical and biological species (Osuntokun *et al*., 2019).

ZnO NPs possesses some antibacterial effect, good thermal qualities, low cost and little toxicity and has found a wide range of applications, including antibacterial, photoluminescence, optoelectronics, solar cells, catalysts, in food packing, nanomedicine, pharmaceuticals and cosmetics (Demissie *et al*., 2020). Biosynthesized ZnO NPs exhibit strong antimicrobial behaviours against bacterial and multifunctional behaviours and dynamic antibacterial activity because of their small size which can help the entrance of NPs through cell membrane of bacteria easily (Nagarajan and Rajagopalan, 2008).

On the basis of Ashe, (2011) investigations, it has been demonstrated that ZnO nanostructures exhibit antimicrobial activity against a broad spectrum of gram negative bacteria such as*, E. coli*, *Pseudomonas aeruginosa(P. aeruginosa), S. paratyphoid* and gram positive bacteria such as *Bacillus subtilis (B. subtilis) and S. aureus.* It is evident that the antibacterial activity of ZnO NPs depends on the surface area and concentration, while the crystalline structure and particle shape have little effect. Further it is also mentioned in this studies that smaller the size of ZnO NPs better is its antibacterial activity. Thus higher the concentration and larger the surface area of the nanoparticles, the better is its antibacterial activity (Ashe, 2011).

The antimicrobial mechanisms of NPs have not yet been clearly identified and that in general, it has been proposed that ZnO NPs inhibits bacteria growth by three main mechanisms; metal ions bind to proteins and deactivate proteins, metal ions can interact with microbial membrane and causing structural changes and permeability and metal ions interact with microbial nucleic acids and prevent microbial replication. Its antimicrobial activity also related to the induction of oxidative stress due to the generation of reactive oxygen species, which may cause the degradation of the bacterial membrane structure and denature the protein functions (Dobrucka and Dlugaszewska, 2016).

In addition, disruption of the bacterial membrane is attributed to per oxidation of the unsaturated phospholipids due to photo-catalytically induced hydrogen peroxide and binding of Zn^{2+} to microorganisms' membranes thus damages the bacterial membrane and cell wall. Consequently, bacterial growth is inhibited and prolongs the lag phase of the microbial growth cycle (Pouraboulghasem *et al*., 2016). However, the easy aggregation into big cluster of ZnO NPs at nanoscale in the solution will weaken the antibacterial effect

and its low photo-inactivation efficiency in visible region also impose a negative influence on their antibacterial activity (Sirelkhatim *et al*., 2015).

Zhang *et al*., (2010) tested the antibacterial activity of ZnO NPs against *E. coli*. ZnO NPs indicate high importance since they can accumulate in bacterial membrane and cytoplasm regions of bacterial cells after increasing the membrane permeability of *E. coli* cells and so slow down the *E. coli* growth rate. Sharma *et al*., (2010) demonstrated that ZnO NPs possessed antibacterial activity even at lower concentrations hence suitable for thin coating applications.

Over the past decades, different physical and chemical methods such as sol-gel, spray pyrolysis, precipitation, micro-emulsion techniques, thermal evaporation, laser ablation, chemical vapour deposition, mechanical milling, molten salt, microwave method and hydrothermal synthesis are widely used for ZnO NPs synthesis. Such synthesis methods are typically costly and labour intensive, require high temperature, involve complex apparatus or processing, use organic solvents, hazardous capping agents or toxic stabilizers which can be hazardous to both the environment and living organisms. Thus, there is a need, for an alternative, simple, cost-effective, high yield synthetic method, safe and environmentally sound means of NPs preparation methods (Agarwal *et al*., 2017).

Bio-synthesis of metal oxide NPs has been proposed as a reliable, low-cost and environment friendly alternative approach compared with classical chemical and physical methods. Bio-synthesis of NPs by using different plants, organisms and environmental friendly materials allows for the large-scale production of metal oxide NPs free of impurities. The biogenic synthesis of metallic oxide NPs leads to the formation of capped nanostructures with bio-molecules from the organism during the biosynthesis. These capping agents prevent NPs from agglomeration and likely play an important role in the stabilization of the nanoparticles. The presence of capping agents may also improve the biocompatibility of biogenic nanomaterial's (Seabra and Duran, 2015).

Bio-synthesis can be carried out with fungi, algae, bacteria, and plants, etc. Among these organisms, plants seem to be the best candidates and they are suitable for the large-scale biosynthesis of nanoparticles. Metal oxide NPs produced by plants are more stable and more varied in shape and size in comparison with those produced by other organisms (Salam *et al*., 2014). Some parts of plants such as leaves, fruits, roots, stem, seeds have been used for the synthesis of various metal oxide NPs due to the presence of phytochemicals in its extract which acts reducing agent. Based on the literature, the

synthesis of ZnO NPs using plants has been successful with extracts of various parts of plant species like *Azadirachta indica*, *Nephelium lappaceum* L.(Yuvakkumar *et al*., 2015), *Costus pictus D. Don*(Suresh *et al*., 2018), *Ocimum basilicum L. var.* (Sivaraj *et al*., 2014) and *Citrus aurantifolia, Vitex negundo L.* (Samat and Nor, 2013).

Nowadays, the use of unique properties of plants attracted a lot of interest (Suresh *et al*., 2018; Vaishnav *et al*., 2017). The *H. abyssinica* plant belongs to the member of the rosaceous family, a species of flowering plant native to the high elevation Afro-mountain regions of central and eastern Africa from Sudan and Ethiopia. *H.abyssinica* is an interesting plant for NPs synthesis because of its bioactive compounds. The main components of *H. abyssinica* plant are flavonoids, alkaloids, tannis, phenolic, and triterpenic acids. From ancient times, the roots of *H. abyssinica* are cooked with meat and the soup drunk for general illness and malaria, while the dried and pounded female inflorescence is used as an anthelmintic (especially for tapeworm) (Wolde *et al*., 2016).

In the case of chemical or green synthesis of NPs, unfortunately, the agglomeration of NPs happens due to their small size and high surface energy. Also it has been demonstrated that using NPs alone is dangerous, because their sizes can affect human health and the environment. To overcome this problem, hybrid processes were introduced by combining NPs with other environmentally friendly inert and stable solid supports, such as kaolinite, montmorillonite (MMT), halloysite, and zeolite to utilize the NPs full properties in wide-range of applications (Honarmand *et al*., 2020; Shu *et al*., 2017).

Among inert and stable solid support materials, low-grade Na-bentonite clays are considered as an appealing substrate for immobilization of a variety of NPs because of being excellent filler, binder, large surface area, good swelling behaviour, high chemical and mechanical stability, high adsorption and ion exchange properties and substrates for metal/metal oxide NPs. Bentonite clays are natural minerals with hydrous aluminium silicates and a layered structure composed of silicate sheets bonded to aluminium oxide/hydroxide. They are used to incorporate the metal oxide into the basal space of its layered structure and make NPs more stable having less size, while inhibits pollution caused by runoff of the NPs removal process. Their adsorption capacities help to attract contaminants into the open pores and therefore raise the efficiency of the dispersed NPs (Honarmand *et al*., 2020).

Moreover, introducing of NPs with other substrates/fillers can result in composites with novel and enhanced properties that cannot be achieved by the individual components.

Nanocomposites are composites in which at least one of the phases shows dimensions in the nanometer range and are created by introducing nanomaterial's (often referred to as filler) into a macroscopic sample material (often referred to as the matrix). Nano composite materials have emerged as suitable alternatives to overcome limitations of micro-composites and monolithic, while posing preparation challenges related to the control of elemental composition and stoichiometry in the Nano cluster phase. These materials can act as antimicrobial agents which are applied and attracted to many fields such as industries, food, synthetic textiles, and environmental remediation in recent years due to the ability to inhibit the growth of micro-organisms (Henrique *et al*., 2009).

Nanocomposites may preserve the antibacterial activity of the NPs while increasing the biocompatibility of the resultant composite structure. NCs with a metal oxide nanostructure could protect the metal oxide NPs against agglomeration and leaching out in real operating medium, improve its dispersibility but also could retain the antimicrobial activity of the metal oxide NPs (Motshekga *et al*., 2013). Interestingly, ZnO attachment on a support can extend life and reusability of the NPs and the surface of the support can be used to prevent the guest particles from aggregation (Hakimi *et al*., 2018a).

Various strategies have been recently developed to achieve ZnO supported materials such as co-precipitation, solid state ion exchange, liquid state ion exchange and hydrothermal methods. These techniques are passing through multiple steps of ultra-sonication and stirring, which take several hours, chemical reduction of the precursor and produce large particle size. Thus, any new synthesis technique that helps to simplify, save time, control particle size and provide uniform dispersion of NPs would be exceedingly thought provoking. Bio-synthesis utilizes the concept of homogeneous dispersion of in situ prepared ZnO NPs into the clay structure generating discrete and uniform distribution of active sites that may have high antibacterial efficacy (Meshram *et al*., 2011).

The research on heavy metal-clay mineral surface interactions is still of great interest because of the well-known toxicity of heavy metal ions and the need for removal of these metals from aqueous solutions. Recent studies on antibacterial activities of clay-based materials are mainly focused on immobilization of inorganic cations such as Zn^{2+}, Cu^{2+} and Ag^{+} onto clay minerals. Montmorillonites clay was recently reported to possess antibacterial properties, facilitated by the exchange of metal ions such as Ag^{+}, ZnO and CuO. Among many noble metal nanomaterial's, Ag NPs with size or shape dependent

physicochemical properties and antibacterial activities have been widely reported, and applied in catalysis, sensors and medical uses (Pourabolghasem *et al*., 2016).

The antibacterial activity of nanoclay-silver has long been known to have a broad spectrum of antimicrobial activities than the above mentioned NCs. The higher antibacterial activity might be related to the large surface of nanoclay and the existence of pillared silver. Antibacterial behaviour of Ag NPs can be attributed to their high affinity for sulphur, oxygen and nitrogen. Ag NPs form a complex with sulphur, present in the cell membrane of the bacteria thus inhibiting the bacterial cell viability. But the main problem of using Ag NPs is, Ag-based compounds has potentially toxic effects on human health and expensive inorganic antibacterial materials (Ghorbanpour *et al*., 2017).

Zinc oxide possesses some antibacterial effect and used as antimicrobial agents in medicine for a long time due to the high safety and broad spectrum antibacterial activity. But the applications of the long-acting antibacterial materials loading zinc ions or rare earth ions are limited due to their relatively poor antibacterial activity. To enhance the antibacterial efficacy of ZnO NPs, hybridization of zinc salt precursors and Na-bentonite is a method that has been largely explored. There are many papers reporting the antibacterial activity of ZnO loaded montmorillonites (Hakimi *et al*., 2018a).

Pouraboulghasem *et al*., (2016) synthesized Zn-MMT and Cu-MMT nanocomposites for use as an antibacterial material against *E. coli and S. aureus* by a quick and simple alkaline ion exchange method. Their investigation clearly showed that nanocomposites samples had viable cells reduction ability for testing strains. Tan *et al*. have synthesized ZnO loaded MMT (ZnO-MMT) by an ion-exchange reaction for use as an antibacterial material against *E. coli*, *S. aureus* and *Candida albinos* (Tan *et al*., 2008). The resulting ZnO-MMT exhibited some antibacterial activity. Their investigation shows the antibacterial activity of ZnO-MMT was enhanced due to the synergistic antibacterial effect of Zn^{2+} than the modified MMT which showed no antibacterial activity. Their studies suggest that modified MMT provide large surface area for the diffusion of active sites.

To the best of our knowledge, biological approach via co-precipitation method using *H. abyssinica* plant leaf extract has been used for the first time as a reducing and capping agent for the synthesis of hexagonal wurtzite ZnO NPs and ZnO-bentonite NCs. Thus, the core objective of this work was to investigate the antibacterial activity of ZnO NPs alone and ZnO-bentonite NCs against *E.coli* and *S.aureus* bacterial strains.

1.1. Statement of the Problem

Drug resistance bacteria are a common problem and different antibacterial agents have been developed from different materials. The most excellent antibiotics nanomaterial's, Ag and ZnO NPs, are widely used in a growing number of applications due to their unique properties.

In recent years, clay mineral-based antibacterial nanoparticles have been prepared by a series of processes between the clay minerals and antibacterial nanoparticles to strength the bonds between clay and NPs. Pouraboulghasem *el al*. (2016) reports showed that clay doesn't cause any side effect, plentiful, non-toxic, and inexpensive, possesses excellent adsorption property and eco-friendly. Nanoparticles loaded into solid clay, slowly released into the environment from its matrix, interact with soil and sediment to form inert aggregate.

Over the past decades, different physical and chemical methods are widely used for ZnO-bentonite NCs and ZnO NPs synthesis. Such manufacturing methods are typically costly, require high temperature, involve complex processing, use hazardous capping agents and can be hazardous to both the environment and living organisms (Suresh *et al*., 2018). Thus there is a need for developing simple methods of synthesizing low cost and nontoxic ZnO NPs and ZnO-bentonite NCs for our communities for health safety and curing various bacteria. In this present study, ZnO-bentonite NCs were prepared from ZnO NPs precursor and bentonite clay by utilization of bioactive compounds present in *H. abyssinica* plant leaf extract and investigated for antibacterial activity.

1.2. Objectives

1.2.1. General Objective

The main objective of this research was to synthesize Zinc oxide nanoparticles and ZnO-bentonite NCs using *H. abyssinica* medicinal plant aqueous leaf extract and investigate their antibacterial activity.

1.2.2 Specific Objectives

The specific objectives of this research are to:

- Extraction of *H. abyssinica* plant leaf and analysis of its phytochemicals.
- To synthesize ZnO NPs from zinc acetate salt by utilization of *H. abyssinica* plant aqueous leaf extract.
- Purification and activation of bentonite clay to form bentonite nanoclay
- To synthesize ZnO-bentonite NCs from $Zn(CH_3COO)_2.2H_2O$ and activated bentonite by utilization of *H. abyssinica* plant aqueous leaf extract.
- To characterize the synthesized ZnO NPs, natural and activated bentonite and ZnO-bentonite NCs using TGA, XRD, UV-Vis, UV-Vis-DRS, AAS, SEM and FT-IR.
- To investigate the antibacterial activities of the synthesized ZnO NPS, Na-bentonite, *H.abyssinica* and ZnO-bentonite NCs against gram positive bacteria *E. coli and* gram negative *S. aureus* bacterial species.

1.3. Significance of the Study

The significance of this study is to utilize locally available natural resources to create new alternative and improved environmentally friendly antibacterial agent.

1.4. Scope of the Study

This research work was limited to green synthesis of ZnO NPs and ZnO-bentonite NCs using *H. abyssinica* medicinal plant aqueous leaf extract, their characterization using TGA, XRD, UV-Vis, UV-Vis-DRS, AAS, SEM and FT-IR techniques and investigating their antibacterial efficacy against bacterial *strains E. coli and S. auras* by using disc diffusion methods.

CHAPTER TWO

2. LITERATURE OVERVIEW

2.1. Nanotechnology

Nanotechnology was a modern field of science which plays a dominant role in day to day life aspects. It deals with production, manipulation and use of material ranging in nanometers. These nanoscale dimension materials provide a large surface area to volume ratio and thus very specific properties. The field of nanotechnology was one of the most active areas of research in modern materials science. In nanotechnology, day-to-day incredible growth has unbolted up innovative applied and fundamental frontiers in a new branch of research, i.e., materials science and engineering, nanobiotechnology, quantum dots, and applied microbiology. Nanobiotechnology was defined as a field that applies the nanoscale principle and techniques to understand and transform bio systems (living and non-living) and which uses biological principles and materials to create new devices and systems integrated from the nanoscale (Vishwakarma, 2013).

2.2. Nanoparticles

Nanoparticles were particles in the nanoscale size between 1nm and 100nm with surrounding interfacial layer which exhibit atom-like behaviours due to high surface energy resulting from high and large specific surface area, high fraction of surface atoms and wide gap between valence and conduction band when divided to near atomic size. Nanoparticles are of great interest due to their extremely small size and large surface to volume ratio, which lead to both chemical and physical differences in their properties (*e.g.* mechanical properties, biological and steric properties, catalytic activity, thermal and electrical conductivity, optical absorption and melting point) compared to bulk of the same chemical composition. The intrinsic properties of a metal nanoparticle are mainly determined by size, shape, composition, crystallinity and morphology (Iravani, 2011).

Nanoparticles can be broadly grouped into two: namely organic and inorganic nanoparticles. Organic nanoparticles may include carbon nanoparticles (fullerenes) while some of the inorganic nanoparticles may include magnetic nanoparticles, noble metal nanoparticles (like gold and silver) and semiconductor nanoparticles (like titanium dioxide and zinc oxide). There is a growing interest in inorganic nanoparticles as they provide

superior material properties with functional versatility. Nanoparticles are used for many bio-applications such as therapeutics, antimicrobial agents, drug delivery agents, biosensors, imaging contrast agents, sunscreen transfection vectors and fluorescent labels (Kaur and Kaur, 2019).

NPs have started being considered as nanoantibiotics because of their antimicrobial activities. Among the known materials used for the antibacterial activities, metal and metal oxide such as Ag, ZnO, TiO_2, WO_3, SnO_2, CuO and MgO nanoparticles have attracted extensive interest. Of the inorganic materials, metal oxides such as TiO_2, ZnO, MgO and CaO are of particular interest as they are not only stable under harsh process conditions but also generally regarded as safe materials to human beings and animals. Nanoparticles also have been integrated into various industrial, health, food, feed, space, chemical, and cosmetics industry of consumers which calls for a green and environment-friendly approach to their synthesis (Appendini and Hotchkiss, 2002).

2.2.1. Zinc Oxide Nanoparticles

ZnO NPs are n-type semiconductor with a conductivity of about 10^{-7}-10^{-3} S/cm, and possess high exciton binding energy of 60 meV and a large band gap of 3.37 eV in the near-UV spectral region, strong oxidation ability, and good photo catalytic property. The high band gap (3.0–3.9 eV) limits the use of ZnO for wider applications, because it is only active in UV light area. Due to these properties, they show various semiconducting properties such as high catalytic activity, wound healing, anti-inflammatory, ultraviolet filtering properties and extensively used in various cosmetics such as sunscreens (Vishwakarma, 2013).

ZnO NPs have drawn considerable attention from researchers and scientists in the past 4-5 years due to its wide applications in biomedical field, in optics and electronics. ZnO NPs are of great interest due to inexpensive to synthesize, safe, easy method of synthesis and environment-friendly as they are compatible with organisms; which makes them suitable for the treatment of water and wastewater. These nanoparticles are used in various biomedical applications too such as antifungal, antibacterial, drug delivery, and anti-diabetic, anticancer. It can absorb a wider range of solar spectra and more light quanta than several semiconducting metal oxides (Jiang *et al*., 2018).

2.3. Synthesis of Nanoparticles

Synthesis of nanomaterials is a complex process; even then a large number of techniques are available for their synthesis. Currently, a large number of top-down (physical method), bottom up (chemical method), Green (biological method), and hybrid methods are available to synthesize different types of nanoparticles. Though physical and chemical methods are more popular for nanoparticle synthesis, the use of toxic, expensive, and inflammable compounds limits their applications (Akram *et al*., 2016).

The physical approach involves methods such as condensation, evaporation and laser synthesis. In case of physical methods nanoparticles are produced directly from their bulk counterpart. However in the case of chemical approach, a salt solution of metal ions is reduced to neutral metal atoms which are then in response to aggregation of atoms, furnishing metallic nanoparticles. Some commonly used chemical methods are thermal, electrochemical, sonochemical, sol-gel and photochemical with different precursors. The development of safe eco-friendly methods for biogenetic production is now of more interest due to simplicity of the procedures, cost effective, energy saver and having environmentally benign protocols technique and versatility (Iravani, 2011).

The choice of synthesis method determines the physicochemical characteristics of the metal oxide nanoparticle, such as the size, dispersibility, type of intrinsic and/or extrinsic defects, morphology and crystal structure. In other way, we make broadly a division of synthesis methods into three categories: solution based (such as sonochemical method, co-precipitation method, solvothermal method sol–gel method, micro-emulsion method, microwave-assisted method), vapour state based synthesis (laser ablation method, chemical vapour based methods, combustion method, template/surface-mediated synthesis) and biological synthesis are metal oxide synthesis methods used most of the time.

2.3.1. Synthesis Methods of Zinc Oxide Nanoparticles

There are different methods used for the synthesis of zinc oxide nanoparticles: direct precipitation, homogeneous precipitation, solvothermal method, sonochemical method, reverse micelles, sol gel method, hydrothermal, thermal decomposition, and microwave irradiation (Talam *et al*., 2012).

A). Sol-gel technique

The Sol-gel technique is bottom up method in which materials containing the desired precursors are mixed in a controlled fashion to form a colloidal solution. The sol-gel process, involves the evolution of inorganic networks through the formation of a colloidal suspension (sol) and gelation of the sol to form a network in a continuous liquid phase (gel). The precursors for synthesizing these colloids consist usually of a metal or metalloid element surrounded by various reactive ligands. The starting material is processed to form a dispersible oxide and forms a sol in contact with water or dilute acid. Removal of the liquid from the sol yields the gel, and the sol/gel transition controls the particle size and shape. Calcinations of the gel produce the oxide; hence it is a chemical technique.

Sol-gel processing refers to the hydrolysis and condensation of alkoxide based precursors (Samat and Nor, 2013).

$MOR + H_2O \rightarrow MOH + ROH$ (hydrolysis) Eq. (1)

$MOH + ROM \rightarrow M\text{-}O\text{-}M + ROH$ (condensation) Eq. (2)

Where, M is metal and R is alkyl group. A novel sol-gel synthesis of ZnO NPs was firstly presented by Jiang *et al.* which mainly involved three major (Jiang *et al*., 2018).

(1). Preparation of zinc precursor

A sample of $Zn(CH_3COO)_2 \cdot 2H_2O$ was dissolved in ethanol, placed into a distillation apparatus, and then refluxed for few hours at atmospheric pressure. The solution was boiled nearly at 80°C and stirred to obtain the condensate and hygroscopic reaction mixture.

(2). Preparation of ZnO clusters: The hygroscopic mixture was diluted to ethanol solution with the addition of $LiOH \cdot H_2O$ powder. The suspension will become transparent with the help of an ultrasonic bath. This procedure could accelerate the release of OH ions, and the reaction at low temperature under air conditions could prevent rapid particle growth and get ZnO sols.

(3). Crystal growth: Crystal growth is a self-induced procedure occurring at room temperature. But the amount of LiOH which could strongly affect the crystals growth rate, shape, and size should be well controlled. LiOH induced ZnO growth can be briefly summarized as follows:

$Zn(CH_3COO)_2 \cdot 2H_2O + 2LiOH \rightarrow Zn(OH)_2 + 2CH_3COOLi + 2H_2O$ Eq. (3)

$Zn(OH)_2 + 2H_2O \longrightarrow Zn(OH)_4^{2-} + 2H^+$ Eq. (4)

$Zn(OH)_4^{2-} \longleftrightarrow ZnO + H_2O + 2OH^-$ Eq. (5)

B). Solvothermal/ Hydrothermal synthesis

In Solvothermal synthesis process the polar solvents are involved in different condition like at temperatures above their boiling points and in the condition of under pressure at versatile low temperature. Hence the reaction does not involve in lower temperature because the solubility of reaction get significantly increases in Solvothermal condition. In solvothermal process, the decomposition of the precursors at a particular solvent depends on the temperature and pressure within the reaction vessel. Two processes are required for crystallization in a supersaturated solution: nucleation and crystal growth. For the solvothermal synthesis in alcohols or glycols, the nucleation as well as the continuing growth of ZnO crystals is similar to those that occur in the hydrothermal process because the solvent also consists of a hydroxyl group, which is a key factor for ZnO nucleus formation in the hydrothermal method (Ghoshal *et al*., 2009).

$Zn(CH_3COO)_2 \cdot 2H_2O + 2R\text{–}OH \rightarrow Zn(CH_3COO)_2 \cdot 2R\text{–}OH + 2H_2O$ Eq. (6)

The zinc cation in zinc acetate is surrounded by a columbic hydration sheath, which remains with it even inside a solvent like alcohol and prevents it to completely dissolve in it. The treatment with ethylene glycol disturbs this hydration sheet which allows the solute to dissolve in an alcohol. ZnO nucleus can be formed either directly by homogeneous precipitation, or through re-dissolution of meta-stable hydrosol-intermediates, such as zinc hydroxide or zinc hydroxyacetate that change into the more stable ZnO.

The hydrothermal method involves the heterogeneous chemical reaction in a solvent (aqueous or non-aqueous) occurring above room temperature and at pressure more than 1atm in a closed system. Normally, hydrothermal reactions are conducted in a specially sealed container or high pressure autoclave under subcritical or supercritical solvent condition. Madathil *et al.*, (2007) synthesized ZnO NPs from methanoic stock solutions of $Zn(CH_3COO)_2.2H_2O$ under continuous stirring with NaOH solution prepared in methanol to control the pH value of reactant. In this method, the source of Zn is in the forms of $Zn(OH)_2$ precipitates and $Zn(OH)_4^{2-}$ species according to the stoichiometric ratio of Zn^{2+} on OH^- .

The $Zn(OH)_2$ precipitates under the hydrothermal conditions would dissolve to considerable extent to form ions of Zn^{2+} and OH- , once the product of $[Zn^{2+}]$ and $[OH^-]$

exceeds a critical value which is necessary for the formation of ZnO crystals, the ZnO crystals will precipitate from the solution. The solubility of ZnO is significantly smaller than that of $Zn(OH)_2$ under the hydrothermal conditions, consequently, the $Zn(OH)_2$ precipitates strongly tended to be transformed into ZnO crystals during the hydrothermal process, by the following reaction.

$$Zn(CH_3COO)_2.2H_2O + NaOH \rightarrow Zn(OH)_2 \rightarrow Zn^{2+} + 2OH^- \rightarrow ZnO + H_2O \quad \text{Eq. (7)}$$

C). Co-Precipitation Methods

Chemical Precipitation is the most popular method for ZnO NPs preparation, which usually involves two reaction reagents: a highly purified zinc forerunner such as zinc acetate ($Zn(CH_3COO)_2 \cdot 2H_2O$), zinc nitrate ($Zn(NO_3)_2$), or zinc sulphate ($ZnSO_4$) and a solution of precipitator such as sodium hydroxide (NaOH), potassium hydroxide (KOH) or ammonium hydroxide ($NH_3 \cdot H_2O$).The precipitation method is used for the synthesis of metal oxides NPs, mixed metal or metal ceramics NCs, produces precipitate that are separated from solution. Inorganic salts are used as precursors, dissolved in water and other solvents to obtain homogeneous solution of ions, and then these salts start precipitating as hydroxides or oxalates by the help of precipitating medium when the critical concentration of species is attained followed by nucleation and growth phases.

Typically, the precipitant is added drop wise to the dissolved zinc precursor until the pH level reached about 10 or above. In the precipitation method, the precipitate can be formed as nuclei and then nuclei grow to become particles. Then, completely mix these solutions to get a white intermediate of $(Zn(OH)_2$. Ultimately, the sample of zinc hydroxide $(Zn(OH)_2)$ was converted to ZnO with a definite crystalline structure after precipitation, filtration and washing is done followed by calcinations or sintering at high temperature (Manzoor *et al*., 2015).

Controlled parameters in this method mainly include the concentration of zinc forerunner and precipitator, the molar ratio of two reagents, and the reaction and calcinations temperature. Bisht *et al*. synthesized ZnO NPs using the chemical precipitation method using $Zn(CH_3COO)_2 \cdot 2H_2O$ and NaOH in a molar ratio of 1: 5. Intermediate products were calcined at 200°C for 2 h in a muffle furnace to obtain white fine powder ZnO with the size of 18.67 ± 2.2nm (Bisht *et al*., 2016).

D). Biological Methods

Physical and chemical methods for NPs preparations utilize less time for synthesizing large quantities of nanoparticles, they require toxic chemicals as capping agents to maintain stability, thus leading to toxicity in the environment. Keeping this in consideration, green nanotechnology has attracted more and more attention because it is mostly environmentally friendly. A broad variety of plant extract are used for the biosynthesis of ZnO NPs such as the leaf of insulin plant (*Costus pictus D.Don*), *azadirachta indica*, *agathosma betulina*, *aloe vera*, *parthenium hysterophorus L.*, *plectranthus amboinicus*, *vitex negundo L.*, and *pongamia pinnata* , the flower extract of *Trifolium pratense*, *Jacaranda mimosifolia*, the seeds of *Physalis alkekengi* L, and so on. Biosynthetic and environment friendly technology for the synthesis of ZnO NPs are believed to be more eco-friendly, economical (low priced), nontoxic, and biocompatible than chemical and physical methods (Suresh *et al*., 2018).

As bio-molecules present in plant were very sensitive to the solution pH and temperature, there is a general need to synthesize metal oxide semiconducting NPs for possible applications in biological sensing, biological labelling, drug and gene delivery, and nanomedicines. In particular, due to their easy fabrication, environmentally friendly nature, and non-toxic synthesis route, ZnO NPs can provide a better option for various biological applications. However, water solubility and biocompatibility of ZnO NPs are the main requisites for biological applications (Vaishnav *et al*., 2017).

NP synthesis using bacteria is also a green approach but it has several disadvantages like screening of microbes is a time-consuming process, careful monitoring of culture broth and the entire process is required to avoid the contamination, lack of control on NP size, shape and cost associated with the media used to grow bacteria is also very high. ZnO nanoflowers and Spherical shaped NPs were synthesized by using *B. licheniformis* and *Rhodococcus pyridinivoran* through an eco-friendly approach which showed photo-catalytic activity and degraded Methylene blue dye (Tripathi *et al*., 2014).

Micro-algae draw special attention because of its ability to degrade toxic metals and convert them to less toxic forms. *Sargassum muticum* and *S. myriocystum* belonging to *Sargassaceae* family have been used for ZnO NP synthesis. Extracellular synthesis of NPs from the fungus is highly useful because of large scale production, convenient downstream processing and economic viability (Azizi *et al*., 2014). Fungal strains are chosen over

bacteria because of their better tolerance and metal bio-accumulation property. ZnO NPs were synthesized from mycelia of Aspergillus fumigatus with the NPs average size of 3.8.

2.4. Properties of Zinc Oxide Nanoparticles

A. Structure of Zinc oxide Nanoparticles

ZnO is an II-VI compound semiconductor whose ionicity resides at the borderline between covalent (SP^3) and ionic semiconductor. The crystal structures shared by ZnO are wurtzite, zinc blende, and rock salt (figure 1). At ambient conditions, the thermodynamically stable phase is wurtzite. The zinc blende ZnO structure can be stabilized only by growth on cubic substrates and the rock salt NaCl structure may be obtained at relatively high pressures. In both cases, the zinc and oxide centers are tetrahedral; the most characteristic geometry for Zn (II). In addition to the wurtzite and zinc blende polymorphs, ZnO can be crystallized in the rock salt motif at relatively high pressures about 10 GPA (Ozgur *et a*l., 2005).

Hexagonal and zinc blende polymorphs have no inversion symmetry (reflection of a crystal relative to any given point does not transform it into itself). This and other lattice symmetry properties result in piezoelectricity of the hexagonal and zinc blende ZnO, and piezoelectricity of hexagonal ZnO. The hexagonal structure has a point group 6 mm (Hermann-Mauguin notation) or C6v (Schoenflies notation), and the space group is P63mc or C6v. The lattice constants are a = 3.25 Å and c = 5.2 Å; their ratio c/a ~ 1.60 is close to the ideal value for hexagonal cell c/a = 1.633. As in most group II-VI materials, the bonding in ZnO is largely ionic ($Zn^{2+}O^{2-}$) with the corresponding radii of 0.074 nm for Zn^{2+} and 0.140 nm for O^{2-}. This property accounts for the preferential formation of wurtzite rather than zinc blende structure as well as the strong piezoelectricity of ZnO. Because of the polar Zn-O bonds, Zn and O_2 planes are electrically charged. To maintain electrical neutrality, those planes reconstruct at atomic level in most relative materials, but not in ZnO because, its surfaces are atomically flat, stable and exhibit no reconstruction at atomic level (Baruah and Dutta, 2009).

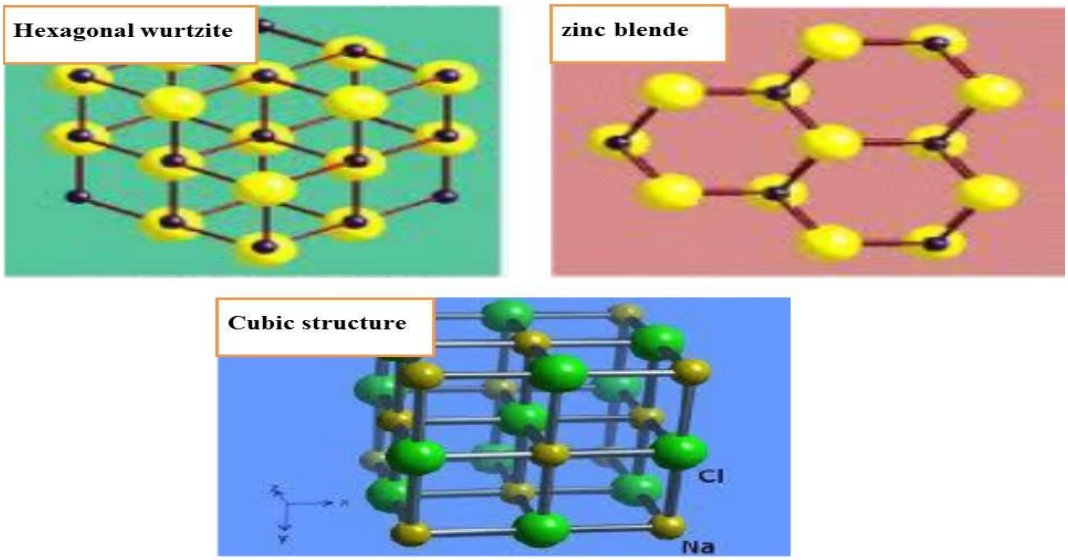

Figure 1: Stick and ball representation of ZnO crystal structures: Hexagonal wurtzite, zinc blende and cubic (rock salt) (Wojnarowicz *et al*., 2020).

B. Mechanical Properties

The mechanical properties of materials involve various concepts such as hardness, stiffness, and piezoelectric constants, Young's and bulk module, and yield strength. Piezoelectricity is the electric charge that accumulates in certain solid materials in response to applied mechanical stress. The word piezoelectricity means electricity resulting from pressure. The piezoelectric effect is understood as the linear electromechanical interaction between the mechanical and the electrical state in crystalline materials with no inversion symmetry. Among the tetrahedral bonded semiconductors, it has been stated that ZnO has the highest piezoelectric tensor. This property makes it a technologically important material for many applications (Desai and Haque, 2007; Espinosa *et al*., 2012).

C. Electronic Properties

ZnO has a relatively large direct band gap of ~3.3 *eV* at room temperature; therefore, pure ZnO is colourless and transparent. Advantages associated with a large band gap include higher breakdown voltages, ability to sustain large electric fields, lower electronic noise, and high temperature and high-power operation. The band-gap of ZnO can further be tuned from ~3.4 eV by its alloying with magnesium oxide or cadmium oxide. Most ZnO has *n*-type character, even in the absence of intentional doping. Native defects such as oxygen vacancies or zinc interstitials are often assumed to be the origin of this, but the subject remains controversial.

D. Optical Properties

ZnO has a wide band gap semiconductor that displays luminescent properties in the near ultra violet and the visible regions. The emission properties of ZnO NPs in the visible region widely depend on their synthetic method as they are attributable to surface defects. The optical properties of a semiconductor are connected with both intrinsic and extrinsic effects. Intrinsic optical transitions take place between the electrons in the conduction band and holes in the valence band, including excitonic effects due to the Coulomb interaction (Ozgur *et al*., 2005).

2.5. Nanotoxicology of Metal Oxide Nanoparticles

Metal oxide nanoparticles have wide applications, primarily in the technology field, including in semiconductor, electroluminescent, in biomedical applications as drug delivery systems for treatment and diagnosis and in environmental decontamination applications. The increasing production and use of metal oxide nanoparticles in numerous applications leads to adverse effects on health. Several studies have demonstrated nanoparticle toxicity and increased cytotoxic potential of these materials. However, a better understanding of the biological mechanisms of cytotoxicity and/or nontoxicity is necessary.

Several studies have compared the toxicity of different metal oxide nanoparticles, but not bio-genically synthesized nanoparticles. CuO, followed by ZnO, is reported to be the most toxic nanoparticle TiO_2 is the least toxic nanoparticle. Cho *et al*. compared the in vivo acute lung inflammogenicity and in vitro cytotoxicity of CuO, SiO_2 , ZnO, and Co_3O_4 nanoparticles. CuO and ZnO were the most toxic nanoparticles in both in vitro and in vivo assays. Baek *et al*. investigated concerning to microbial toxicity of metal oxide nanoparticles such as CuO, ZnO and Sb_2O_3 on *S. aureus, E. coli and Bacillus subcillu*. CuO nanoparticles were the most toxic because this material significantly reduced the colony forming units, followed by ZnO and Sb_2O_3 nanoparticles (Baek *et al*., 2011).

Dasai *et al.* compared the toxicity of different metal oxide nanoparticles to *E. coli,* both in the dark and under irradiation, in terms of the oxidative stress, amount of reduced glutathione, release of metal ions and lipid peroxidation. Under dark condition, the ranking of toxicity was $ZnO > CuO > Co_3O_4 > TiO_2$. Under light irradiation, the toxicity was $ZnO > CuO > TiO_2 > Co_3O_4$. In both cases, ZnO was the most toxic, followed by CuO.

The production of ROS was negligible in the dark and enhanced under light irradiation. ZnO and CuO were reported to be the most toxic nanoparticles (Dasai *et al*., 2013).

2.5.1. Cytotoxicity of Zinc Oxide Nanoparticles

The increasing production and use of metal oxide nanoparticles in numerous applications leads to adverse effects on health. ZnO solutions toxicity was measured by bioluminescence technique used for microbiological and molecular genetics evaluation of the nanomaterials influence on micro-biogenesis species. The method measures inhibition of bioluminescence intensity of the genetically modified photo-bacteria strain *E. coli* affected by the NPs present in the studied sample as compared to the control sample. Alteration in the bioluminescence intensity of the tested object in the analysed sample as compared to the control sample containing no toxic agents was taken as the effect criterion (Zakharova *et al*., 2019).

Several studies have demonstrated nanoparticle toxicity and increased cytotoxic potential of these materials. However, a better understanding of the biological mechanisms of cytotoxicity or genotoxicity is necessary. Exposure of cells to certain type nanoparticles can induces cytotoxicity and many effects like oxidative injury, inflammation, fibrosis, and release of pro-inflammatory mediators. The pathophysiological responses have also been found like generation of ROS (Reactive oxygen species) in cells when cells are exposed to nanoparticles. The generation of ROS is the initiating factor for toxicity of nanoparticles that exposed to organism cells (Seabra and Durán, 2015).

Another initiating factor was lysosomal destabilization loss of mitochondrial membrane integrity cause cell death. Nanoparticles cause toxicity because: a) nanostructures have an electronic, optical and magnetic property that tells about the physical dimensions and breakage in the nanostructures that can lead to a unique toxic effect that is unpredictable. b) The surfaces of nanostructures are involved in many catalytic and oxidative reaction .These reactions may induce cytotoxicity. Cytotoxicity can be greater in the nanomaterial than a bulk material because surface area to volume ratio for nanoparticle is more. c) Some nanostructures contain metals or compound with toxicity when breakdown can induce toxic responses to the components themselves. Common assumption about the nanostructures is that smaller size of nanostructures can easily enter into tissues, cells, organelles and functional bio-molecular structures, as the actual size of engineered nanostructures is similar to many biological molecules and structures. The entry of the

nanostructures into biological systems can cause damage, which can cause harm to human health (Sharifia *et al*., 2016).

2.6. Application of Metal Oxide Nanoparticles

Table 1: Application of nanoparticles in different field.

No	Applied field	Application
1	Nanomedicines	Nano drugs, Medical devices, Tissue engineering
2	Chemical and Cosmetics	Nanoscale chemicals and compounds, paints, coatings etc.
3	Materials	carbon nanotubes, biopolymers, points, coatings
5	Military and Energy	Biosensors, weapons, sensory enhancement
6	Electronics	Semiconductors chips, memory storage, optoelectronics
7	Scientific Tools	Atomic force and scanning tunnelling microscope
8	Food, Environment and Energy science	Processing, nutracetical food, nanocapsules. Water and air purification filters, fuel cells, photovoltaic

2.6.1. Application of Zinc Oxide Nanoparticles

2.6.1.1. Biomedical Applications of Zinc Oxide Nanoparticles

ZnO NPs, as a new type of the low-cost and low-toxicity nanomaterial, it have attracted tremendous interest in various biomedical fields such as anticancer, antibacterial, antioxidant, Anti-diabetic, sunscreen and anti-inflammatory activities, as well as for drug delivery, bio-imaging and used as an ultraviolet (UV) radiation filter in sunscreen cosmetics (creams, balms, lotions) applications. ZnO NPs less than 100nm are considered to be relatively biocompatible and biodegradability, which support their biomedical applications and represent a powerful property in promoting the biomedical research (Zhang and Xiong, 2015).

2.6.1.2. Antibacterial Activity of Zinc Oxide Nanoparticles

The antibacterial and antifungal properties of ZnO NPs have become the focus of interest of pharmacy, biomedicine and dentistry due to their low toxicity to the human and organism. ZnO NPs can be selected as an antibacterial material because of its superior properties, such as high specific surface area and high activity to block a wide scope of pathogenic agents. But recently, the antibacterial activity of ZnO NPs is still scarcely

known. Prior reports had suggested the main antibacterial toxicity mechanisms of ZnO NPs were based on their ability induce excess ROS generation, such as superoxide anion, hydroxyl radicals, and hydrogen peroxide production. The antibacterial activity may involve the accumulation of ZnO NPs in the outer membrane or cytoplasm of bacterial cells and trigger Zn^{2+} release, which would cause bacterial cell membrane disintegration, membrane protein damage, and genomic instability, resulting in the death of bacterial cells (Jiang *et al*., 2016).

Biosynthesized ZnO NPs were tested against gram positive bacteria such as *S. aureus*, *B. subtilis* and gram negative bacteria *E. coli*, *P. aeruginosa*, *Salmonella paratyphoid* (Dobrucka and Długaszewska, 2016). Jiang *et al*. reports the potential antibacterial mechanisms of ZnO NPs against *E. col* (Jiang *et al*., 2016). It showed that ZnO NPs with an average size about 30nm caused cell death by directly contacting with the phospholipids bilayer of the membrane, destroying the membrane integrity. The addition of radical scavengers such as mannitol, vitamin E, and glutathione could block the bactericidal action of ZnO NPs, potentially revealing that ROS production played a necessary function in the antibacterial properties of ZnO NPs.

2.6.1.3. Application of Zinc Oxide Nanoparticles in Cosmetics

The rapid development of nanotechnology has resulted in an increasing number of nanomaterial-based consumer products and industries. Because of their unique physical properties, nanomaterials have dramatically transformed the function and application of commercial products, including wound dressings, cosmetics, detergents, food packaging, drug delivery, biosensors, and antimicrobial coatings. Recently, TiO_2 and ZnO NPs have gained popularity as inorganic physical sunscreens because they can reflect and scatter UVA and UVB radiations while preventing skin irritation and disruption of the endocrine system typically induced by chemical UV filters. Also, these NPs may be transparent and pleasant to touch (Lu *et al*., 2015).

However, safety concerns regarding their utilization in consumer products have recently emerged. In literature Li *et al*. report suggested that sunscreen NPs induce cytotoxicity and genotoxicity through oxidative stress. Physicochemical characterization of nanomaterials particle size, particle size distribution, aggregation, agglomeration state, shape, surface area, composition, surface charge, and solubility/dispersibility were critical for the identification of test materials before toxicological assessment (Li *et al*., 2012).

Sunscreens are used to provide protection against adverse effects of ultraviolet (UV) B (290–320 nm) and UVA (320–400 nm) radiation. Solar ultraviolet (UV) radiation of (UVA-2, 320–340 nm; and UVA-1, 340–400 nm) rays can reach our skin and cause biological and metabolic reactions**.** Minerals like zinc oxide (ZnO) and titanium dioxide (TiO_2) are frequently used as inorganic physical sun blockers. They are preferred above organic compounds that solely absorb UV radiation. Advantages offered by sunscreens based on inorganic compounds comprise absence of skin irritation and sensitization, inertness of the ingredients, limited skin penetration, and a broad spectrum protection. The natural opaqueness of these micro-sized sunscreen components is eliminated without reducing their UV blocking efficacy by utilizing nanosized ZnO and TiO_2 particles. Since the surface area to volume ratio of particles increases as the particle diameter decreases, nanoparticles (NPs), i.e., nano-objects with all three external dimensions in the nanoscale, may be more reactive than normal bulk materials (Smijs and Pavel, 2011).

2.6.1.4. Anticancer Activity of Zinc Oxide Nanoparticles

Today cancer is one of the leading causes of death worldwide, which is mainly treated with chemo therapy, radiation, and surgery. While chemotherapy and radiotherapy suffer from severe toxic side effects to normal tissues, surgery in most occasions could not remove all cancer cells in the human body. Nanomedicine can offer a more targeted approach in the treatment of cancer. Nanoparticles with their small size preferentially enter into the leaky vascular tumor tissues, and are then retained in the tumour bed, by a process recognized as the enhanced permeation and retention effect (Jiang *et al*., 2018).

Zinc oxide (ZnO) belonging to a group of metal oxides is a wide band-gap semiconductor which absorbs in the UV region. ZnO NPs are biocompatible having antibacterial properties and show inherent differential toxicity against rapidly dividing cancer cells. Generation of intracellular reactive oxygen species (ROS) is a major cytotoxic mechanism of ZnO NPs leading to cell death. For nanoscale ZnO large numbers of valence band holes and/or conduction band electrons are available on the surface due to crystal defects. These electron-hole pairs get trapped by dissolved oxygen in the aqueous solution inside the cell resulting in the production reactive of oxygen species (ROS). Generally cancer cells themselves produce more ROS than normal cells owing to their faster metabolic rate. Therefore, exogenous ROS-generating agents like ZnO NPs produces more ROS in cancer cells than normal cells resulting in huge oxidative stress in the cancer cell and eventually killing the cell (Vasuki and Manimekalai, 2019).

2.6.1.5. Photo-catalytic Activity of Zinc Oxide Nanoparticles

Over the past few years, the preparation of nanomaterials with divergent morphologies via green methods has given a boost to the application of these materials in catalysis and in the manufacture of commercial products. Water sources have suffered an unprecedented contamination due to the huge volume of organic dyes being discharged from textile industries. These dyes are mostly not biodegradable, toxic to the ecosystem and are carcinogenic to the cell. Various methods have been reported for the removal of dyes from solutions such as reverse osmosis, oxidation using chemical action, membrane filtration, and coagulation and adsorption techniques. The materials used in these methods are either expensive or results in the formation of waste that are non-biodegradable and non-recyclable. In an attempt to overcome this snag, ZnO NPs synthesized via green method is cheap and nontoxic nanoparticles which have a significant photo-catalytic activity for dye removal (Osuntokun *et al*., 2019).

Photo-catalytic activity is based on the interaction between a photo-catalyst, usually a semi-conductor, and light to produce reactive hydroxyl radicals or superoxide species that could interact with dye molecules, resulting in enhanced degradation process of the organic dyes. ZnO NPs have been reported as good photo - catalyst in the degradation of organic dyes due to their high stability, electron binding energy and large surface area. They exhibit photo-catalytic degradation ability similar to TiO_2 due to their close band gap energies; thus, an efficient alternative for the degradation of organic dyes and potential environmental pollutant. The nanoparticles have oxygen vacancy-induced band gap narrowing which enhances its visible light photo-catalytic activity (Ji and Ye, 2008).

ZnO is one of the most promising materials for executing removal of large quantities of cyanide, degrading pesticide, carbetamide, herbicide triclopyr, and pulp mill bleaching wastewater, 2-phenylphenol, phenol, methylene blue, and acid red as an alternative to the widely used, relatively expensive titanium oxide (TiO_2). This superiority of ZnO photo-catalytic activity is because of its more active sites possesses a high surface to volume ratio, vacancies and uncoordinated atoms at corners and edges, higher reaction rates, and is more effective in generating hydrogen peroxide. The mechanism of photo-catalytic degradation of methylene blue could be illustrated thus: when incident UV light irradiated the ZnO nanoparticles, it created electron–hole pair via oxidation and reduction processes which ultimately generated -OH radicals in the presence of O_2. These photo-generated hydroxyl

radicals, superoxide radicals were responsible for the photo-catalytic degradation of methylene blue over ZnO NPs (Bagabas *et al*., 2013).

2.7. Clays

Clays are natural minerals with hydrous aluminium silicates and a layered structure composed of silicate sheets bonded to aluminium oxide/hydroxide. Structure of clay particles is perceived in layers where each layer is composed of two types of structural sheets: octahedral and tetrahedral. Clays are plastic due to their water content and become hard, brittle and non-plastic upon drying or firing. Clay is composed mainly of silica, alumina and water, frequently with appreciable quantities of iron, alkalies and alkali earths. Clay deposits and clay minerals generally vary in nature; no two or more deposits can have exactly same clay minerals. Their physical and chemical properties (swelling ability, plasticity, cation exchange capacity etc.) vary typically within and between deposits due to the differences in the degree of chemical substitution within the smectite structure and nature of exchangeable cations present, and also due to the type and amount of impurities present. Bentonite, kaolinite, mica (illite), serpentine, pylophyllite (talc), vermiculite and sepiolite are some of the classes of clays (Nayak and Singh, 2007).

2.7.1. Bentonite Clay

Bentonite is an aluminium phyllosilicate generated frequently from the alteration of volcanic ash, consisting predominantly of smectite minerals, mostly montmorillonite (MMT) (80-90 % by weight). Two types of bentonite exist: swelling bentonite which is also called sodium bentonite and non-swelling bentonite or calcium bentonite. The layers present in MMT are composed of a 2:1 structure i.e. two tetrahedral silica sheets sandwiching a central octahedral alumina sheet (T-O-T) (Abdullahi and Audu, 2017).

Tetrahedral sheets consist of corner-linked tetrahedral with oxygen in the corners and cations in the center. The dominant cation Al^{3+} is substituted for Si^{4+} frequently, up to half of the Si. Fe^{3+} is substituted for Si^{4+} occasionally; the tetrahedral rest on a triangular face and share all three oxygen with three other tetrahedral. The sheet of linked tetrahedral has hexagonal symmetry. Octahedral sheets consist of edge-linked octahedral with OH in the corners and cations in the center. The cations are usually Al^{3+}, Mg^{2+}, Fe^{2+} or Fe^{3+}, but all other transition elements and Li are possible. The octahedral sheets can be described as composed of two planes of closest-packed hydroxyls with cations occupying the octahedral sites between the two planes (Belachew and Bekele, 2020).

The structure of bentonite is characterized by one Al octahedral sheet placed between two Si tetrahedral sheets. Due to an isomorphic substitution within the layers (e.g., Al^{3+} for Si^{4+} in the tetrahedral sheet and Fe^{2+}or Mg^{2+} for Al^{3+} in the octahedral sheet) the clay layers have negative crystal charge which is balanced by exchangeable cations such as Na^{+}, K^{+}, Ca^{2+} in the interlayer together with water molecules bonded by ion-dipole forces. The hydration of these inorganic cations causes the clay mineral surface to be hydrophilic (Abdullahi and Audu, 2017).

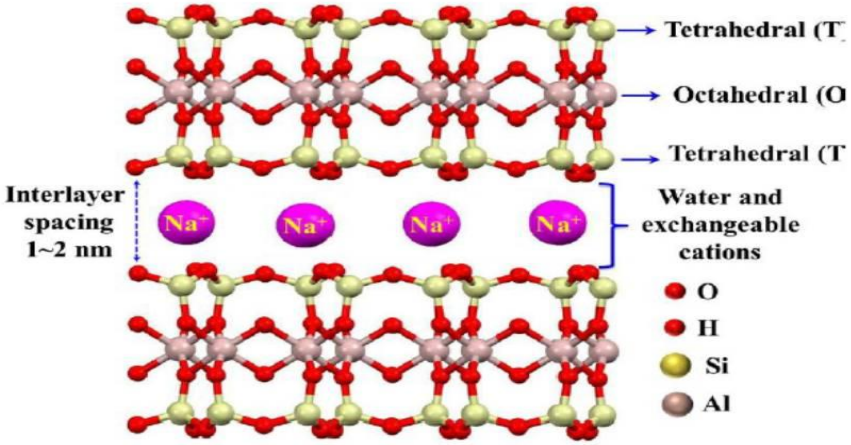

Figure 2: Atomic model of bentonite clay (Komine and Ogata, 1996).

Montmorillonite is the most studied swelling clay mineral due to its physical-chemical properties and its ability to increase the space between its layers after being subjected to an activation process (acidic, alkaline, thermal or mixed). It is a layered material with a negative structural charge due to isomorphic substitutions, which impart a cation exchange capacity (CEC) of about 100 meq/100 g and hydrophilic properties to its surface. The distribution of cations in the montmorillonite system is dependent on various parameters such as pH, ionic strength, and the type of adsorbed cation. Chemical compositions of bentonite are SiO_2, Al_2O_3, Fe_2O_3, CaO, Na_2O, MgO, K_2O, TiO_2, and P_2O_5. The most abundant oxides in both of the bentonite samples are SiO2 and Al_2O_3. The most common impurities in bentonite clay are quartz, calcite, feldspar, cristobalite, beotite, kaolinite, mica and organic matter while hydrated iron oxide, ferrous carbonate and pyrite are being the minor impurities depending on the nature of their genesis (Aguilar *et al*., 2020).

2.7.2. Synthesis of Na-Bentonite Nanoclay

Nanoclay is the new class of nanomaterials belonging to clay minerals, which offers cheap and eco-friendly source for different novel applications. In nature, the clay minerals are layered as hydrous silicate sheets, stacked one over the other. They can be obtained from clay minerals through various methods such as centrifugation, freeze drying, energetic stirring, cross-flow filtration, or through ultracentrifugation. These methods can separate clay minerals into individual sheets which can give a high aspect ratio, at least in one dimension. The synthesis of nanoscale particles without toxic chemicals overcomes the difficulties in its use in biomedical field with enhanced properties and with lesser side effects (Bukit *et al*., 2013).

Bentonite can be used without any modification or can be modified using certain physiochemical treatments based on their applications. The incorporation of any molecules within the nanoclay system does not affect the nature of the molecules. Purification of bentonite is used to prepare nanoclay with the requirement of high montmorillonite content, high swell potential, small particle size, and high specific surface area and the exchangeable Na^+, which imparts many of beneficial properties. Purification of bentonite clay can pass through four steps; eliminate the impurity levels of non-swelling components, eliminate the impurity levels of Fe, eliminate the impurity levels of Al and concentrate montmorillonite in the sample using centrifuge. The purification methods of bentonite generally classified into mechanical purification methods and chemical purification methods (Ismaeel, 2017).

The first step of bentonite nanoclay preparation is purification of clay sample. The clay samples collected along the bentonite bed at an interval of one sample for each ½ meter. The sample crushed using 1 MZ-400 W tungsten type samples pulverizes. The step of bentonite purification which takes four steps:

- ✓ Elimination of the impurity levels of non-clay minerals from bentonite clay using sieves.
- ✓ Elimination of the impurity levels of Fe using magnetic separation device.
- ✓ Elimination of the impurity levels of Al by chemical process using HCl solution.
- ✓ Concentration of montmorillonite done through stirring and centrifugation.

The second step of bentonite nanoclay preparation is activation of purified clay by using sodium compounds namely Sodium Carbonate (Na_2CO_3), Sodium Hydroxide (NaOH),

Sodium Chloride (NaCl) and Sodium Silicate (Na_2SiO_3) or acid like HCl. The Na-montmorillonite obtained by soda activation has high montmorillonite content, high swell potential, small particle size, and high specific surface area than Ca-montmorillonite. This suggests that Na^+cations replaced Ca^{2+} cations in the montmorillonite interlayer. The percentage of Na_2O is high when treated with Na_2CO_3 (Evangeline*et al*., 2009).

Table 2: Percentage of Na_2O and CaO present in bentonite treated with sodium compound (Evangeline *et al*., 2009).

Name of Na-comp.	Oxide analysed	Presence of Na_2O/CaO in %			
		Na-comp. (%)	Na-comp. (2.5%)	Na-comp. (5%)	Na-comp. (7.5%)
NaCl	Na_2O%	1.46	4.16	4.95	4.51
	CaO%	2.19	1.49	1.31	0.68
NaOH	Na_2O%	1.46	4.81	5.21	6.03
	CaO%	2.19	1.38	1.08	1.10
Na_2CO_3	Na_2O%	1.46	6.62	8.28	8.07
	CaO%	2.19	1.64	1.33	1.48
Na_2SiO_3	Na_2O%	1.46	3.78	4.40	4.88
	CaO%	2.19	2.08	1.26	1.41

2.7.3. Application of Bentonite Clay

Bentonite clay is mainly used in structural polymers, ceramic bodies, drilling fluids, in adsorption catalytic processes, animal feed additive, wastewater treatments and biomedical applications.

A. Bentonite as Antibacterial agent

Some studies employ bentonite-type clay minerals as drug carriers or drug recipients, three types of nanoclays (bentonite, MMT and halloysite) used as potential carriers for antimicrobial peptides nisin and pediocin and other pharmaceutical applications. Due to their considerable chemical and mineralogical diversity and complexity, a variety of specific clay minerals have been widely employed in pharmaceutical and biomedical applications as active ingredients.

A variety of physical and/or chemical processes can make clays antibacterial. Physical bactericide can occur by surface attraction between clay minerals and bacteria, which can

hamper (hinder) passive and active uptake of essential nutrients, disrupt cell envelopes or impair efflux of metabolites. The investigation of the antibacterial activities and physicochemical characteristics of clays in laboratory studies demonstrated that an iron-rich clay show a broad-spectrum in *vitro* antibacterial activity to treat Buruli ulcer (Williams *et al*., 2011).

However, further investigation revealed that among "healing" clays, relatively few deposits exhibit antibacterial properties. Bentonite clay is one of the healing clays from the smectite group. They are called living clays appropriately since they prolong life by detoxing the toxic burden in our bodies. Native American tribes call bentonite 'Ea-Wah-Kee' which means 'The Mud that Heals." In the book the Clay Cur (Behroozian *et al*., 2020).

B. Bentonite for recycled automotive oil purification

Motor oils play an important role in the operation and performance of a vehicle, being one of the products in greatest demand. Because of the development of new technologies and the eminent industrial and automotive market growth, it is projected that the motor oil demand increases in time. The increasing motor oil demand combined with the decreasing petroleum availability. Un-purified motor oil needs to be purified because; it has a dangerous waste which could contaminate drinking water due to the presence of heavy metals, polycyclic aromatic compounds, polychlorinated biphenyls, among others. Nowadays, the un-purified motor oil purification technologies consist of four stages: (i) dewater and light defuel, (ii) de-asphalt, (iii) fractionation and (iv) finishing. The finishing is the stage in which some substances (chlorine, nitrogen, sulphur, oxygen, peroxides, among others) are removed from un-purified motor oil. These substances give color to the oil and increase its acidity degree. The finishing can be performed by adsorption process. The most common adsorbent materials used are natural clay, activated clay, silica, activated carbon, etc. (Aguilar *et al*., 2020).

C. Bentonite in Nano Particle Material as intercalation or Filler Nanocomposite

Natural bentonite was used in nano particle material as filler and reinforcement of thermoplastic high density polyethylene that has mechanical properties and good thermal properties and can be used as one component in the automotive industry. The fillers were often added to polymeric materials that are capable of homogeneously into the matrix. Filler would provide varied nature of the material properties in order to obtain the physical and mechanical properties that meet the requirements. Bentonite is a type of rock that

contains a lot of minerals in it that has the properties of a typical montmorillonite namely; may inflate in water, intercalation and ion exchangers are making this material interesting organo clay used to be a catalyst nano and nano clay polymer composites. Nano fillers can be applied to the polymer material to produce nano composite material with improved some basic properties of polymers, such as thermal resistance properties, mechanical properties, chemical resistance and flammability (Bukit *et al*., 2013).

Na-bentonite nanoclay was excellent filler, binder, intercalation and supporting materials, and substrates for metal/metal oxide NPs due to its large surface area, swelling behaviour, and high adsorption and ion exchange properties. Their adsorption capacities help to attract contaminants into the open pores and therefore raise the efficiency of the dispersed transition metal oxides NPs such as titanium oxide (TiO_2), zinc oxide (ZnO), zirconium oxide (ZrO_2), tin oxide (SnO_2), manganese oxide (MnO_2), etc. Chakraborty et al., (2019) reports that the catalytic activity of these oxides was reinforced when they were supported on a bentonite clay which contain a high specific surface area and low cost. A large number of ion exchange sites available in clays are also beneficial for incorporation of electro-active species and nanoparticles.

D. Bentonite in Cosmetic Products

Recent research shows that clay minerals can be used in sunscreens as UV filters instead of inorganic and organic compounds, which can cause unexpected photo-catalytic effect and damage the skin surface and can be absorbed into the skin and cause allergic reactions. Clay's minerals are the potential candidate as natural UV filters in sunscreens, due to their positive impact on human health and chemical inertness and high specific surface area, therefore providing effective coverage of skin surface (Dusenkova *et al*., 2015).

Their magnitude of UV protection depends on the clay mineralogical composition. The presence of carbonates can cause alkaline media, therefore reducing the efficiency of clay mineral separation from non-clay minerals and can be irritating to the skin. The presence of iron oxides and hydroxides (iron containing minerals) also reduce the efficiency of clay mineral purification and in most cases gives the color to clays. After the removal of theses iron containing minerals the clay samples become lighter in color (from light greenish gray to white), therefore expanding their application possibilities, because in cosmetics color is an essential property (Smijs and Pavel, 2011).

2.8. Synthesis Methods of Metal Oxide-Bentonite NCs

As mentioned above, every nanomaterial has its own drawbacks. For example, the light adsorption of TiO_2 NPs and ZnO NPs is limited in the ultraviolet light region due to their big band gap energies. Recent investigations on nanoparticles have revealed their potentials in biomedical application and wastewater treatment, especially in the area of adsorption. However, there are demerits of the direct use of nanoparticles in wastewater in terms of their aggregation in fluidized systems, difficulty in separation from the treated water and their fates in the treated water. The agglomeration of nanoparticles happens due to their small size, and consequently decreases their catalytic activity. To avoid the agglomeration of nanoparticles, hybrid processes (nanocomposites) were introduced by combining metal oxide nanoparticles with other environmentally friendly materials of inert and stable materials like clay to utilize nanoparticles' full properties in wide range applications (Mustapha *et al*., 2020).

Metal oxide-clay NCs are the combination of metal oxide NPs and nanoclay particle. Because of high specific surface area, high chemical and mechanical stability and excellent binder and fillers for metal oxide, bentonite clays are used to incorporate the metal oxide into the basal space of their layered structure and make NPs more stable. Clay minerals are a big family of silicates showing diverse structural arrangements and morphologies with topologies able to accommodate a variety of NPs of semiconductors such as TiO_2 and ZnO (Ruiz-Hitzky *et al*., 2019).

In recent years, the synthesis of various metal oxide-clay nanocomposites has become the most active subject in the field of nanomaterials such as TiO_2, ZnO, Fe_3O_4, CdO, Mn_2O_3, WO_3, SnO_2, Ce_2O, CuO and MgO. Among various metal oxides, ZnO is one of the most popular which possesses some antibacterial effect, good thermal qualities, and color stability, with low cost and little toxicity(Tan *et al*., (2008). ZnO-bentonite NCs synthesis operation is accomplished by hybridizing zinc salt precursors and Na-bentonite. The synthesis of uniform sized nanocomposites is very important because their properties include optical, magnetic, electrical and biological properties depending on their size and dimensions (Hakimi *et al*., 2018b).

Composites of metal oxide NPs supported on clay can be synthesized by various techniques. However, their formulation is still mostly based on prescribed techniques such as ion exchange processes, γ-irradiation, hydrothermal synthesis, chemical reduction

methods, solvothermal methods, electrolysis plating and sol-gel. The preparation methodologies of ZnO-layered clay based materials mainly include the in situ formation of ZnO NPs in the presence of the clays or organo-clays in aqueous media followed by diverse Zn salt precursors and experimental conditions (Hakimi *et al*., 2018a).

2.8.1. Ion Exchange Method

Ion exchange methods can be further classified into liquid phase ion exchange (LSIE) and solid state ion exchange (SSIE). In the liquid phase ion exchange method, cations in the interlayer space of clay minerals such as Na^{+} or Ca^{2+} can be converted into various inorganic or organic Cations like Zn^{2+} via an ion-exchange reaction. Therefore, ion-exchanged cations occupy the interlayer space in natural clays. Finally, by applying heat treatment, the ion-exchanged cations undergo dehydration reaction and are converted to metal oxide clusters in the interlamellar space of clay particles. In most studies done so far, LSIE method has been used to prepare composites (Hakimi *et al*., 2018b).

The solid method has been recently used in a number of studies to prepare various antimicrobial composites. In this method, a zinc salt such as $ZnCl_2$ and $ZnSO_4$ are mixed with bentonite and heated at around the melting temperature of a zinc salt. Synchronized application of heat and ion exchange creates a fast process· SSIE is simpler and faster than LSIE and precipitation methods (Pouraboulghasem *et al*., 2016).

2.8.2. Precipitation Method

The precipitation method is used for the synthesis of metal oxides NPs, mixed metal or metal ceramics nanocomposites, produces precipitate that are separated from solution. Inorganic salts are used as precursors, dissolved in water and other solvents to obtain homogenous solution of ions, and then these salts start precipitating as hydroxides or oxalates when the critical concentration of species is attained followed by nucleation and growth phases**.** In the precipitation method, the precipitate can be formed as nuclei and then nuclei grow to become particles. Nuclei formation and growth depend on the concentration of precursor solution and reaction time. The size and shape of particles is greatly influenced by solution pH, reducing agent, temperature and concentration of salt (Stankic et al., 2016).

After precipitation, filtration and washing is done followed by calcinations to convert hydroxide into oxides with a definite crystalline structure. The precipitating medium

usually employed includes NaOH, NH_3 or NH_4OH, Na_2CO_3 etc. The method offers the advantage of being low cost, simple, water based reaction, flexibility, mild reaction conditions and size control**.** Previously, Kutlakova *et al.* synthesized ZnO-bentonite NCs by the precipitation method from the reaction of zinc salts such as $ZnCl_2$ with bentonite in basic solutions containing NaOH to complete the precipitation, leading to the formation of a white gel by heating mixture at around the melting temperature of a zinc salt (250 ℃) (Kutlakova *et al*., 2015)...

2.8.3. Hydrothermal Synthesis Method

The hydrothermal and solvothermal synthesis of inorganic materials is an important methodology in nanomaterial synthesis. The hydrothermal method involves the heterogeneous chemical reaction in a solvent (aqueous or non-aqueous) occurring above room temperature and at pressure more than 1atm in a closed system. Normally, hydrothermal reactions are conducted in a specially sealed container or high pressure autoclave under subcritical or supercritical solvent conditions. Under such conditions, the solubility of reactants increases significantly, enabling reaction to take place at lower temperature. In previous literature, Madathil *et al*. and Farias *et al*. synthesized ZnO-bentonite NCs from an aqueous suspension containing bentonite and the $Zn(CH_3COO)_2.H_2O$) with alkalization by NH_4OH and hydro-thermallization at 100 ℃ in a microwave reactor (Madathil *et al*., 2007; Farias *et al*., 2011).

2.8.4. Sol-Gel Method

Sol-gel is a methodology of producing small particles in material chemistry. It is wet-chemical technique mostly used for the synthesis of nanoparticle. The inorganic nanostructures are formed by the sol-gel process through formation of colloidal suspension (sol) and gelation of the sol to integrated network in continuous liquid phase (gel).The initial step of this process is converting monomers or the starting material into a sol, i.e., a colloidal solution which is the precursor for the further formation of a gel. This gel is made up of discrete particles or polymers. Sol-gel process is preferred due to its economic feasibility and the low temperature process which gives us control over the composition of the product achieved (Samat and Nor, 2013).

A gel is formed when solid and liquid phases are dispersed in each other. In this process, initially, colloidal particles are dispersed in a liquid forming a sol. Deposition of this sol can produce thin coating on any substrate by the means of spraying, spinning or coating.

The steps involved in the sol-gel synthesis are mixing, casting, gelation, aging, drying and densification. Sol–gel process involves inorganic precursors that undergo various chemical reactions, resulting in the formation of a 3D molecular network. One of the most common routes is via hydrolysis and condensation of metal alkoxides to form larger metal oxide molecules that polymerize to form the coating.

However, the fundamental problem of aqueous sol-gel chemistry is the complexity of process and the fact that the as-synthesized precipitates are generally amorphous. Nowadays, the family of metal oxide NPs is synthesized by non-aqueous processes and ranges from simple binary metal oxides to more complex ternary, multi-metal and doped systems. This method is cost effective but possibility of contamination is higher due to the precursor chemicals.

The advantage of sol–gel method are the synthesis of nanostructures containing more than one component, since the slow reaction kinetics allows good structural engineering of the final product and the reactions are conducted at low temperatures or at room temperature. According to Xu *et al*., (2015) report, the synthesis of ZnO-bentonite NCs by the sol-gel method involves the reaction of Zinc acetate ($Zn(CH_3COO)_2 \bullet 2H_2O$ with ethanol: water (3:1) mixture and calcination at 200 ℃ for 4h.

2.8.5. Microwave Synthesis Method

Metal oxide-bentonite NCs can be synthesized by using Simple Microwave Synthesis method. In this method the mixture of metal oxide solution and clay mineral was loaded into a microwave Teflon container and the reaction were performed in a microwave digestion system under various conditions. Foroughi *et al*., (2017) synthesized CdO-Clay NCs successfully with the aid of CdO NPs and bentonite clay. According to their report, CdO NPs was prepared by a solid-state thermal decomposition with the aid of Cd $(CH_3COO)_2.2H_2O$ without any surfactants or additive and bentonite clay was prepared by rapid and facile microwave method. In this method $Cd(CH_3COO)_2.2H_2O$ powder was put into a small quartz boat. The quartz boat was entered into the proper position of the tube furnace and it was held in the heating zone at 250 ^{0}C and then it was slowly dragged out of the furnace. The sample was naturally cooled down in ambient conditions**.**

2.8.6. Bio-Synthesis Methods

Usually, chemical or physical method is used to prepare the metal oxide-bentonite NCs.

However, the physical and chemical methods are generally expensive, use harmful and inflammable solvent and have limitations such as incomplete removal, slow process, high-energy requirement and production of secondary pollutants that require further disposal. But the biological methods are a cost effective, energy saver and having environmentally benign protocols technique for green synthesis of metal oxide-bentonite NCs from different microorganisms like plant. This method of biosynthesis is very simple, requiring less time and energy in comparison to the physical and chemical methods with predictable mechanisms (Iravani, 2011).

Among many organisms plants seem to be the best candidates and they are suitable for large scale biosynthesis of metal oxide-bentonite NCs. Plant materials contain biogenic molecules capable of acting as modifiers and capping agents for the synthesis of nanocomposites. These bio-molecules are vital in the green synthesis of environmental-benign metal oxide-bentonite NCs, and are good alternatives to the chemicals used in conventional methods. According to Honarmand *et al*. report, the advantages of using plant and plant-derived materials for biosynthesis of metal oxide-bentonite NCs have attracted the interest researchers to investigate mechanisms of metal ions uptake and bio reduction by plants, and to understand the possible mechanism of metal oxide-bentonite NCs formation in plants (Honarmand *et al*., 2020).

Henrique *et al*. reports that metal oxide-clay NCs are the combination of metal oxide NPs and nanoclay particle; hence they can have a combination or have markedly different mechanical, electrochemical, electrical, catalytic, thermal and optical properties from the component materials (Henrique *et al*., 2009).

2.9. Hagenia Abyssinica Plant

H. abyssinica plant is a member of the Rosaceae family, is a species of flowering plant native to the high-elevation Afro-mountain regions of central and eastern Africa from Sudan and Ethiopia. It is known in English as African redwood and East African\rosewood and in Amharic language kosso and in Oromo language as Hexo. *H. abyssinica* is a slender tree up to 20m tall, with a short trunk and thick branches. The roots are cooked with meat and the soup drunk for general illness and malaria, for intestinal parasites , especially against cestodes while the dried and pounded female inflorescence is used as an anthelmintic (especially for tapeworm) (Desta, 1995).

The leaf extract of *H. abyssinica* (kosso) was used because of its medicinal properties. It is rich in phytochemical sparticulary secondary metabolites such as tannins, terpenoids, flavonoids, Saponins, alkaloids, phlobathanins and phenol compounds which act as reducing, stabilization agents and that have been demonstrated to have antibacterial properties. These bioactive compounds such as phenol compounds are act as a ligand, particle size controller, antioxidant and bind to metal ions and reduce them and cap them to form nanoparticles due to their high inclination towards chelating the metals. Phenol compounds contain hydroxyl and carboxylic groups which have very high tendency to bind metal ions. Metal ions in solution interact with polyphenol compound and helps in the nucleation and formation of NPs (Murthy *et al*., 2020).

The antimicrobial activity of NPs can be attributed to the presence of bioactive compounds on the surface of NPs as capping and stabilizing agents. Thus, synergistic effect of bioactive compounds such as tannins, phenol and glycoside of *H. abyssinica* leaf extract coupled with ZnO NPs can enhance the antibacterial activity of ZnO NPs against pathogens by reducing its oxidation state. Therefore, the phytochemical screening result reveals that the presence of these phytochemical constituents supports the use of *H. abyssinica* plant in folklore medications and it is probable that these phytochemicals are responsible for the healing properties of these plants which have been claimed by the peoples in the area of this study. Generally, this is a strong medicine that must not be taken in large quantities; it is sometimes taken as an abortifacient (Wolde *et al*., 2016).

Figure 3 shows the unaffected *H. abyssinica* plant leaves and flower. Traditionally the dried female Kosso flowers are used as decoction or suspension in water. The powdered material is usually macerated with water. Children infested with the parasite resist taking the drug and are sometimes punished by their parents in order to force them to drink concoction. Infections with *Taenia saginata* are common in the country due to the regular traditional consumption of raw meat and treated with *H. abyssinica* plant flower water suspension.

Figure 3: *Hagenia abyssinica* plant (Assefa *et al*., 2010)**.**

2.10. Characterization of Nanoparticles and Nanocomposites

Nanoparticles and nanocomposites are generally characterized by thermal stability, their size, optical properties, chemical composition, morphology, functional group, and surface charge, using advanced microscopic techniques such as TGA, XRD, UV-Vis, AAS, SEM, TEM, DLS, AFM etc. The average particle diameter, their size distribution and charge affect the physical stability and the in vivo distribution of the nanoparticles. Particle size distribution and morphology are the most important parameters of characterization of NPs and NCs. Thermal stability and decomposition properties of materials are determines by using thermo-gravimetric analysis, crystal structure and average particles sizes using XRD, optical and electrical properties using UV-Vis, morphology, the size distribution, and shape using SEM and DLS, TEM, AFM and SEM are characterization techniques used for determining nanoparticle size.

For SEM characterization, nanoparticles solution should be first converted into a dry powder, which is then mounted on a sample holder followed by coating with a conductive metal, such as gold, using a sputter coater. The sample preparation for TEM is complex and time consuming because of its requirement to be ultra-thin for the electron transmittance. The nanoparticles dispersion is deposited onto support grids or films. To make nanoparticles withstand the instrument vacuum and facilitate handling, they are

fixed using either a negative staining material, such as phosphotungstic acid or derivatives, uranyl acetate, etc., or by plastic embedding

2.11. Application of Metal Oxide-Bentonite NCs

The applications of metal oxide-bentonite NCs in different sectors had been widely recognized. ZnO-bentonite NCs have drawn considerable attention from researchers and scientists in the past 4-5 years due to its wide applications in the biomedical field (antifungal, antibacterial, drug delivery, anti-diabetic, anticancer), agriculture/ food, in environment (as adsorbents, photo-catalysts and sensors), optics and electronics (catalytic activity, wound healing, anti-inflammatory, ultraviolet filtering properties and extensively used in various cosmetics such as sunscreen).

2.11.1. As Antibacterial Agent

Several biosynthesized metal oxide-bentonite NCs applications to biomedical and antimicrobial areas have been explored. The mechanism of the antibacterial activity of clay-based nanocomposites can be classified into two stages namely: adhesion and killing. The application of NPs and NCs strongly depends on the classes or types of bacteria in water and the physicochemical characteristics of the nanomaterials (Mustapha *et al*., 2020). Pouraboulghasem *et al*. synthesized ZnO-bentonite NCs by a quick and simple alkaline ion exchange method and tested against gram-negative *E. coli* bacteria as a model (Pouraboulghasem *et al*., 2016). According to their report composites of ZnO-bentonite show good antibacterial properties, confirming that they can be used alone for antibacterial action. The results indicate that composites synthesized through longer ion exchange time yield greater beneficial effects in inhibiting bacterial growth. The enhanced antibacterial activity of the composites can be attributed to the chemical and physical properties of the nanoparticles with a large surface area of the clay. This implies that a great amount of ZnO is highly dispersed per unit area of the bentonite surfaces, thereby, maximizing antibacterial activity.

The antibacterial properties of metal oxide-bentonite NCs have been utilized in food packaging materials for controlling food-borne pathogens and deactivating many other bacteria. The antibacterial study on ZnO-nanoclay hybrids against *E. coli* and *S. aureus* was conducted under the influence of contact time and temperature by Garshasbi *et al*. (2017). Krishnan and Mahalingam also reports the antibacterial activity of Mn_3O_4-bentonite NCs synthesized by facile thermal decomposition method. They conduct

antibacterial test against a Gram- negative (*E. coli* and *P. aeruginosa*), Gram-positive (*S. aureus* and B. subtilis) bacterial and fungal (*Candida albinos*) pathogens. The results showed that nanocomposite of Mn_3O_4-bentonite clay NCs have enhanced the antimicrobial activity than pristine Na^+- bentonite clay (Krishnan and Mahalingam, 2017).

Because of storage of antibacterial samples for long period of time reduce the toxicity of samples; fresh solutions of samples was used for highest antibacterial effect. In Pouraboulghasem *et al*. previous report; stability analysis showed that the highest antibacterial effect was produced by less stable solutions containing the largest aggregates (*Pouraboulghasem et al*., 2016).

2.11.2. As Photo-catalyst

ZnO NPs have been used in a variety of applications such as semiconductors catalysts because of the strong ultraviolet absorption properties. ZnO, a wide band-gap compound II–VI semiconductor has a direct band gap of about 3.37eV at room temperature, is a well-known material suitable for generating ultraviolet (UV) light. Furthermore, a large exciton binding energy of about 60 meV in ZnO,), ensures efficient excitation emission at room temperature under low excitation energy (Meshram *et al*., 2011).

Among environmentally harmful organic contaminants, phenols and dyes are primary toxic contaminants which are detrimental even at ppb levels to the aquatic/human life. Similarly, hexavalent chromium [Cr (VI)] is a toxic inorganic industrial pollutant. The removal of both inorganic and organic pollutants from wastewater can be done through several chemical and/or physical methods such as biological methods, activated sludge process, trickling filter, membrane bioreactor, and suspended-bio-film reactor, exposing contaminated water in UV light etc. But these methods get incomplete removal of pollutants and also suffer with problem of mud formation as well as adsorbent regeneration (Sasikala *et al*., 2019).

Metal oxides-clay NCs are economically and technically attractive photo catalyst used for degradation of these combinations of pollutants and for various water purification and recycling processes. Among many metal oxides-clay NCs such asTiO_2, ZnO, ZrO_2, SnO_2, MnO_2, ZnO-bentonite NCs is one of the interesting due to its non-toxic nature, comparatively high photo-catalytic ability, chemical and thermal stability, synthesis feasibility and low solubility in aqueous solutions (Mustapha *et al*., 2020). Chakraborty *et al*., (2019) synthesized ZnO-bentonite NCs an efficient catalyst for discharge of dyes,

phenol and Cr (VI) from water. According to their report the catalytic activity of these oxides was reinforced when they were supported on a suitable substance such as natural clays like bentonite, which contain a high specific surface area and low cost.

2.11.3. In Drilling Fluids

The rheology of drilling fluids plays an important role in controlling the drilling operations. Several drilling problems like lost circulation, pipe sticking, formation damage and high torque and drag are common in extending a reach drilling operation that limits the performance and are mainly responsible for huge financial losses in the form of expensive drilling fluids additives and lost production time. So using ZnO-bentonite NCs was an interesting method to maintain the remarkable colloidal suspension thus enabling homogeneous drilling fluids recipes (Haneef and Abdo, 2012). In literature it is found that, Nizamani *et al*. also synthesized TiO_2-bentonite NCs by using cost effective hydrothermal method for water-based drilling fluids application (Nizamani *et al*., 2017).

2.11.4. As Sunscreens

Sunscreens are used to provide protection against adverse effects of ultraviolet (UV) B (290–320 nm) and UVA (320–400 nm) radiation. According to the United States Food and Drug Administration, the protection factor against UVA should be at least one-third of the overall sun protection factor. Inorganic materials can absorb, reflect, or scatter the ultraviolet radiation, depending on their particle size, unlike the organic blockers, which absorb the UV irradiation. Due to its physical and chemical stability in addition to its transparency in the visible region with ultraviolet protective activity, ZnO can be used in sunscreen applications (Smijs and Pavel, 2011).

Indeed, ZnO is attractive for sunscreen formulization, due to its modest refractive index (2.0), its absorption of the small fraction of solar radiation in the UV range ≤375 nm, its high probable recombination of photo-generated carriers (electrons and holes), large direct band gap, high exciton binding energy, non-risky nature, and high tendency towards chemical and physical stability. However, the photo-catalytic activity of inorganic UV absorbers has raised much concern in many UV protection applications. On absorption of UV light by ZnO, the electrons in the occupied valence band are excited by the UV light into the unoccupied conducting band. The conduction band electrons and valence band holes thus created can migrate out to the particle surface to react with electron donors or

acceptors (water or oxygen) that are adsorbed on the particle surface, they produce reactive superoxide ($\bullet O_2^-$) and hydroxyl (•OH) free radicals (Tsuzuki *et al*., 2012).

A significant issue for ZnO use in sunscreens is that it can generate ROS in the presence of UV light because of its photo-catalytic activity. Therefore it is essential to make a non-photo-catalytic ZnO material through doping with other metals. Several efforts have been made to deactivate the photo-catalytic activity of ZnO by using inorganic surface modifiers. However, to solve the cosmetic drawback of these opaque sunscreens, nanosized ZnO have been increasingly replaced by ZnO-bentonite NCs (<100 nm) (Tsuzuki *et al*., 2012).

One approach to reduce the photo-catalytic activity of ZnO NPs is to coat the particles with non-conductive materials such as SiO_2 or Al_2O_3 and clays. This is based on the assumption that, if the coating layer is sufficiently thick for photo-exited electrons and holes to cross through, photo-generated excitons would be trapped within the coating layer so that free radical generation would be inhibited. Silica is a barrier materials between ZnO and surrounding materials, because of its hydrophilic, safe, low cost and stable nature against biodegradation (Wang *et al*., 2009). Clays are also potential candidate as natural UV filters in sunscreens based on their chemical composition, due to their positive impact on human health, chemical inertness and their high specific surface area, therefore providing effective coverage of skin surface (Dusenkova *et al*., 2015; Mueen *et al*., 2020).

There are a number of reports on the risks from exposure to UV rays from sunlight, such as skin aging, sunburn and sun-tanning photo-toxicity, and skin cancer. Most of them relate to the risks from the generation of reactive oxygen species (ROS), which are created during UV exposure. For this reason, the demand for efficient UV-protection has become very urgent. Utilization of composite of nanosized ZnO NPs and bentonite nanoclay may improve a broad-band UV protection (opaqueness of nanocomposites). Skin exposure to NP-containing sunscreens leads to incorporation of ZnO NPs in the stratum corneum, which can alter specific NPs attenuation properties due to particle-particle, particle-skin, and skin-particle-light physicochemical interactions (Mueen, 2020).

CHAPTER THREE

3.0. MATERIALS AND METHODS

3.1. Study Sites Description

The plant *H. abyssinica* was collected from Roomie regional state, East Arsi Zone (Qarsa town) 235km from Addis Ababa. Bentonite clay was collected from Afar Regional State, Gewane. Bio-synthesis of ZnO NPs and ZnO-bentonite NCs using *H. abyssinica* medicinal plant leaf extract was carried out in the Applied Chemistry laboratory of Adama Science and Technology University (ASTU). The UV-Vis characterization and antibacterial activity were tested in the Applied Biology laboratory; TGA, UV-Vis-DRS and XRD analysis were conducted at the Materials Science Engineering laboratory, ASTU. Analysis of bentonite was conducted at Geological Survey of Ethiopia laboratory and FTIR analysis were performed at Addis Ababa University.

3.2. Chemicals and Apparatus

All the chemicals and reagents used for the preparation of ZnO NPs and ZnO-bentonite NCs were purchased from the local market in Addis Ababa and used without further purification.

3.2.1. Chemicals

Zinc acetate ($Zn(CH_3COO)_2{\cdot}2H_2O$)-99.9% AR analytical reagent (Guandong Guanglua Sci-tech co., Ltd, France), distilled water (H_2O), ethanol (CH_3CH_2OH), sodium carbonate (Na_2CO_3), dimethylsulfoxide (DMSO)-(Sisco, Research laboratories Pvt. Ltd, India), sodium hydroxide (NaOH), Mueller Hinton agar (Sisco. Research laboratories Pvt. Ltd, India), ethyl acetate ($CH_3CH_2OOCCH_3$), ammonia (NH_3), Iodine (I_2), potassium iodide (KI), methanol (CH_3OH), 2, 4- dinitrophenyl hydrazine (2,4-DH), and hydrochloric acid (HCl) were used. All aqueous solutions were prepared using distilled water.

3.2.2. Apparatus

Glass ware (beaker, conical flask, pipette, quartz cuvete, volumetric flask, funnels, measuring cylinder), electronic balance, magnetic stirrer with hot plate, petri-dish crucible, mortar and pestle, dropper, ball milling, oven, furnace and centrifuge were used.

3.3.Experimental Procedure

3.3.1. Collection of *H. Abyssinica* Plant Leaves

H. abyssinica plant leaves were collected from around Qarsa Town, in East Arsi Zone Oromia Regional State, Ethiopia. The study site was chosen based on the social studies on *Hagenia abyssinica* plant to get basic information on medicinal value of plant. Plant leaf was selected other than root and flowers due to its high content of phytochemical and Medicinal value is better in antibacterial. The leaf samples were washed several times with tap water followed by distilled water to remove extraneous matter. The cleaned leaves were dried in open air under shadow for two weeks (15 days) to reduce the moisture content of the leaves. The dried leaves were crushed by using an electrical grinding machine to produce small particle size which easily homogenized in solvent and form better surface contact with extraction solvents; then packed in a brown glass bottle to protect it from light. Figure 4 shows the process of preparing *H.abyssinica* leaves powder.

Figure 4: *H. abyssinica* plant; wet leaves, dried leaves and leaves powder.

3.3.2. Preparation of Aqueous Plant Leaf Extract

H. abyssinica plant aqueous leaf extract was prepared fresh prior to the synthesis of the nanomaterial. Aqueous solvent was selected as a measure of the solvent efficiency to extract specific components; because selected plants had abundant polar compounds

compared to non- polar compounds. For preparing the fresh leaf extract, 25 g of the powdered leaves of *H. abyssinica* was taken in a 1000 ml conical flask containing 400 ml of distilled water. The flasks were then covered with aluminium foil; to prevent the effect of light. After that, the contents of the flask were stirred using a magnetic stirrer for 90 min without heating for efficient extraction to occur, the solvent must make contact with the target analytes and allowed to warm at 50 ˚C for 1 h followed by cooling to room temperature. The contents of the flask were left as such overnight. The prepared solution was centrifuged at 5000 rpm for 10 min. to obtain a clear solution. The clear extract was stored at 4 ℃ till required.

3.3.3. Phytochemical Screening of *H. abyssinica* Plant Leaf Extract

A. Test for saponins (Frothing test).

3 mL of the plant leaf extract was mixed with 5 mL of distilled water in a test-tube. The test-tube was stoppered and shaken vigorously by hand for about 5 min., allowed to stand for 30 min and observed for honey-comb froth (appearance of creamy miss of small bubbles), which was indicative of the presence of saponins (Auwal *et al.,* 2014).

B. Test for flavonoids:

Determination of flavonoids was done according to the methodology by Wolde *et al*. with little modification (Wolde *et al*., 2016).

To 2 ml of the plant leaf extract, 10 mL of ethyl acetate was added and heated in a steam bath for 3 min. The mixture was then filtered and 4 mL of the filtrate was shaken with 1 mL of dilute ammonia solution and a yellow coloration was observed, which was indicative of the presence of flavonoids.

C. Test for alkaloids: Wagner's test

5 ml of plant leaf extract was mixed with 1.27 g of iodine and 2 g of KI in 100 ml of water and shaked for 3 min. Reddish brown color was formed which showed the presence of alkaloids (Vaishnav *et al*., 2017).

D. Test for terpenoids: Salkowski's test

The test was done according to the methodology by Wolde *et al*. with little modification (Wolde *et al*., 2016). 2 ml of the plant leaf extract was mixed with 5 mL of methanol. 2 mL of this mixture, was treated with 1 mL of 2, 4- dinitrophenyl hydrazine dissolved in 100 mL of 2 M HCl. Yellow-orange coloration was observed as an indication of terpenoids.

E. Test for tannins: Ferric chloride test

A few drops of 10 % ferric chloride ($FeCl_3$) solution were added to 2 mL of the aqueous solution of the plant leaf extract. The occurrence of blackish blue color showed the presence of tannins (Auwal *et al.,* 2014).

F. Test for Phenols

1 mL of the plant leaf extract was taken in a test tube and treated with a few drops of 2 % of $FeCl_3$. The observation of bluish green or black coloration indicated the presence of phenols (Vaishnav *et al*., 2017).

G. Test for Phlobatannins

2 mL of the plant leaf extract was added to 2 mL of 1 % HCl and then the mixture was boiled. Greenish yellow precipitate was formed which showed no presence of phlobatannins (Auwal *et al.,* 2014).

3.3.4. Synthesis of Zinc Oxide NPs using *H. abyssinica* Leaf Extract

For comparison of antibacterial activity of ZnO NPs with ZnO-bentonite NCs, ZnO NPs were synthesized using different ratios of leaf extract and $Zn(CH_3COO)_2{\cdot}2H_2O$ by adopting the procedure of upadhyaya *et al*. with slight modifications (upadhyaya *et al*., 2018). A 0.2 M aqueous solution of $Zn(CH_3COO)_2{\cdot}2H_2O$ was prepared by dissolving 11 g of the $Zn(CH_3COO)_2{\cdot}2H_2O$ in distilled water. Different volume of leaf extract (0, 10, 20, 30, 50 and 100 mL) was added to 100 mL of 0.2M $Zn(CH_3COO)_2{\cdot}2H_2O$ solution in ratios of 0:100, 1:10, 1:5, 3:10, 1:2 and 1:1 slowly under continuous stirring at 60 ˚C for 2 h on a magnetic stirrer heater until a white, light white, pale white and light yellow precipitate was formed. The solution pH was adjusted to pH 12 by drop wise addition of 1 M NaOH. The precipitate was centrifuged at 5,000 rpm for 5 min followed by washing with copious amounts of distilled water and ethanol to remove any impurities and then collected in a ceramic crucible. The precipitate was further oven dried at 50 ˚C for 6 h. The dried sample was ground by mortar and pestle to obtain a fine powder. The ZnO powder was calcined at 450 ˚C (brightened in color) carefully packed in plastic sample holder till required for characterization. The reaction mechanism proposed for the formation of ZnO NPs is given below (Sasikala *et al*., 2019):

$$Zn(CH_3COO)_2{\cdot}2H_2O + HOH/Ar\text{-}OH \longrightarrow Zn^{2+} + HOOCCH_3/CH_3CO\text{-}O\text{-}Ar \qquad \text{Eq. (8)}$$

$$Zn^{2+} + HOH/OH^- \longrightarrow [Zn(OH)_2]\,(aq) \qquad \text{Eq. (9)}$$

$$Zn\text{-}OH + Zn(CH_3COO)_2{\cdot}2H_2O + NaOH \longrightarrow Zn\text{-}O\text{-}Zn + 2CH_3COONa \quad \text{Eq. (10)}$$

$$ZnO\ /Zn\ (OH)_2 \xrightarrow[\Delta]{60\ ^\circ C,\ pH\ 12} ZnO\ NPs \quad \text{Eq. (11)}$$

Where, Ar is Aromatic compound containing alcohol functional group. Figure 5 shows the process of bio-synthesis of ZnO NPs using *H.abyssinica* leaves powder.

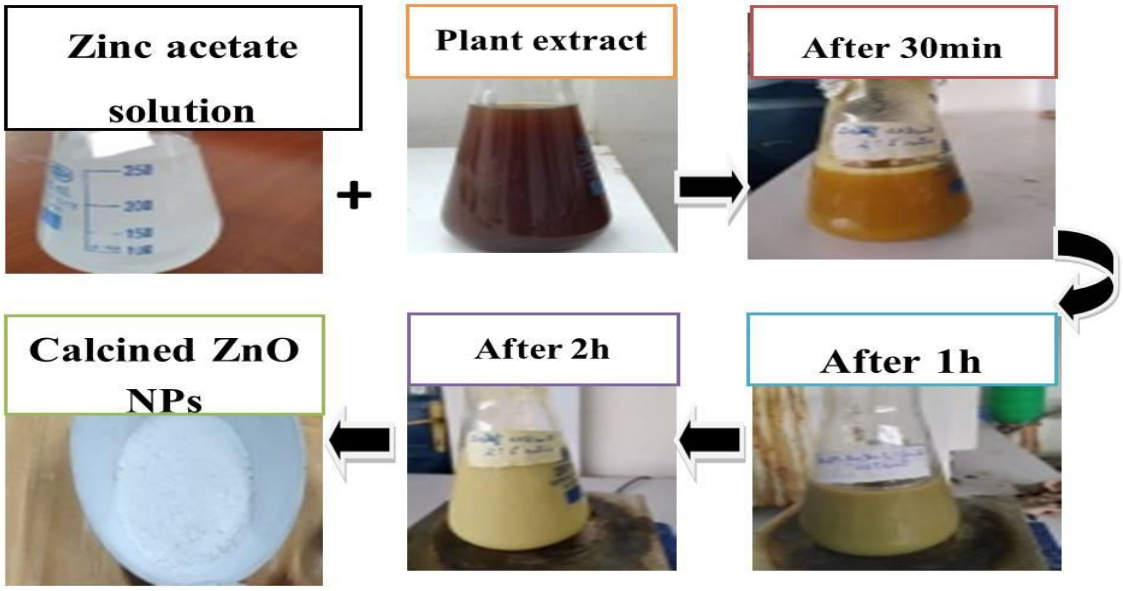

Figure 5: Change in the colour observed during ZnO NPs synthesis.

3.3.5. Synthesis of Bentonite Nanoclay

3.3.5.1. Purification of Bentonite

The collected natural bentonite was dried at room temperature for one week and crushed to particle size 125 µm using a ball mill at 350 rpm. To remove quartz, carbonates, calcites, and iron hydroxide ($Fe(OH)_2$); 100 g of the ground bentonite was dispersed in 1 L distilled water at room temperature and stirred for 1 h. The suspension was allowed to stand for 24 h to settle the impurities. The clear supernatant was decanted and the solid sample was separated from the suspension and centrifuged at 3000 rpm for 20 min to obtain the bentonite. This process was repeated four times, in order to guarantee obtaining samples in a pure form. The bentonite clay was dried in an oven at 60 ˚C for 12 h, then ground using ball mill and sieved using a 63 µm mesh sieve, and stored in tightly closed plastic bottles till required for the further experiments (Gong *et al*., 2016).

3.3.5.2. Activation of Bentonite by Sodium Carbonate

Activation of bentonite by sodium carbonate was conducted by using the procedure detailed by Shah *et al*. with slight modification (Shah *et al*., 2013). A 100 g of purified bentonite powder was dispersed into 1 L boiled distilled water to form a suspension. Then, 5 g of Na_2CO_3 was added to the suspension to obtain a stable aqueous dispersion. The suspension was stirred slowly with a magnetic stirrer and boiled for 1h. After activation, the suspension was allowed to cool to room temperature and diluted with 1 L distilled water. The diluted suspension was allowed to stand for 24 h to settle the impurities. The supernatant was decanted and the impurities settled at the bottom of the beaker were discarded. The bentonite suspension was centrifuged at 3000 rpm for 20 min and then dried in an oven at 60 ˚C for 12 h to obtain Na-exchanged bentonite ($Al_2H_2Na_2O_3Si_4$). The dried sample was then ground to obtain fine powder for further experiment.

3.3.5.3. Tests for Natural and activated bentonite Properties

A. Swelling power

The swelling capacity was determined according to the US Pharmacopeia method (Pharmacopeia, 2007). 2 g of non-activated and activated bentonite sample was added slowly to a 100 ml graduated cylinder containing 100 ml of distilled water and the apparent sediment volume was determined after 2 h by measuring sediment volume. The experiment was repeated three times.

B. Gel formation

The technique based on European pharmacopeia (Dardir *et al*., 2013) was used to measure the sedimentation volume or gel formation. 6 g of non-activated and activated bentonite sample were added to 200 mL distilled water and subsequently homogenized with a domestic high-speed mixer at 5,000 rpm. Then 100 mL of each suspension was added to a 100 mL graduated cylinder. The sedimentation volume was then measured by determining the clear supernatant volume after 24 h. The experiment was repeated three times.

C. pH measurement

Following the pharmacopoeia specifications for bentonite (US Pharmacopeia, 2007a), the pH values of non-activated and activated bentonite clay suspensions (4 g/ 200 mL) were measured in triplicate after 2 h continuous stirring (Oliveira *et al*., 2013).

D. Cation exchange capacity (CEC)

The determination of CEC was carried out according to the Standard Test Method for Methylene Blue Index of Clay, according to the ASTM C 837-81 (Higgs, 1988). 2 g of non-activated and activated bentonite clay were soaked separately in a 600 mL beaker containing 300 mL of distilled water and sufficient 0.1 M H_2SO_4 was added to bring the pH within the range of 2.5 to 3.8. After adjusting the pH, a burette was filled with methylene blue solution (0.028 N) and 5 mL of the solution was added to the suspension, and stirred for 2 min. Following this, a drop of slurry was placed on the edge of a filter paper. A 2 mL increment of methylene blue solution was added to the suspension with 2 min of stirring after each addition, and a drop added on a filter paper. The end point was indicated by the formation of a light blue halo around the drop.

3.3.6. Bio-synthesis of Zinc Oxide-Bentonite Nanocomposites using *H. abyssinica* Aqueous Leaves Extract

ZnO-bentonite NCs were synthesized using different mass of $Zn(CH_3COO)_2{\cdot}2H_2O$ to bentonite ratios by adopting the procedure of Honarmand *et al*. with slight modifications (Honarmand *et al.*, 2020).

Table 3: The effect of $Zn(CH_3COO)_2.2H_2O$ to bentonite ratio in bio-synthesis of ZnO-Bentonite NCs.

ZnO-bentonite NCs code	Mass of $Zn(CH_3COO)_2.2H_2O$ (g)	Volume of solvent (DW:DMSO: ethanol) (mL)	Volume of Plant extract (mL)	Mass of bentonite (g)
ZnO-bentonite NCs(2:1)-ZB1	4.4	50:25:25	100	2.2
ZnO-bentonite NCs(1:1)-ZB2	2.2	50:25:25	100	2.2
ZnO-bentonite NCs(1:2)-ZB3	1.1	50:25:25	100	2.2

100 mL of $Zn(CH_3COO)_2{\cdot}2H_2O$ solutions (0.2 M, 0.1 M and 0.05 M) and 2.2 g of solid Na-bentonite were mixed together separately in 1000 mL beakers. 100 mL aqueous extract of *H. abyssinica* was added drop wise under vigorous stirring on magnetic stirrer for 30 min at room temperature. During this time, the colour of the contents of the flasks changed from white(creamy) to dark brown. After 30 min, the mixtures were transferred to a heated

oil bath and stirring continued at 80 ˚C for a further 30 min at pH 12 adjusted by addition of 1 M NaOH solution. The rust like colour (dark brown) precipitate formed was then centrifuged at 5000 rpm for 5 min followed by washing with double distilled water three times. The samples were dried at room temperature for five days, calcined at 550 ˚C and stored in glass bottle till required. Figure 6 shows the process of bio-synthesis of ZnO-benonite nanocmposites using *H.abyssinica* leaves powder.

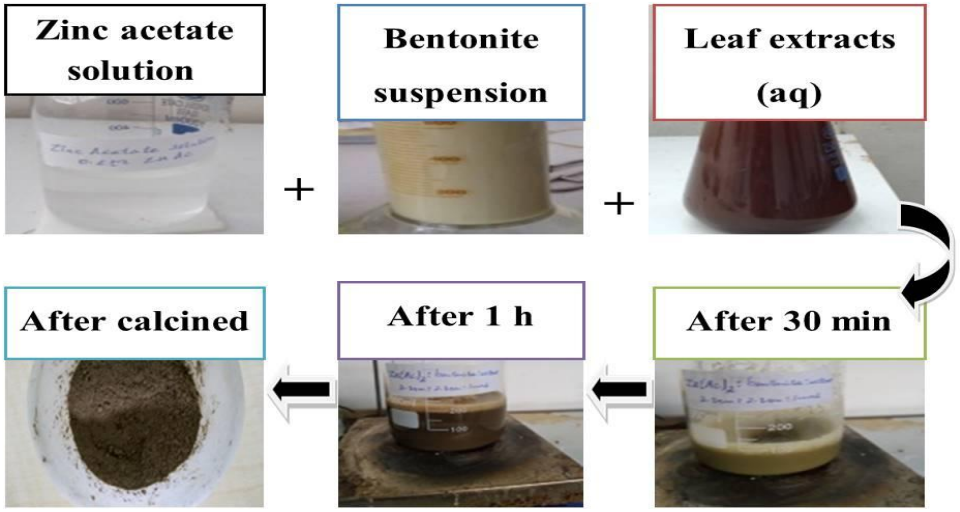

Figure 6: Basic steps in the synthesis of ZnO-benonite nanocmposites.

3.3.7. Characterization Techniques

A. Thermal Analysis (TGA/DTA)

Thermal analysis was conducted to evaluate the thermal stability of ZnO NPs, bentonite nanoclay and ZnO-bentonite NCs by using a TGA (model DTA-60H, Shimadzu Co., Japan). 11.902 mg of ZnO NPs, 15.946 mg bentonite and 13.88 mg ZnO-bentonite NCs sample were analysed under 50 [ºC/ min] nitrogen flow rate with a heating rate of 10 ºC at the temperature range of 23-1000 ºC.

B. X-RAY Diffraction (XRD)

Crystalline structure and the average crystalline size of the synthesized ZnO NPs, bentonite nanoclay and ZnO-bentonite NCs were characterized using an X-ray diffractometer (XRD-700, Shimadzu Co., Japan) equipped with a Cu target for generating a Cu Kα radiation with λ = 1.54056 Å XRD spectra were recorded from 10 ° to 80 ° for ZnO NPs and 0 ° to 80 ° for bentonite and ZnO-bentonite NCs with 2θ angles using Cu Kα radiation operated

at 40 kv and 30 mA in continuous scan mode with scan rate 3 (deg/ min). The crystallite sizes (D) of the powders were calculated by using Scherrer's equation:

$$D = \frac{0.089\lambda}{\beta \cos\theta} \quad \text{Eq. (12)}$$

Where $K = 0.94$ is Scherrer's constant, λ is the X-ray wavelength, θ is Bragg's diffraction angle, and β is the Full width at half maximum (FWHM) of the diffraction line at half of the maximum intensity.

C. UV-visible Spectroscopy (UV–Vis)

The optical properties of the ZnO NPs, bentonite nano-clay and ZnO-bentonite NCs were determined by UV–Vis spectroscopy (SM-1600 Dual beam UV-VIS Spectrometer, Azzota Corp., USA). The 0.01 g samples powder was re-suspended in 15 mL de-ionized water to note the UV- Visible spectra. The absorbance of samples was recorded in the wavelength range: 200 nm to 800 nm and their maximum absorbance was recorded. Base line correction of the spectrophotometer was carried out by using a blank reference. The UV-Vis absorption spectra of the samples were recorded.

D. Diffuse Reflectance Spectroscopy (DRS)

Absorption spectra and band gab of ZnO NPs and ZnO-bentonite NCs were measured by a UV-Vis diffusive reflectance spectrophotometer (UV-Vis-NIR Spectrophotometer, UV-3600plus, Shimadzu, Japan), in the wavelength range of 200-1000 nm.

E. Bentonite Analysis

The pristine bentonite and bentonite nanoclay samples were characterized by using AAS to determine their chemical composition. For complete silicate analysis of both samples 0.1 gram of each was added separately to 1.5 g of lithium boron oxide ($LiBO_2$) and the mixtures was heated in a furnace for 45 min at 950 °C. After they were cooled overnight, the mixtures were stirred by a magnetic stirrer, washed and transferred to round bottom flasks with addition of lanthanum chloride ($LaCl_3$). The prepared solutions were used to determine metals like Ca, K, Al, K, Mg, Fe, Na, etc. The amount of silica was determined by taking 0.1 g each samples, 3 mL of HCl and 2 mL of boric acid directly read by the instrument and the amount of TiO_2 and P_2O_5 was determined by UV-Vis spectrophotometer.

F. Scanning Electron Microscopy (SEM) analysis

The morphological features of the ZnO NPs, activated bentonite and ZnO-bentonite NCs were determined by using scanning electron Microscopy (model JEOL JCM-6000plus, Japan), using electron beam energy of 15 Kv and magnification of 1000. Powdered samples were mounted on a sample holder followed by coating with a smart coater (gold) and scanned. The surface characteristics of the samples were obtained from the secondary electrons emitted from the sample surface.

G. Fourier Transforms Infrared Spectroscopy (FTIR) analysis

The functional groups present in dried powders of *H. abyssinica* crude extract, ZnO NPs, bentonite clay and ZnO-bentonite NCs were analysed by a FTIR (Perkin Elmer, Spectrum 65 FTIR, and USA). The spectra were acquired in the range 4000-400 cm^{-1} using KBr disc.

3.3.8. Antibacterial Assay

Qualitative antimicrobial assay of the synthesized *H. abyssinica* crude extract powder, ZnO NPs, bentonite nano-clay and ZnO-bentonite NCs were carried out against two bacterial strains; gram-negative *E. coli* and gram positive *S. aureus* bacteria in the Microbiology laboratory of ASTU by the disc diffusion method according to the procedure detailed by Bauer *et al*. with slight modification (Bauer *et al*., 1966). In this test, first of all bacterial strains were grown aerobically in Muller-Hinton agar nutrient broth for 24 h at 37 ˚C until the concentration of bacterial suspensions was achieved to1.5×10^8 CFU mL^{-1} by comparison with the 0.5 McFarland Standard. Bacterial cultures were maintained on nutrient Muller-Hinton agar at 37 ˚C, the antibiotic Ceftriaxone was used as the positive control, and DMSO solvent was used as the negative control. 100 µL of 24 h standardized culture of test bacteria was first evenly spread onto the surface of the Muller-Hinton agar plates using sterile cotton swabs. The plates were then turned upside down and incubated at 37 ˚C for 24 h in an incubator. 200 mg of prepared samples were dissolved in 1mL of DMSO. From 200 mg/ mL concentration of each sample, 150, 100 and 50 mg/ mL were diluted. 6 mm diameter disc were saturated with each concentration and 30 mg/ mL of Ceftriaxone (positive control) and placed on a plate covered with lids and incubated at 37°C for 24 h. Antibacterial activity was then evaluated by measuring the diameter (mm) of the inhibition zone around the disc against the test organisms using a capillary.

CHAPTER FOUR

4. RESULTS AND DISCUSSION

4.1. Phytochemical Screening of *Hagenia abyssinica* Plant Aqueous Leaf Extract Results.

H. abyssinica plant extracts were rich in different phytochemicals (table 4) with different functional group such as OH^-, $-COO^-$, -CHO, etc. which acts as a capping agent.

Table 4: Phytochemical screening of the *H. abyssinica* plant leaves aqueous extracts.

Serial No.	Phytochemical assessment	Observation	Result
1	Saponins	Soap like foam	+
2	Tannins	Brownish green	+
3	Flavonoids	Yellow color	+
4	Terpenoids	Yellow color	+
5	Alkaloids	Reddish brown color	+
6	Phenols	Bluish green	+
7	Phlobatannins	Greenish yellow	_

In the present study the qualitative analysis of *H. abyssinica* aqueous leaves extracts were carried out for aqueous solution of plant samples. Saponins, tannins, alkaloids, flavonoids, terpenoids and phenolic compounds were revealed to be present in extracts of *Hagenia abyssinica* which are known to have antimicrobial activity (Table 12). Most of the phytochemicals from plant sources such as phenolic and flavonoids have been reported to have high content associated with their antioxidant activities and antibacterial that play a role in the prevention of the development of bacterial disease, particularly cause by oxidative stress (Oloyed, 2005).

Wolde *et al*., report on preliminary screening for phytochemicals in the plant extracts revealed presence of terpenoids, phenolic, Saponins, tannins, alkaloids and flavonoids which could confer antibiotic property on the plant. Therefore, the phytochemical screening result reveals that the presence of these phytochemical constituents supports the use of *H. abyssinica* plant in folklore medications and it is probable that these phytochemicals are responsible for the healing properties of these plants which have been claimed by the peoples in the area of this study.

These phytochemicals species also plays a critical role in nanoparticles synthesis to prevent agglomeration. XRD result showed that increasing the volume of plant extract cause the formation of small particle size nanoparticles.

4.2. Thermal Analysis (TGA/DTA)

The thermal analysis of synthesized sample was investigated with TGA/ DTA analytical instrument. The uncalcined ZnO NPs, bentonite clay and ZnO-bentonite NCs TGA analysis was measured from room temperature to 1000 ˚C at the heating rate of 10 ˚C/ min. TGA curve shows mass loss of the sample, whereas the DTA curve indicates the energy gain or loss during the process.

A. TGA of ZnO NPs

Figure 7 (a) shows the TGA/DTA result of bio-synthesized ZnO NPs. TGA curves showed three transition states occurred at 62.73 ˚C, 170.83 °C and 450 °C temperature. At these temperature, ZnO NPs losses -0.23 mg (-1.932 %), -0.45 mg (-3.78%) and -1.44 mg (-12.098 %) due to dehydration of adsorbed water and decomposition of organic binder from $Zn(OH)_2$. TGA showed a -1.44 mg (-12.098 %) weight loss of ZnO sample. The corresponding DTA curve showed two endothermic peaks at 59.17 ^oC and 188.84 ^oC temperatures. DTA curve also showed two exothermic peaks at 332.46 ^oC and 873.84 ^oC due to sample decomposition of $Zn(OH)_2$ to form ZnO and organic binders. The exothermic peak observed at 873.84°C on the DTA curve might be due to the phase transition to form stable ZnO NPs, and no considerable loss in mass is observed after 450°C temperature up to 1000 °C. This indicates that the biosynthesized ZnO NPs are thermally stable after 450 ˚C; so could calcined at this temperature. Similar result was reported by (Demissie et al., 2020).

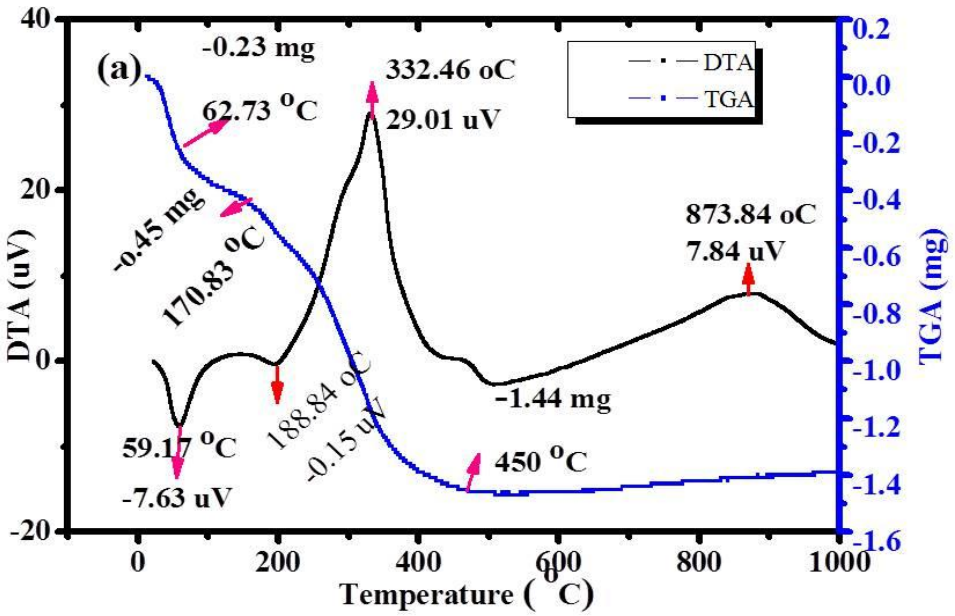

Figure 7: Thermal analysis of synthesized ZnO NPs (1:2)

B. TGA Result of Purified Bentonite

TGA/DTA transition curve for purified bentonite clay in figure 8 (b) shows a loss of weights at 95.42 °C (-0.7 mg, 4.389 %), 412.98 °C (-1.5 mg, 9.406 %) and 650 °C (-1.89 mg ,11.852 %) in the temperature range of RT-650 ˚C. A significant weight loss is observed in the clays in the range between 100 and 650 °C, which can be attributed to the de-hydroxylation of the clay minerals present in the purified bentonite and sample decomposition. The sample also gained -15.61 uV and 10.9 uV of energy at the temperature of 81.33 ˚C and 536.52 °C respectively during sample decomposition up to 650 ˚C. The presence of double endothermic peaks up to 536.52 °C is related to the presence of coordinated water to Ca^{2+} and Mg^{2+}. No considerable loss in mass is observed after 650 ˚C temperatures up to 1000 ˚C. According to the result presented in figure10 (b), this material showed a weight loss of 1.890 mg (11.852 %).

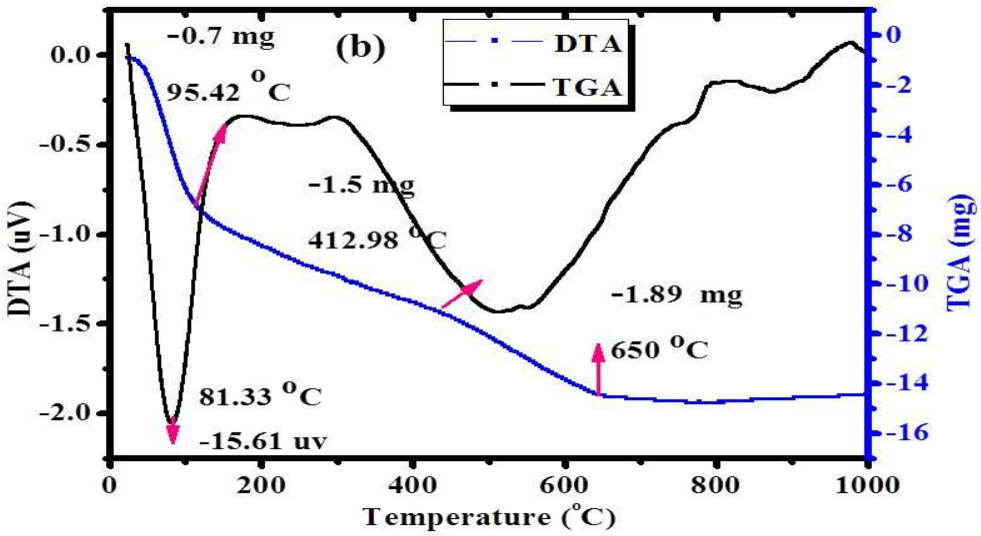

Figure 8: Thermal analysis of purified bentonite clay.

C. TGA Result of ZnO-Bentonite NCs

Figure 9 shows typical TG-DTA curves of the biosynthesized ZnO-bentonite NCs. ZnO-bentonite NCs losses a weight of 4.2170 mg (30.38 %) in the temperature range of 23-450, and very small mass loss 0.279 mg (2 %) in the temperature range of 450- 550 with nearly a constant plateau. Hence, annealing at 550 ºC seems to guarantee the formation of stable ZnO-bentonite NCs. Stability of ZnO-bentonite NCs at this temperature confirm that the sample could not loss mass above this temperature. The first two stages of weight loss occurs at temperatures below 23 ºC, which indicates the separation and vaporization of the surface water and might be attributed to the loss of volatile surfactant molecules adsorbed on the surface of zinc based complexes during synthesis. Whereas the third stage of weight loss takes place from decomposition of organic materials. The DTA curves of ZnO-bentonite NCs shows the presence of endothermic peaks recorded at 73.12, and 193.35°C that might be due to dehydration of adsorbed water and decomposition of organic binder from the composites and another exothermic peak was observed at 369.85 due to sample decomposition.

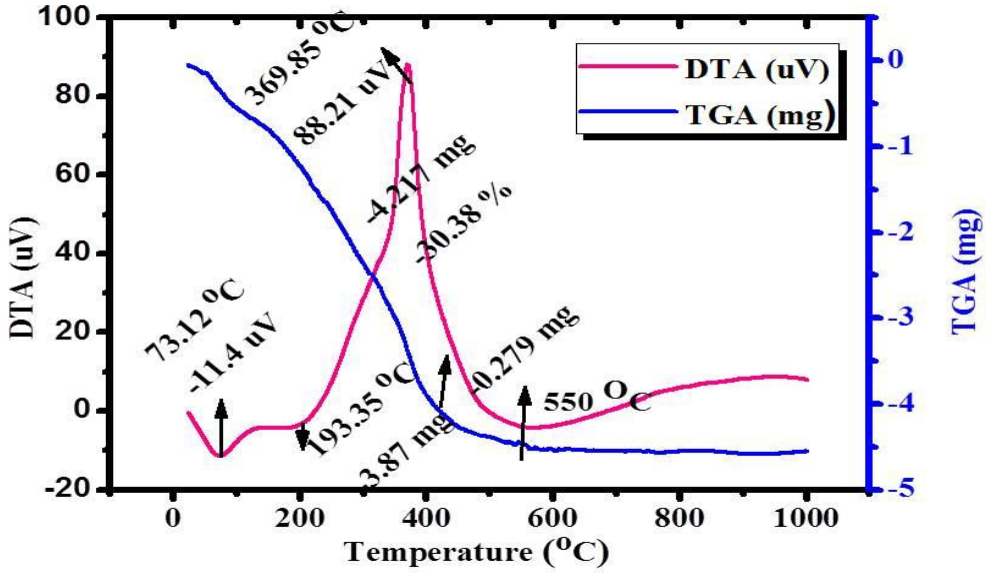

Figure 9: TGA/DTA spectra of ZnO-bentonite nanocomposites (1:1).

4.3. XRD Results

A. XRD Results of ZnO NPs

Figure 10 shows the XRD spectra of the calcined and uncalcined ZnO NPs synthesized by using various ratios (0:100, 1:1, 1:2) of plant leaf extracts to precursor. The XRD pattern of nanostructure of ZnO shows that the diffraction peaks at around the angles 31.82 °, 34.46 °, 36.3 °, 47.62 °, 56.64 °, 62.9 °, 68 ° and 69.18 ° which corresponds to the crystal planes of (100), (002), (101), (102), (110), (103), (112) and (201) in the wurtzite structure showed similarity to that obtained by Salam *et al*. using *Ocimum basilicum L.var. purpurascens* extract (Salam *et al*., 2014). All the peaks observed were coordinated with the hexagonal phase (wurtzite structure) in comparison with the data from JCPDS card No. 36-1451.

Similar XRD results are also checked in the Chemingui *et al*. report for ZnO NPs Chemingui *et al*., 2019). All XRD profiles exhibit 8 distinguishable Bragg diffractions are noticed in accordance with zincite phase of ZnO.

Table 5: The XRD data for synthesized ZnO NPs**.**

ZnO NPs	Peaks position(degree)	Miller indices	Peaks intensity (%)	(FWHM)	Width
Calc. ZnO(1:1) -ZOA	31.806	(100)	38.89	0.4095	2.811
	34.457	(002)	37.74	0.3273	2.600
	36.281	(101)	67.29	0.4152	2.511
Uncalc. ZnO(1:1)-ZOB	31.827	(100)	20.7	0.4382	2.809
	34.503	(102)	22.52	0.3189	2.697
	36.327	(101)	35.66	0.4128	2.570
Calc. ZnO(1:2) -ZOC	31.902	(100)	40.31	0.3963	2.803
	34.546	(002)	40.63	0.298	2.694
	36.373	(101)	70.24	0.3947	2.567
Calc. ZnO(0:100)-ZOD	31.827	(100)	60.7	0.2987	2.809
	34.479	(002)	50.56	0.2660	2.699
	36.309	(101)	100	0.3073	2.572

A definite line broadening of the XRD peaks indicates that the prepared material consist of particles in nanoscale range and the narrow and strong diffraction peaks indicate the well crystalline nature of ZnO. The obtained 2θ and Miller indices (hkl) values have been keenly indexed as hexagonal wurtzite phase of ZnO with lattice constants around $a = b = 0.325$nm, $c = 0.521$nm, c/a=1.61 and space group of C_{6v}^4 or $P6_3mc$ (JPCDS card number: 36-1451) (Demissie *et al*., 2020). It also confirms the synthesized nanopowder was free of impurities as it does not contain any characteristics XRD peaks other than ZnO peaks. The crystal structure of ZnO belonging to space group *P63mc* was characterized by the interconnection of two sub-lattices made of Zn^{+2} and O^{-2} in such a way that each Zn^{+2} ions is surrounded by four O^{-2} ions and vice-versa. By using the corresponding reticular plane distance's relation $d_{hkl}= (4/3(h^2+ hk + k^2)/a^2+ l^2/c^2)^{-1/2}$, the average values of the lattice parameters a_{exp} and c_{ap} have been derived.

The average values of Lattices parameters of ZnO NPs were calculated by using two major peaks. Lattice constants *a* and *c* of hexagonal wurtzite phase of ZnO NPs can be calculated from (100) and (101) planes; where

$$a=2\sqrt{\frac{d_{100}^2}{3}} \qquad \text{Eq. (13)}$$

$$\frac{1}{d_{101}^2} = \frac{4}{3a^2}(h^2 + hk + k^2) + \frac{l^2}{c^2} \qquad \text{Eq. (14)}$$

For ZnO(0:100); $\frac{1}{d_{100}^2} = \frac{4}{3a^2}(h^2 + hk + k^2) + \frac{l^2}{c^2} \Rightarrow a$=0.3243nm and c (101) = 0.521nm

For ZnO (1:1); $\frac{1}{d_{100}^2} = \frac{4}{3a^2}(h^2 + hk + k^2) + \frac{l^2}{c^2} \Rightarrow a$ = 0.325nm and c (101) = 0.5189nm

For uncalcined ZnO (1:1); a (100) = 0.324nm and c (101) = 0.586nm

For ZnO (1:2); $\frac{1}{d_{100}^2} = \frac{4}{3a^2}(h^2 + hk + k^2) + \frac{l^2}{c^2} \Rightarrow a$ = 0.324nm and c (101) = 0.5187nm.

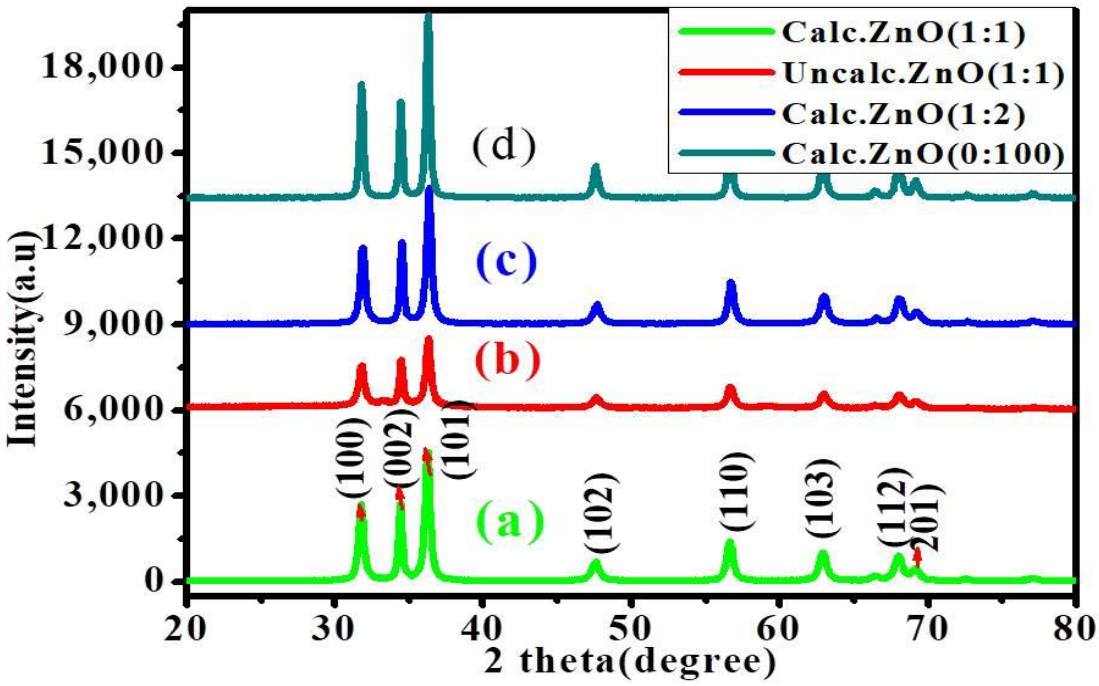

Figure 10: XRD result of calcined (a) and Uncalcined (b) ZnO(1:1), Calcined ZnO(1:2)(c) and ZnO (0:100)(d).

The average diameter of crystallites (D) is calculated by using Debye-Scherer equation.

The average particle size of the calcined and uncalcined ZnO (1:1), calcined ZnO (1:2) and ZnO (0:100) was found to be 21.67nm, 21.5nm, 23.07nm and 28.4nm which was derived from the FWHM of more intense peak corresponding to 100, 102 and 101 using Scherrer's formula. The difference in sizes could be due to the effect of the volume of plant extract on

ZnO NPs. This result confirms that the uncapped nanomaterial has a larger particle size than the capped one and as concentration of plant leaf extract decrease particle size increase. This was due to the fact that the greater amount of the plant extract used during the synthesis process results in effective capping and stabilizing the synthesized nanoparticles and hindered from aggregation. Therefore, the crystallinity of ZnO prepared using high volume of plant extract is better.

Table 10 also shows that the average crystal size of uncalcined ZnO NPs synthesized by using 1:1 ratios by volume of precursor salt and plant extract was less than their corresponding calcined ZnO NPs. This may also be due to the high concentrations of bio-molecules from plants that remain in the uncalcined NPs that could highly stabilize the nanoparticles by capping and hinders further crystal growth. This study is clearly agree with previous report (Demissie *et al*., 2020).

The XRD results clearly suggest that there was a systematic increase in peak intensity and peak width (FWHM) for calcined ZnO NPs than uncalcined one. In addition the peak intensity and peak width for ZnO (1:1) NPs was decrease and increase in ZnO (1:2).

The inter-planar d-spacing of ZnO NPs were calculated from their major peaks by using Bragg's Law equation;

$$2d \sin \theta = n\lambda \qquad \text{Eq. (15)}$$

Where, θ is Bragg's angle of diffraction, λ is X-ray wavelength, i.e. 1.5406Å and n= 1.

Dislocation is a crystallographic defect or irregularity, within a crystal structure. The presence of dislocations strongly influences many of the properties of materials. Where dislocation densities are calculated using the formula:

$$\delta = {}^{1}/_{D^2} \qquad \text{Eq. (16)}$$

Where D is the crystallite size, δ is the dislocation density and ε is micro-strain;

$$\varepsilon = {}^{\beta}/_{4\tan\theta} \qquad \text{Eq. (17)}$$

It is observed from table 6 dislocation density is indirectly proportional to particle size. Dislocation density increases while particle size decreases. This might be due the increase of surface area of nanoparticle. As the surface area of nanoparticles increase the probability of missing few ions in a layer might be increase (Suresh *et al*., 2015).

The strain effect in the crystal lattice at the nanoscale has been explained by the high surface energy of the nanoparticles. This assumption takes into account that materials at the nanoscale possess a large fraction of under-coordinated surface atoms presenting a bond order deficiency compared to their bulk equivalent form. This effect induces the compression of the lattice parameters and unit cell, increasing the internal pressure as the particle size decreases (Andrade *et al*., 2017).The micro-strain of the crystal lattice decrease with increasing particle size. The increasing of crystallite size and decreasing of micro-strain leads to the growth of particle size and increasing of the ZnO lattice parameter. The high strain in the crystal lattice may lead to lattice contraction in order to relieve the strain.

Table 6: Average particle size, inter-planar d-spacing, dislocation density and micro-strain for the major peaks of ZnO NPs**.**

Sample	Peak 2θ(°)	d(Å)	β(rad)	D(nm)	Average	$\delta(*10^{-5})$	$\varepsilon(*10^{-3})$
Calc. ZnO-1:1	31.806	2.81	0.007144	19.96	21.67nm	213	16
	34.457	2.6	0.00571	25.14			
	36.281	2.47	0.007243	19.92			
Uncalc. ZnO-1:1	31.827	2.81	0.007644	18.6	21.5 nm	216	17
	34.503	2.59	0.005563	25.2			
	36.327	2.47	0.007201	20.7			
Calc. ZnO-1:2	31.902	2.80	0.006913	20.63	23.07nm	188	15
	34.546	2.59	0.005198	27.62			
	36.373	2.47	0.006885	20.96			
	31.827	2.81	0.005211	27.36	28.4nm	124	13
Calc. ZnO 0:100	34.479	2.59	0.00464	30.94			
	36.309	2.47	0.005361	26.9			

B. XRD Results of Purified and Activated Bentonite

The characterization of the clay samples by XRD aimed to verify the existence of associated minerals and clay minerals. Figure 11 presents the x-ray diffraction results of the purified and activated bentonite clay which shows the diffraction peaks at around the

angles 15.8 º, 19.66 º, 26.04 º, 30.62 º, 34.78 º, and 61.4 ° which corresponds to the crystal planes of (211), (220), (0 0 4), (332), (431), and (842) as majority phases. The diffraction angle 2θ of purified bentonite was 8.44 ˚ with their corresponding inter planar distance of 10.1557 Å. While the diffraction angle 2θ of activated bentonite was 8.72 º and inter planar distance of 10.468 Å, where inter-planar distance calculated according to Bragg equation: $2d\sin\theta = \lambda$. The inter-planar distance of purified bentonite was smaller than activated bentonite. This indicated that the when Ca^{2+} ions of large atomic radius were replaced by Na^{+} ions of less atomic size, inter-planner distance increase due to the hydration energy of Na^{+} ion is larger than Ca^{2+}. Similarly, Meshram *et al*. reported d-spacing of natural bentonite is 1.87, while it increases to 1.98 nm when bentonite nanoclay is formed (Meshram *et al.* 2011). In the XRD patterns of the bentonite clays obtained in this study, the presence of quartz and kaolinite as impurities were also observed. Similar XRD results were obtained by Oliveira *et al*. when they performed the characterization of bentonite clays from Cubati, Paraíba (Northeast of Brazil) (Oliveira *et al*., 2016).

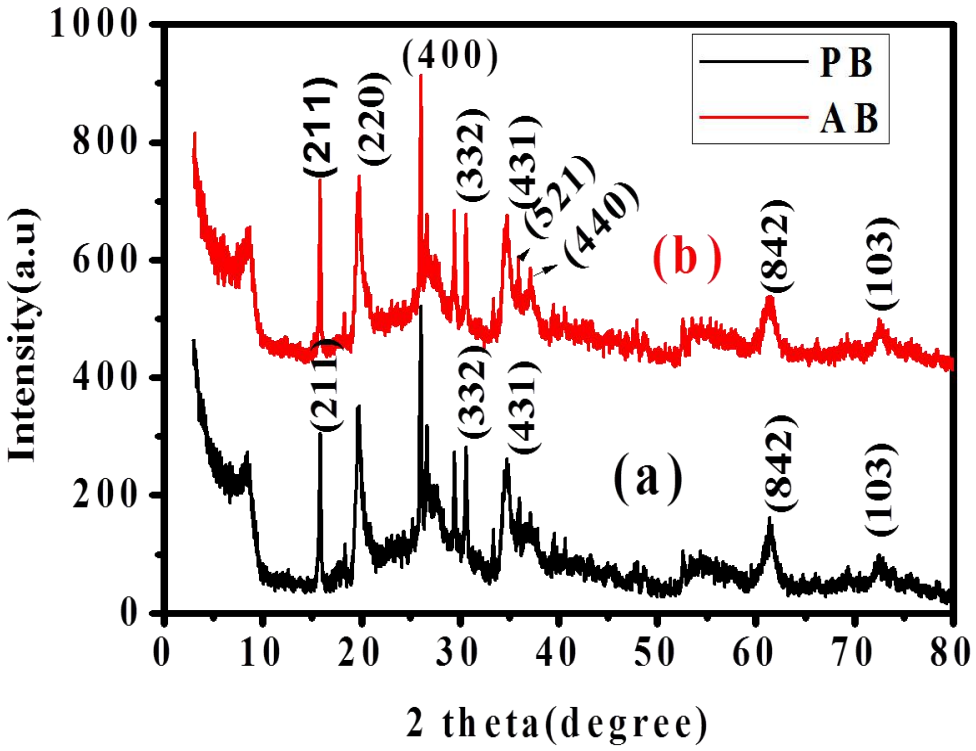

Figure 11: XRD result of purified bentonite (PB) (a) and activated bentonite (AB) (b).

In the clay composition, the characteristic peaks of montmorillonite (M), gypsum (G), kaolonite (K), and quartz (Q) were presented in table 8.

Table 7: XRD results of purified and activated bentonite.

Purified bentonite				Activated Bentonite			
2θ	Miller index	d (Å)	Reflection	2θ	Intensity	d (Å)	Reflection
8.44		10.20	MMT (M)	8.7		10.44	MMT (M)
15.86	(211)	5.5	Kaolinite (K)	15.8	(211)	5.6	Kaolinite (K)
19.76	(220)	4.4	MMT (M)	19.78	(220)	4.5	MMT (M)
26.04	(400)	3.42	Kaolinite (K)	26.02	(400)	3.45	Kaolinite (K)
29.42	(330)	3.04	Quartz (Q)	29.42	(330)	3.06	Quartz (Q)
30.62	(332)	2.9	Gypsum (G)	30.6	(332)	2.95	Gypsum (G)
34.78	(431)	2.5	kaolonite (K)	34.74	(431)	2.59	Kaolonite (K)
36.04	(521)	2.5	Quartz (Q)	35.92	(521)	2.498	Quartz (Q)
37.2	(440)	2.46	MMT (M)	36.3	(440)	2.477	MMT (M)
61.4	(842)	1.52	MMT (M)	61.26	(842)	1.55	MMT (M)

Activation of bentonite by Na_2CO_3 clearly causes a decrease in peak intensity which demonstrates that changes have occurred in their mineral composition. Also, the quartz content, which is seen as an impurity, decreased. As observed from table 7 the increase d-spacing of montmorillonite of activated bentonite than purified bentonite clay indicate that swelling property enhanced after activation. Shah *et al.* suggested that the Na^+ ions replaced Ca^{2+} ions in the montmorillonite interlayer and cause the increase in swelling properties of activated bentonite (Shah *et al*., 2013). The reduction in intensity indicate that the crystallinity of the montmorillonite considerably affected by activation. The change in MMT composition is significant; because high content of MMT in bentonite clay enhance the rheological properties of clay.

C. XRD Results of ZnO-bentonite NCs

Figure 12 illustrates the XRD patterns of activated bentonite and Zn^{2+}-exchanged bentonite. Figure 14a shows the XRD patterns of activated bentonite diffraction peaks located at $2\theta\sim$ 8.6 °, 15.8 °, , 20.08 °, 26.04 °, 29.42 °, 30.68 °, 34.74 ° which corresponds to (001), (211), (220), (400), (330), (332), (431) planes and peaks near 26.02 ^{0} are due to the silicate unit. As shown in figure 14(b, c and d), after the immobilization of ZnO NPs on bentonite, ZnO NPs characteristics peaks are observed at $2\theta\sim$ 31.76 °, 34.42 °, 36.24 °, 47.56 °, 56.62 °, 62.84 °, 67.88 °, which corresponds to (100), (002), (101), (102), (110), (103), (112) planes and bentonite characteristics peaks are observed at $2\theta\sim$ 8.6 °, 15.8 °, , 20.08 °, 26.04 °, 29.42 °, 30.68 °.

As observed from XRD spectra (figure 12), the synthesized ZnO-benonite NCs were composed of ZnO and bentonite phase. In XRD peaks of ZnO-bentonite, bentonite characteristics peaks intensity is weaker than that of pure bentonite. The ZnO NPs characteristics peaks present in ZnO-bentonite NCs decrease as the concentration of ZnO precursor decrease. Hence, the ZnO characteristics peak intensity present in ZnO-bentonite NCs is decrease from ZnO-bentonite NCs (2:1) followed by ZnO-bentonite NCs (1:1) and ZnO-bentonite NCs (1:2). It's observed that the intensity of ZnO characteristic peaks in ZnO-bentonite NCs (1:2) is very weak, difficult to see. The widening of the peaks probably results from the ability of ZnO to bridge the neighbouring silicate units between the layers.

In XRD spectra of all ZnO-bentonite NCs, the left hand peaks (below 2θ of 30 °) are strongly shows the bentonite character and right hand peaks (above 2θ of 30 °) are strongly shows the ZnO character which are compressed as a result of ZnO bridged the neighbouring silicate units of bentonite. As reported by Meshram *et al*., after the modifications of natural bentonite due to chemical reactions, the peak of ZnO–bentonite NCs shifted towards to lower angle side when compared with natural-bentonite and the reflections due to ZnO were also seen at higher angle region (Meshram *et al*., 2011).

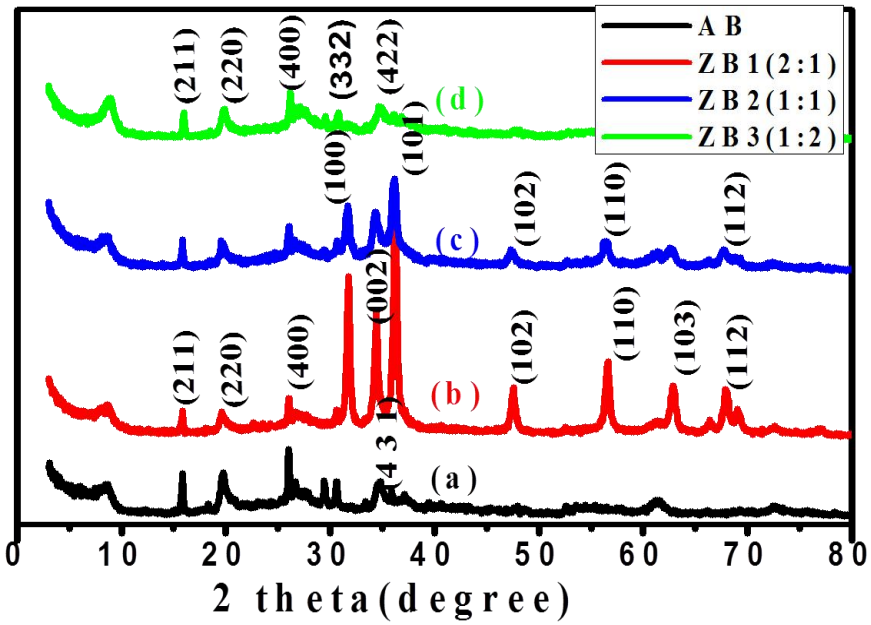

Figure 12: XRD analysis result of AB (a), ZnO-bentonite NCs (ZB1 (2:1) (b), ZB2 (1:1) (c) and ZB3 (1:2) (d)).

The X-ray diffraction patterns of Na-bentonite displayed a diffraction peak at the 2θ value of 8.55 °, 15.81 °, 19.76 °, 26.01 °, 29.41 °, 30.60 °, 34.76 °, 61.5 ° which correspond to basal spacing of 10.44, 5.6, 4.49, 3.43, 3.03, 2.92, 2.58 and 1.51Å respectively.

The X-ray diffraction patterns of ZB1 displayed a diffraction peak at the 2θ value of 8.73 °, 15.88 °, 19.75 °, 26.07 °, 31.76 °, 34.42 °, 36.24 °, 47.52 °, 56.55 ° , 62.83 ° , 67.92 ° which correspond to basal spacing of 10.12, 5.58, 4.49, 3.42, 2.82, 2.6, 2.48, 1.91, 1.62, 1.48, and 1.38 Å respectively.

The X-ray diffraction patterns of ZB2 displayed a diffraction peak at the 2θ value of 8.56 °, 15.88 °, 19.76 °, 26.07 °, 31.68 °, 34.42 °, 36.12 °, 47.38 °, 56.41 ° , 62.56 ° , 67.72 ° which correspond to basal spacing of 10.32, 5.57, 4.49, 3.42, 2.82, 2.6, 2.48, 1.91, 1.63, 1.48, 1.38 respectively. The basal spacing of the Na-bentonite was decreased after exchanged with Zn^{2+}, this might be due to the replacement of smaller ionic radius of Zn^{2+} (0.074 nm) with that of Na^{+} (0.095 nm) of larger ionic radius. In addition the bentonite characteristic peak at 2θ value of 30.60 °, 34.76 ° and 61.5 ° decreased in intensity, almost disappeared. It's clearly observed that the basal spacing of ZnO-bentonite NCs is decreased as the number of ZnO loaded on Na-bentonite increase. This might be due to large number of smaller ionic radius Zn^{2+} is replaces large number of bigger ionic radius Na^{+}.

In XRD patterns of figure 12(b, c), the 2θ and Miller indices (hkl) values obtained in between 30°-40° have been keenly indexed as hexagonal wurtzite phase of ZnO NPs with lattice constants around $a = b = 0.325$nm and $c = 0.521$nm and space group of *P*63*mc* (JPCDS card number: 36-1451) except ZB3 (1:2).

Lattice constants *a* and *c* of hexagonal wurtzite ZnO phase in ZnO-bentonite NCs can be calculated from (1 0 0) and (1 0 1) planes; where $a=2\sqrt{\frac{d_{100}^2}{3}}$ and *c* from formula.

For ZB1 (2:1); $\frac{1}{d_{100}^2} = \frac{4}{3a^2}(h^2 + hk + k^2) + \frac{l^2}{c^2} \Rightarrow a = 0.325$nm, c (101) = 0.521nm

For ZB2 (1:1); $\frac{1}{d_{100}^2} = \frac{4}{3a^2}(h^2 + hk + k^2) + \frac{l^2}{c^2} \Rightarrow a = 0.3258$nm, c (101) = 0.5243nm

In XRD patterns of figure 12(d), the 2θ and Miller indices (hkl) values obtained in between 30°°-40 ° have been keenly indexed as cubic phase of ZnO NPs with lattice constants around $a = c = 2.05$nm and space group of *Pm*3*m* (JPCDS card number: 25-1257). In ZnO-bentonite NCs of ZB3 (1:2) the ZnO phase has a cubic structure.

$$d_{hkl} = \frac{a}{\sqrt{(h+k+l)^2}} \qquad \text{Eq. (18)}$$

For ZB3 (1:2); $d_{422} = \frac{a}{\sqrt{(h+k+l)^2}} \Rightarrow a = 2.05$nm = c, cubic with *pm*3*m* space group

For ZB3 (1:2); $d_{332} = \frac{a}{\sqrt{(h+k+l)^2}} \Rightarrow a = 2.33$nm = c, cubic with *pm*3*m* space group

The 2θ and Miller indices (hkl) values obtained at below 30 °have been keenly indexed as bentonite phase and the ZnO characteristics peaks are shown above 35 ° with a very weak intensity dominated by bentonite peak. .

The average diameter of crystallites (D) is calculated by using Debye-Scherer equation.

Inter-planar d-spacing was also calculated using Bragg's Law equation (Table 9): $2d \sin\theta = n\lambda$, Where, θ is Bragg's angle of diffraction and n= 1.

Table 8: Average particle size and inter-planar d-spacing for the major peaks of ZnO-bentonite NCs and bentonite.

Sample	Peak 2θ	sin θ	d(Å)	cos θ	β(rad)	D(nm)	Aver.(nm)
ZB1-2:1	31.7564	0.274	2.81549	0.96185	0.006301	22.62	21.78
	34.4236	0.296	2.60320	0.95522	0.006899	20.81	
	36.2352	0.311	2.47710	0.95042	0.006582	21.92	
ZB2-1:1	31.6791	0.273	2.82219	0.96203	0.009080	15.69	13.33
	34.4242	0.296	2.60316	0.95522	0.013926	10.31	
	36.1225	0.31	2.48457	0.95073	0.010315	13.98	
ZB3-1:2	8.8784	0.077	9.95205	0.997	0.020771	6.62	8.48
	26.2289	0.227	3.39493	0.97392	0.011304	12.45	
	34.9554	0.30	2.56481	0.95383	0.022416	6.41	
AB.	15.8131	0.138	5.5998	0.99049	0.003471	39.88	31.69
	19.7600	0.172	4.4893	0.98517	0.011328	12.29	
	26.0046	0.225	3.4237	0.97436	0.003279	42.92	

As can be seen in Figure 12, the XRD pattern of the ZnO-bentonite NCs displays small changes in intensity and in the position of the interlayer spacing (d_{400}) of montmorillonite from 3.42371 Å to 3.41510, 3.41547 and 3.39493 Å for ZnO-bentonite clay hybrids. These changes resulted from the expansion of the interlayer spaces, which may be caused by the intercalation of ZnO NPs.

In this study XRD pattern of the ZnO-bentonite clearly shows in the presence of high concentration of zinc solution (2:1); the composite characteristics peak intensity and particle size increase, but in ZnO-bentonite NCs with low concentration of zinc solution (1:2) the composite characteristics peak intensity and interlayer spacing value decrease. However, decreasing amount of ZnO content is accompanied with formation of smaller size NCs. This might be due to more enough amount of bentonite clay responsible for capping and preventing ZnO NPs from agglomeration. For the smaller particles the peak broadening are larger and some of the peaks begin to overlap to a rather large extend. As the particles become smaller the signal also gets weaker.

Generally, in XRD data analysis of ZnO-bentonite NCs in the range 2θ = 30-36. 2 ° it is evident that increasing amount of ZnO samples led to the increased intensity of reflections

and their narrowing. Increase of the intensity and the narrowing is caused by the recrystallization and further growth of ZnO crystallites as proved also by visual observations (figure 12). Diffraction peaks corresponding to impurities were not found in the XRD patterns of ZnO-benonite NCs, confirming the high purity of the synthesized products..

As the amount of organic phase diffused in the aqueous phase is sufficient in the matrix, ZnO nanoparticles formed in between interlayer of bentonite clay can easily capped; and resulted in lower particle size. According to Fessi *et al*. reports, the diffusion of the organic solvent in the aqueous medium in the presence of lipophilic surfactant or stabilizer under magnetic stirring decrease the particles size of nanomaterials (Fessi *et al*., 1989). In the present study the *H. abyssinica* plant extracts can acts as a natural stabilizer and efficient reducing agent. DMSO can act both as capping and dispersant agent. It is believed that DMSO can make good dispersions of ZnO NPs with bentonite for easy diffusion of Zn^{2+} throughout the bentonite structure. It is also used to increase the interlayer space of bentonite due to its large size.

4.4. UV-Vis spectrophotometry

A. UV-Vis of ZnO NPs

The biosynthesis of ZnO NPs from different ratios of $ZnO(CH_3COO)_2.2H_2O$ and *H. abyssinica* plant leaves extract results are shown in Table 9. ZnO NPs synthesized from different ratios showed different color. The products with different colors obtained might be due to the formation of ZnO NPs with different sizes and optical properties. In this regard *H. abyssinica* leaf extract plays a crucial role in the conversion of $ZnO(CH_3COO)_2.2H_2O$ to $Zn(OH)_2$ or $Zn(OH)_4^{2-}$ through weak hydrogen bonds with Zn^{2+} and in capping ZnO NPs.

Table 9 shows the effect of plant extract volume on the color and size of nanoparticles. As it is observed from table using different plant extract volume was the reason for synthesis of different nanosized ZnO NPs.

Table 9: The effects of plant extract on the color of ZnO NPs.

№	Volume of leaf extract (mL)	Volume of 0.2M $Zn(CH_3COO)_2.2H_2O$ (mL)	Extract to Precursor ratio	Color of ZnO NPs	Nanosize (nm)
1	0	100	0:100	white	28.4
2	50	100	1:2	Pale white	23.07
3	100	100	1:1	light Yellow	21.67

Upon evaporation of the precipitate, characteristic white, creamish/ pale white and light yellow precipitate was formed and the powder obtained showed more brightness in color upon annealing (figure 5). As it's seen in table 9; change in plant extract concentration cause the change in ZnO NPs optical properties and particle size. As plant extract concentration increase, the nanoparticles size decrease; this causes a shift of absorption edge to the shorter wavelength or higher energy (blue shift).

Figure 13 shows the UV–visible spectra of the ZnO NPs prepared using different concentration of the plant extract. ZnO powder suspension in de-ionized water showed strong absorbance peaks in the range of 374-377 nm. The absence of other absorbance peaks in the spectra confirms that the synthesized materials were pure ZnO NPs. The occurrence of these absorption peaks was due to the surface plasmon resonance property of the nanoparticles, which occurs due to the oscillations of free electrons on the surface of the nanoparticles when they align in resonance with the wavelength of irradiated light. This may be due to the electron transitions from the valence band to the conduction band (O2p–Zn3d). In the present study, increasing the volume of the plant extract was used to optimize the size of the ZnO NPs synthesized. A decrease in particle size was observed when increasing the volume of plant extract from 0 mL to 100 mL. In previous studies, Awwad *et al.* and Zak *et al.* obtained absorbance peaks at 377 nm and 375 nm respectively for ZnO NPs ((Awwad *et al.,* 2014; Zak *et al*., 2014).

Furthermore, according to Demissie *et al.* reports, the peak positions of UV-visible spectra are related with size of nanoparticles and blue shifted or shifted to lower wavelength or higher energy as the crystal size of the nanoparticles decreased (Demissie *et al*., 2020). The wavelength of maximum absorption and particle size have a strong correlation (Sundrarajan *et al*., 2015, Bagabas *et al*., 2013). The blue shift indicated the reduction in the diameter of the ZnO NPs synthesized. However, a further increase in extract volume

resulted in a substantial broadening of absorbance peak. This might be due to the increase in absorbance which could be attributed to the smaller particle size of ZnO NPs, which in turn increases its Rayleigh scattering ray. Different volumes of extracts contain different concentrations of organic binder. This indicates that at higher extract concentrations, the biomolecules act as reducing agent and cap the nanoparticles surfaces protecting them from aggregation.

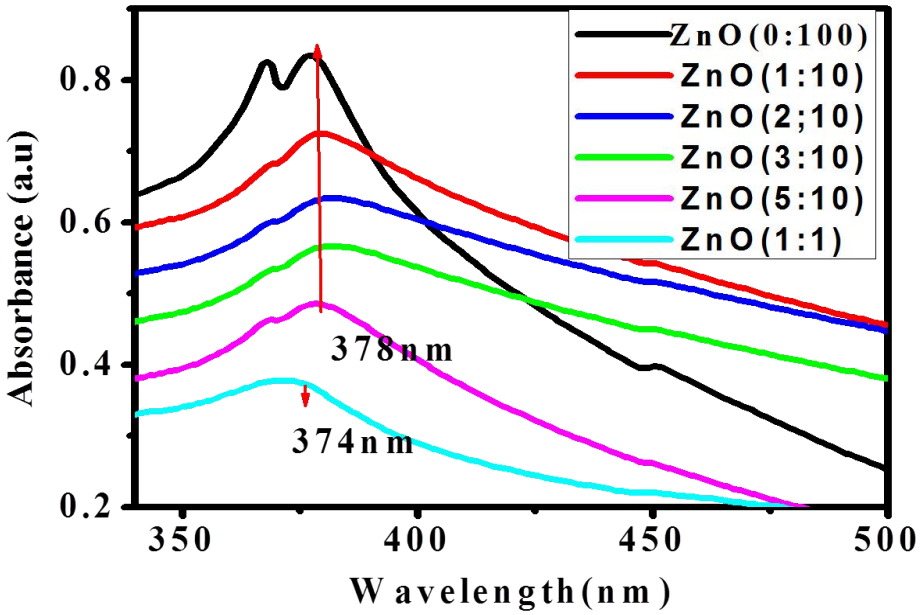

Figure 13: UV-Vis absorption spectra of ZnO NPs synthesized by different ratios of plant extract to $Zn(CH_3COO)_2.2H_2O$ solution.

UV-Vis result on figure 15 indicates the absorbance profile which starts decreasing near 377 nm and 374 nm. This value is in good agreement with previous report on band-gap of ZnO and the purity and the single phase nature of the biosynthesized ZnO NPs obtained after annealing at 450 ^{0}C (Narayanan *et al*., 2016). The broad absorbance band near 374 and 377 nm was a particular band for the hexagonal wurtzite ZnO.

Optical Characterization Studies and Mechanism for the Formation of ZnO NPs

The results of the Diffuse Reflectance spectroscopy (UV-Vis-DRS) can be used for calculating the optical band-gap of the materials. The band gap can be calculated by the intercept of the tangent to the $(F(r)\ hv)^2$ versus photon energy (hv) plot using Kubelka Munk function.

To calculate the optical band gap, Kubelka Munk function was applied; by plotting [F(R) hν]^2 vs. hν where;

F(R) =K/S.....Kubelka Munk function Eq. (19)

K = (1-R)^2.....Molar absorption coefficient Eq. (20)

R = R%/ 100..... Reflectance data Eq. (21)

S = 2R.....Scattering factor Eq. (22)

Energy (hν) = 1240/λ.....Photon energy, λ is wavelength, h is Planks constant and ν is speed of light.

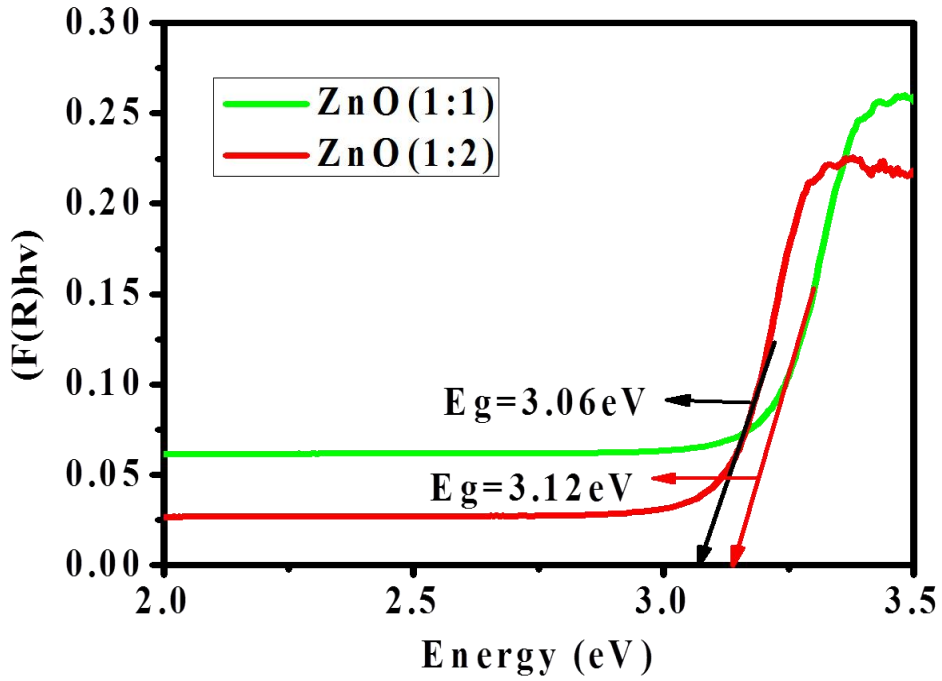

Figure 14: The band gap of ZnO NPs.

As showed on figure 13 and 14, it is observed that ZnO (1:2) has an absorption peak at 377 nm with E g of 3.06 eV and ZnO (1:1) NPs has an absorption peak at 374 nm with Eg of 3.12 eV in the UV–visible spectrum. In comparison to the ZnO (1:2), the observed blue shift in ZnO (1:1) NPs may be due to the size effect (decrease in size). The variation in Eg for the ZnO NPs synthesized at different ratios could be due to variation in average crystal size of the NPs. In case of the present study; when the size of a ZnO NPs decreases, the band gap is increase. Demissie *et al*. reports the band-gap energy values of ZnO NPs synthesized from 9:1, 3: 2, and 1:1 ratios were found to be 3.05, 3.11, and 3.21 eV,

respectively which is closely similar to the band gap value obtained in the present studies(Demissie e*t al*., 2020). The energy band gap of ZnO NPs synthesized by Zak *et al*. was reported as 3.3 eV (Zak *et al*., 2014). It is known that bulk ZnO has an absorption peak at 387 nm with 3.37 eV Eg value which is higher than the as-prepared ZnO NPs (374 nm and 377 nm). In comparison to the bulk ZnO, the observed higher blue shift in ZnO NPs may be due to the size effect. From this experiment it is concluded that the volume of plant extract can reduce the size of ZnO NPs and semiconductor nanoparticles experience a change in optical property compared with their bulk counterpart due to quantum confinement (Osuntokun et al.,2019).

As can be seen from Figure 15, Osuntokun *et al*. proposed the mechanism of formation of the biosynthesized ZnO NPs (Osuntokun *et al*., 2019). Based on literature, the growth mechanism for the formation of ZnO NPs was as a result of the reaction of the Zn^{2+} with the polyphenols and flavonoids among phytochemical present in the plant extract forming complexation Zn $(OH)_4^{2-}$ as growth species in a strongly alkaline solution. At high pH Zn^{2+} exists as Complex ion $[Zn(OH)_4]^{2-}$ or radical $[ZnO_2]^{2-}$, in solution. This is followed by hydrolysis reaction to form $Zn(OH)_2$ due to the presence of the OH^- group in the polyphenol or in the flavonoids. Calcination and decomposition reaction shortly follows to form ZnO NPs. The accumulation of ZnO NPs may refer to the presence of chemical compounds in the *H. abyssinica* plant such as phenols, and flavonoids, which can act as reducing agents plus as stabilizing agents by reducing the Zn^{2+} to the 0-valence state (Osuntokun *et al*., 2019).

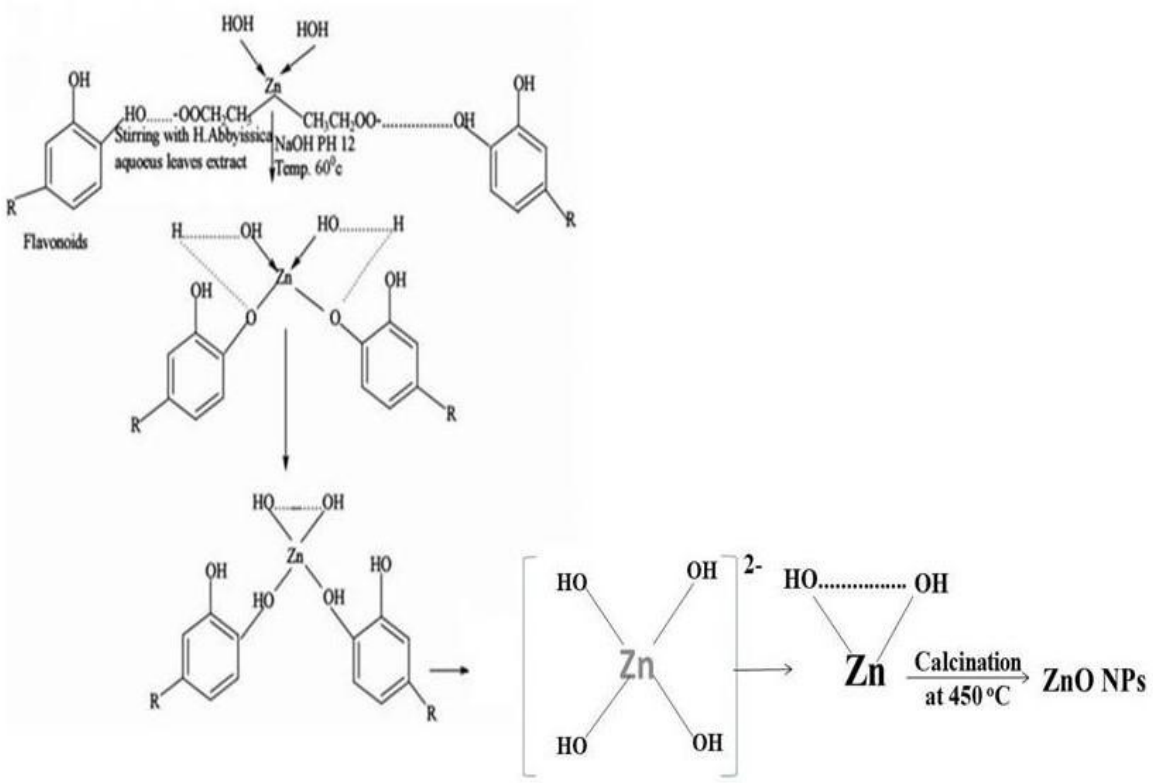

Figure 15: Proposed reaction mechanism for the formation of ZnO NPs using leaves extract (Osuntokun *et al*., 2019).

B. UV-Vis Absorbance of Activated Bentonite and ZnO-Bentonite NCs

The UV-Vis absorption spectra of ZnO NPs, activated bentonite, and Zn^{2+}-exchanged bentonite NCs are shown in figure 17. The UV-Vis spectrum of ZnO NPs and activated bentonite shows an absorption peak at approximately 377 nm and 276 nm respectively. After the ion exchange process, the intensity of the absorbance bands of bulk ZnO and bentonite decreases. The peak of the ZnO NPs shifts a red shift (higher λ) by 2nm from 377 nm to 379 nm and the bentonite peak shifts from 276nm to 282nm. From this observation it is expected that the Na^+ ions in Na-MMT have been exchanged by Zn^{2+}. Hence it was concluded that; the spectra attributed to the formation of ZnO-bentonite NCs, because the spectra has both the ZnO and bentonite characteristic peak. This indicates the slight decreases in the size and distribution of ZnO NPs formed in the complexes. Another interesting wavelength around 282 nm can be observed as a shoulder peak in the spectra of bentonite which denotes the presence of a conjugated system attributed to the $\pi \rightarrow \pi^*$ transition of the Si=O functional group.

In synthesis of ZnO-bentonite NCs, when ZnO NPS are included as reactant, large size ZnO NPs were densely deposited on the surface of the activated bentonite and prevent uniform distribution of Zn^{2+} in the whole nanocomposites matrixs. This affects the properties and application of ZnO-bentonite NCs. Hence, in situ pillaring of ZnO in between bentonite clay interlayer could result in smaller size of ZnO NPs in between TOT layer and uniform distribution of Zn^{2+} in the whole nanocomposites matrixs with enhanced properties and applications. Figure 16 showed that the cation exchange process (the existing Na^{+} captions were replaced by the Zn^{2+} cations) occurred in between the TOT layer. From equation 14-16; it is observed that the reaction was performed and the exchanged Zn^{2+} cations were converted into mixture of $Zn(OH)_2$ and ZnO by the effect of reducing group present in the plant extract.

Upon calcination at 550 °C, the intermediate compound $Zn(OH)_2$ was converted to ZnO. It is believed that the ion exchange process was first initiated inside the layers of Na-bentonite with CH_3COO^- ions as good complexing ligands for Zn (II) as described by following equations (Sasikala *et al*., 2019).

$$Zn(CH_3COO)_2.2H_2O + HOH/OH^- \longleftrightarrow Zn\text{-}OH + (HOOCCH_3/CH_3COOO^-) \quad \text{Eq.(23)}$$

$$Zn\text{-}OH + Zn\text{-}O\ OCCH_3 + NaOH \longleftrightarrow Zn\text{-}O\text{-}Zn + \text{-}OOCCH_3 \quad \text{Eq. (24)}$$

$$ZnO/Zn\text{-}OH + \text{Na-bentonite} \xrightarrow[\Delta]{80\,^{\circ}C,\ pH\ 12} \text{ZnO-bentonite NCs} \quad \text{Eq. (25)}$$

Figure 16 shows how ZnO NPs are formed in between the inter layer of bentonite clay. In this figure it is observed that Zn^{2+} ions substitute the Na^{+} ions of clay and form $Zn(OH)_2$ which was then reduced to ZnO NPs by plant extract.

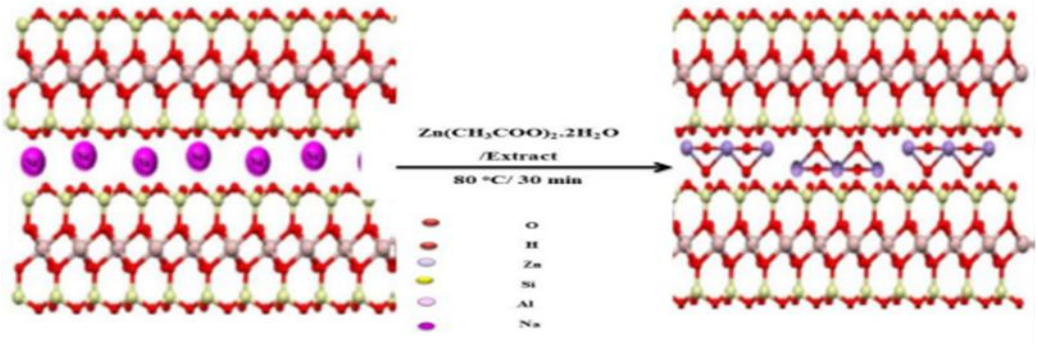

Figure 16: Schematic representation of ZnO-Bentonite NCs (Krishnan and Mahalingam, 2017).

The color of the parent bentonite nanoclay was cream-colored. The nanoclays alkaline ion exchange with $Zn(CH_3COO)_2.2H_2O$ reduced by the phytochemicals present in the plant leaf extract changes the color of the ZnO-bentonite NCs to rusty (Figure 6). It seems that this variation in color may result from the amount of ion-exchanged Zn^{2+} or aggregation of the Zn^{2+} diffused into the bentonite structure and the effect carbon present in organic phase.

Figure 17 shows the UV-Vis spectra of bentonite, ZnO NPs (1:2) and ZnO-bentonite NCs. In this figure it is observed that as composite was the hybrid of ZnO NPs and Na-bentonite, the spectra also shows the presence of characteristic peaks of each component. In this study ZnO NPs characteristics peak in composite was weekend and shifted to higher wavelength(less energy) at around 379 nm after ion exchange, which is associated with the formation of nanocomposites.

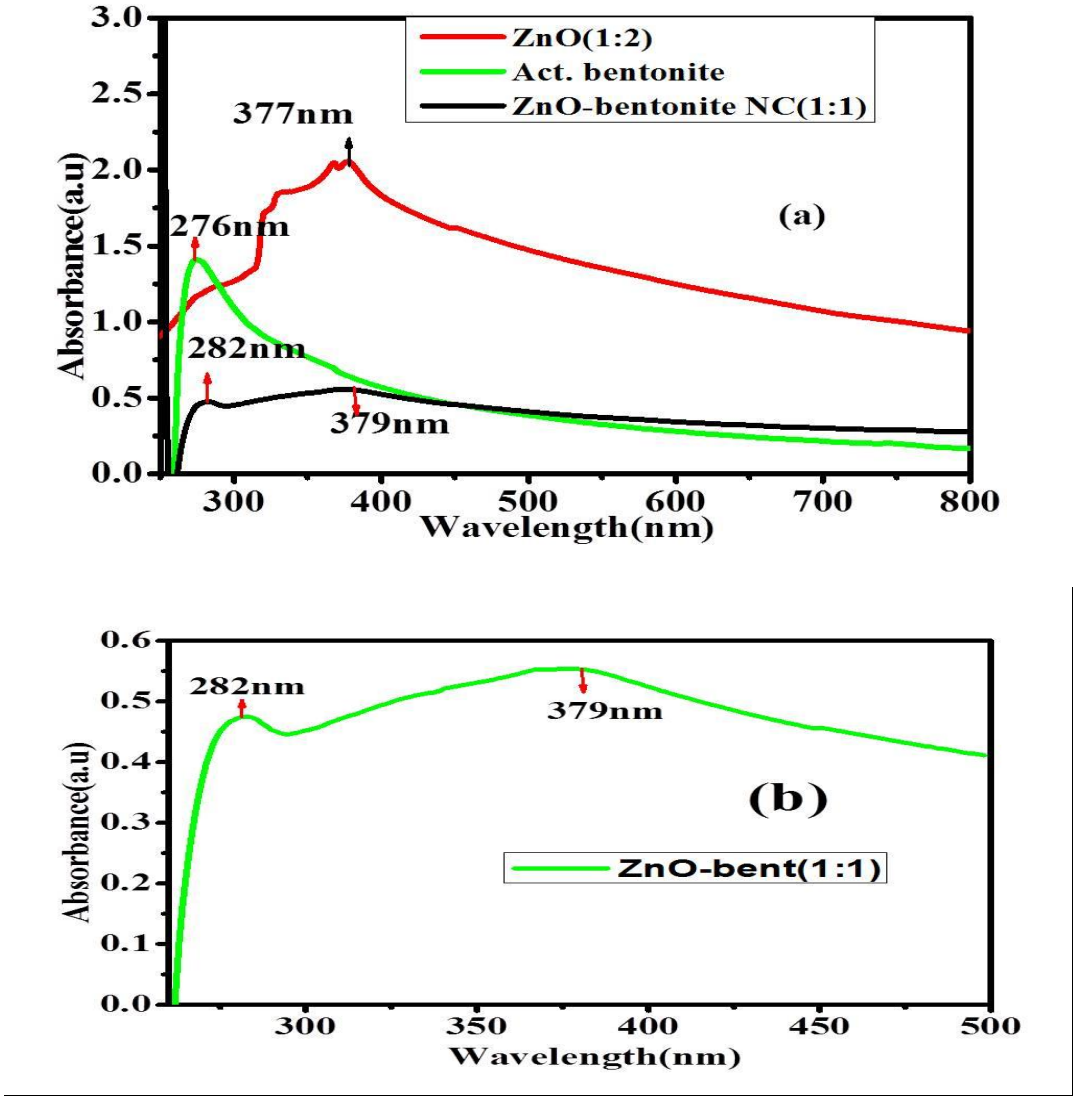

Figure 17: UV-Vis absorption spectra of ZnO NPs, bentonite and ZnO-bentonite NCs.

According to previous reports of Hakimi *et al*., the calculated band gap energy (Eg) value for ZnO NPs is 3.2 eV, which corresponds to the near-UV region emission. The corresponding Eg values calculated for the composites is 3.14 eV (Hakimi *et al*., 2018b). It is expected that the activated bentonite substrate *s*eems to have lowered the band gap which is observed in some previous investigations as well (Fernandez *et al*., 2008).

Figure 18 shows the variation in band gap of synthesized ZnO-bentonite NCs as the amount of ZnO NPs loaded on activated bentonite layer is changed. According to UV-Vis-DRS result the calculated band gap energy (Eg) value for the ZnO (1:2) NPs was 3.06 eV, and Eg values calculated for the ZB1 and ZB2 composites are 3.15 eV and 2.8eV respectively. In the present experiment it's explained that the band gab of ZB2 is less than ZB1 due to sufficient thickness of bentonite substrate used for trapping photo-exited electrons and holes cross through it (Wang *et al*., 2009).

Hakimi *et al*. reported shows that the bentonite substrate present in ZnO-bentonite NCs could reduce the band gab of composite (Hakimi *et al*., 2018b). This may be due to non-conducive nature of bentonite clay. This is based on the assumption that, if the coating layer is sufficiently thick for photo-exited electrons and holes to cross through, photo-generated excitons would be trapped within the coating layer, and cause the decrease in Eg.

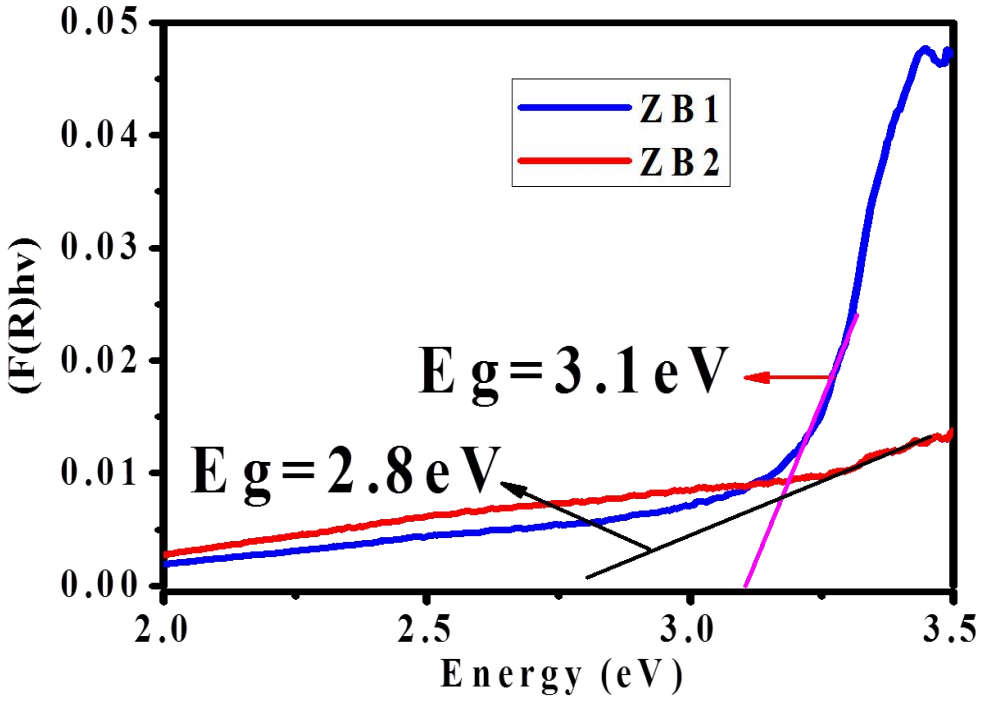

Figure 18: The band gap of ZnO-bentonite NCs (ZB1-2:1) and (ZB2-1:1).

4.5. Bentonite Analysis

4.5.1. Tests for Natural and Activated Bentonite properties

The effect of Na_2CO_3 on Ca-bentonite was observed by testing select bentonite properties as shown in table 10. In Na_2CO_3-beeentonite activation, Na_2CO_3 reacted and exchanged with Ca^{2+} in the bentonite clay; as a result bentonite clay were dispersed and deflocculated and change in its properties were observed. Evidently, as AAS analysis shows (table 11); the percentage of CaO decrease (3.15 % to <0.01 %) consistently and the percentage of Na_2O increases (1.41% to 5.92%).This might be due to greater hydration energies of smaller ions and thus within the inter-layers of clay can attract more water than large ions.The degree of attraction to the clay surface by Na^+ is less and the attraction of Ca^{2+} for adjacent surfaces is stronger (Unnithan, 2017).

Table 10: Rheological properties of Ca- bentonite treated with Na_2CO_3.

Properties of bentonite	Ca-bentonite	Na- bentonite	US Pharmacopeia
pH	10.35	10.6	9-10.5
Swelling capacity (mL)	25	35	24
Gel formation (mL)	2	1.5	≤ 2
CEC (meq/ 100 g)	81.2	88.2	≥ 80

Swelling power is the capacity of bentonite clay to absorb water to a greater extent. The swelling capacity of bentonite clay is upgraded through every step of purification. The result of bentonite properties test showed that swelling capacity of Na-bentonite was greater than Ca-bentonite; because of the weak electrostatic interaction between the Na^+ and the negatively charged bentonite layer, allowing the entrance of excess water molecules. Na^+ located between the inter-layers allow water to hydrate the clay mineral through absorption and results in its high swelling properties. This improved swelling value of the bentonite is due to the enhancement in surface area and breakup limit of nano-sized bentonite clay (Unnithan, 2017).

The bentonite properties test result also shows pH of Na-bentonite was also higher than that of Ca-bentonite because; Na_2CO_3 molecule is quite basic, or alkaline, meaning that it increases the pH of clay (Unnithan,2017).. The cation exchange capacity (CEC) is one of

the basic properties of clay minerals. CEC of bentonite clays was determined by adsorption of methylene blue method; because of its good sorption properties for a number of substances containing cation. As the result in table 10 showed the CEC of activated bentonite clay was greater than Natural bentonite clay. Figure 19 showed that the volume of 0.028 N methylene blue consumed by natural and activated bentonite clay during titration. The blue halo color was formed after 58 ml of methylene blue was consumed by natural and 63 ml of methylene blue was consumed by activated bentonite. As the concentration of methylene blue in bentonite slurry increase, the replacement of Na^+ with $C_{16}H_{18}N_3^+$ increases. At optimum flocculation" point, due to traces of free methylene blue, halo blue color and monomolecular coverage of the surface was attained. So, CEC of bentonite clay can be calculated by using;

$$\text{CEC (meq/ 100 g)} = \frac{V\,(ml)_{MB}}{\text{Weigth of clay}} * N_{MB} * 100 \qquad \text{Eq. (26)}$$

As a result he CEC of natural bentonite was 81.2 meq/100 g and 88.2 meq/100 g for activated bentonite. In adsorption of methylene blue by bentonite clay, the charges of the clay mineral or the surface area of the clay mineral control the amount of substances adsorbed on the clays. In this experiment surface area of activated bentonite clay is larger than raw bentonite. This might cause the increase CEC of activated bentonite. At low methylene blue concentration the CEC can be determined by charges of the clay on the surface, while with increasing concentration of methylene blue the adsorption rate is controlled by the surface area of the clay (Amman, 2003).

The layers in T-O-T layered silicates are overall negatively charged and are neutralized by the presence of cations in the interlayer space. The existing cations in clay may be exchanged with other cations when the clay is exposed to cations-containing solutions. In CEC determination using methylene blue method, methylene blue cation ($C_{16}H_{18}N_3^+$) replaces cations of clay. This indicates that the possible exchangeable cations number in activated bentonite clay is greater than that of raw bentonite (Bujdak *et al*., 2001).

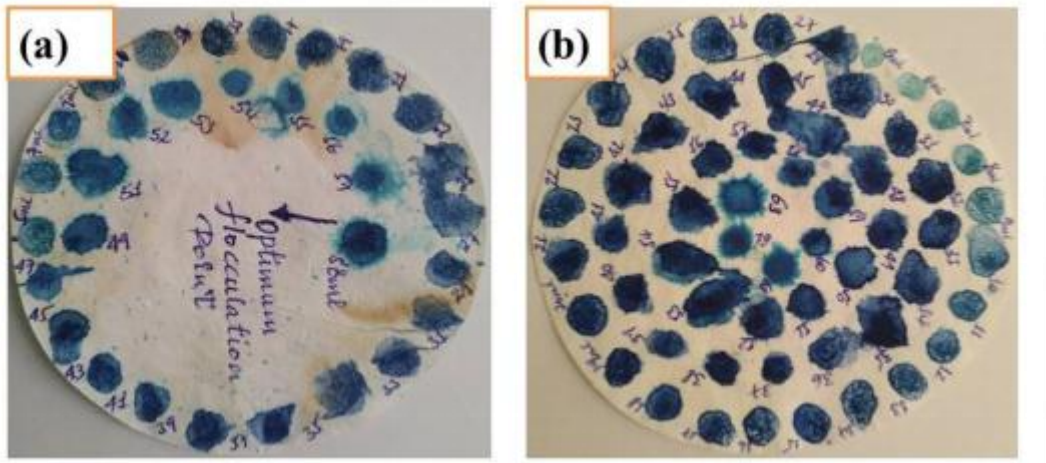

Figure 19: Methylene blue method test for CEC of natural bentonite (a) and activated bentonite (b).

4.5.2. AAS bentonite Analysis

Natural and activated bentonites chemical compositions analysis results are indicated in the table 11.

Table 11: AAS bentonite Analysis result.

Oxides (%)	Natural bentonite	In activated bentonite (5%- Na_2CO_3)
SiO_2	55.54	55.14
Al_2O_3	12.65	12.25
Fe_2O_3	7.75	6.96
CaO	3.15	<0.01
MgO	2.8	2.71
Na_2O	1.41	5.92
K_2O	0.98	0.95
P_2O_5	0.64	0.57
TiO_2	1.35	1.36
H_2O	4.38	5.32
LOI	9.8	8.8

In the table 11, silicate analysis results showed that the percentage chemical composition of raw bentonite is higher than that of activated bentonite, except the results of for Na_2O and H_2O. The percentages of Na_2O and H_2O in raw bentonite are less than that of 5 % Na_2CO_3 activated bentonite. This result of Na_2O percentage changes from 1.41 % to

5.92 % confirmed the replacement of high percentage of calcium ions in MMT by sodium ions. The percentage increase in Na_2O is much higher than the percentage reduction in CaO hence it can be concluded that divalent ions other than Ca^{2+} like Mg^{2+} also got replaced by Na^+ (Evangeline, 2009).

The increase in percentage of H_2O in activated bentonite is also related to activation of bentonite; because the swelling capacity of Na-bentonite was greater than Ca-bentonite; due to the weak electrostatic interaction between the Na^+ ions and the negatively charged smectite layer, allowing the entrance of excess water molecules. The sodium ions located between inter-layer allow water to hydrate in the clay mineral and result in its high swelling properties. Smaller ions tend to have greater hydration energies, and thus within the interlayer of clays can attract more water than large ions. In previous report, it was found that free swell of Ca Bentonite was 16 ml/ 2 mg and Free swell of Na Bentonite was 22 ml/ 2 mg. Addition of $NaCO_3$ shows increase in the free swell (Unnithan, 2017).

The result shows the natural and activated bentonite contain high concentration of SiO_2 followed by Al_2O_3. The decrement in fewer amounts of Al_2O_3 and SiO_2 might be due to the formation of Sodium Aluminium Silicate Hydrate ($Al_{12}Na_{12}O_{48}Si_{12}{\cdot}H_{36}O_{18}$), Sodium Silicate ($Na_2SiO_3$), and Sodium Aluminium Oxide ($NaAlO_2$) etc. Also the percentage of Fe_2O_3, Al_2O_3 and CaO are decreased in the activated bentonite clay, which indicated that the removal of non-clay minerals and impurities level of Fe and Al due to purification processes. This result agreed with the result reported by Ismael *et al.* (Ismaeel *et al*., 2017). The decrease in loss on ignition (LOI) values follows the decrease of silicates amount in activated bentonite. The decrease in the percentage of P_2O_3 can be attributed to the formation of Calcium lacto phosphate. This result was agreement with previous report.

4.6 Scanning Electron Microscopy (SEM)

The surface morphologies of biosynthesized ZnO NPs, activated bentonite and ZnO-bentonite NCs were studied by using SEM and the results are presented in Figure 20. Figure 20(a & b) shows the SEM image of calcined ZnO NPs synthesized by using 1:1 ratio of plant extract to precursor. The images of NPs were found to be nearly spherical in shape even though flower-shaped structures were also observed later. The SEM images show agglomerations of individual ZnO NPs. A closer look at the agglomerated lump shows the presence of several NPs aggregates. The individual growth unit of micro-flower is evident at higher magnification (Figure 20a). The high magnification images of the

micro-flowers reveals that the flower structures are made up by the accumulation of several small spherical particles. In figure 20 (b), some particles appear to be aggregated, hexagonal, spherical shaped and some individual crystals are clearly viewed as large in size. The similar shape was reported by Upadhyaya *et al.* (Upadhyaya *et al*., 2018).

The result of scanning electronic microscope shown in Figure 20 (c and d) which indicated that the activated bentonite has typical layered structure with clearly visible flat structure, irregular platelets form and in a sheet like morphology, partials were close to each other formed aggregates, and obvious hole. The morphological observations of activated bentonite sample surface, was shaped like aluminium silicate mineral layered structure. At higher magnification less nanoclay aggregate and larger holes were observed Figure 20 (c), while figure 20 d shows large aggregate, less hole and large flatter surface area.

Figure 20(e and f) shows the SEM image of calcined ZnO-bentonite NCs (1:1), which confirms the diffusion of Zn^{2+} to the clay surfaces. Activated bentonite has been used to minimize the agglomeration of ZnO NPs and facilitate more active sites of ZnO NPs exposed. After modification with ZnO NPs, the overall parent structure of bentonite remains unchanged and the bentonite clay surface was completely changed with few aggregates. However, holes were detected on the surface of the nano-ZnO–bentonite composite and the bentonite particles were covered by continuous layer of ZnO NPs after in situ pillaring of ZnO NPs to the bentonite structure. As shown in Figure 20 a and c, the morphology of ZnO NPs and activated bentonite were spherical and sheet, respectively. As ZnO shape reported by Garshasbi *et al.* the spherical ZnO NPs on bentonite are observed obviously in the SEM image of ZnO-bentonite NCs (Figure 20 e) (Garshasbi *et al*., 2017).

Thus,Zn^{2+} in the bentonite intermediate layer is “composed of silicate sheets bonded to Al_2O_3/ $Al(OH)_3$.

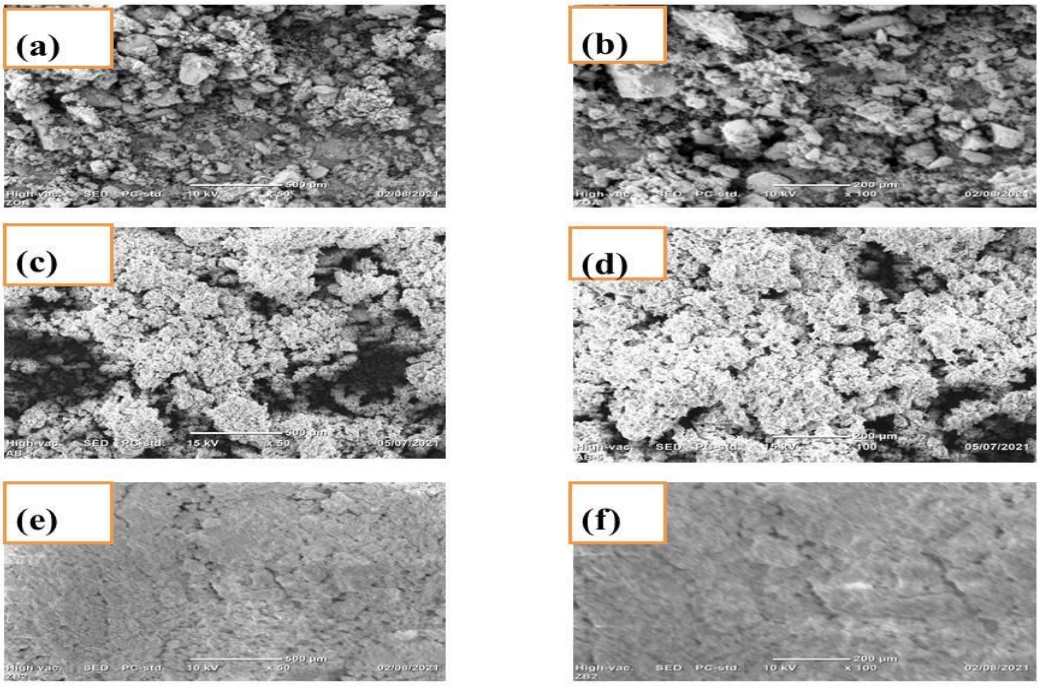

Figure 20: SEM images of ZnO (1:1) NPs (a & b), activated bentonite (c & d) and ZnO-bentonite NCs (1:1) at different magnifications (e &f).

4.7. Fourier Transforms Infrared Spectroscopy (FT-IR)

A. FT-IR Results of *H. Abyssinica* crude leaf extracts and ZnO NPs

FTIR was employed to investigate the possible functional groups in the *H. abyssinica* extract and the biosynthesized nanoparticles. Figure 21 presents the FTIR spectra of the *H. abyssinica* extract, uncalcined ZnO (1:1) and calcined ZnO (1:1). In the spectrum of the *H. abyssinica* extract (Figure 21 a) a broad peak around 3336 cm^{-1} could be assigned to the stretching vibration of the hydroxyl group of phenol, which also overlapped with the N-H of the amines due to different bioactive compounds present in *H. abyssinica* extract. Two low intensity peaks around 2926 $cm^{-1}$to 3000 cm^{-1} corresponded to the symmetric and asymmetric, C–H of the aliphatic group. The band around 1732 cm^{-1} was assigned to the C=O stretching vibration and the peak around 1615 $cm^{-1}$was attributed to C=C or C=N functional groups. The peak around 1446, 1358, 1184 and 1049 cm^{-1} suggests the presence of C-C, C-N, C-O and C-Cl stretching vibration.

Figure 21(b) shows the FTIR spectrum of ZnO before calcinations NPs which was resulted in various peaks at 3408, 2923, 2851, 1575, 1417, 1026, 673 and 466 cm^{-1}. The FTIR band around 1026, 1417, 1575 and 3408 cm^{-1} suggests the presence of bio-molecules present in

leaf extract on ZnO NPs which acted as reducing and capping agents. The broad band peaks at 3408 cm^{-1} correspond to H bonded OH stretching of polyphenols and flavonoids (Jamdagni *et al*., 2018). Two low intensity peaks around 2923 cm^{-1} and 2851 cm^{-1} corresponded to the symmetric and asymmetric C–H of the aliphatic group and C–H stretching vibrations of an aromatic aldehyde. The 1575 cm^{-1} peak results from the stretching bands of C = C or C=N functional group. The peak at 1417 cm^{-1} refers to the amine –N=O vibration stretch in amide linkages (Jamdagni *et al*., 2018). The 1200 cm^{-1} peak results from aromatic amines and C-N stretch of aliphatic amines. The 1026 cm^{-1} and 673 cm^{-1} peaks correspond to alkanes and supposedly, C-H bend in alkynes, respectively and the peak in the region between 400 and 600 cm^{-1} is assigned to Zn-O stretching vibration, confirming ZnO NPs are synthesized using *H. abyssinica* extract as a reducing and capping agent (Dobrucka and Długaszewska, 2016). The peaks at 466 cm^{-1} , 1575 cm^{-1} , 2923cm^{-1} , 3408 cm^{-1} suggests the presence of biomolecules present in leaf extract on ZnO NPs which acted as capping and stabilizing agents.

Figure 21(c) shows the FTIR spectrum of calcined ZnO NPs which resulted in various peaks in the region of 400 cm^{-1} to 4000 cm^{-1}. The band around 3394cm^{-1} was assigned to the O-H stretching vibration. The Peaks at 2920 cm^{-1} and 2854 cm^{-1}corresponds to stretching of the symmetric and asymmetric C–H of SP^3 (Kahsay, 2021). The Peaks at 2342 cm^{-1} corresponds to stretching vibration of CO_2 added during calcination. The stretching vibration at 1743 cm-1 and 1430 cm-1were attributed to C=O (carbonyl group) and the C-C stretching of aromatic ring respectively (Suresh *et al*., 2018).

The intense band located at 1022 cm^{-1} and 880 cm^{-1} illustrates the presence of C-N, and C-O cm^{-1} stretching vibration. The peak around 456 and 451 cm^{-1} is due to Zn–O stretch. The stretch for ZnO NPs was found in the region 400-600 cm^{-1}. Therefore the synthesized nanoparticles were surrounded by metabolites such as terpenoids and flavonoids having functional groups.

Generally from FTIR spectra absorption band of *H. abyssinica* extract at 3336 cm^{-1} can be ascribed to the stretching mode of -OH groups and its shifted to higher frequency 3408 and 3394 cm^{-1} in synthesized uncalcined ZnO (1:1) and calcined ZnO (1:1) NPs; due to formation of $Zn(OH)_2$ and calcination temperature. There was a shift to lower frequency in the following peaks: 2926→2923→2920 cm^{-1}, 1732→1575→1430 cm^{-1}, 1615→1417cm^{-1}→disappearance, 1049→1026→1022 cm^{-1}due to reduction of Zn^{2+} by

secondary metabolise, the capping of ZnO NPs via coordination with OH, -NH, C=O, C=N. The band at 880 cm^{-1} is due to asymmetrical and symmetrical stretching of zinc carboxylates resulting from the involvement of carboxyl groups of *H. abyssinica* extract strong bands at 466 cm^{-1} and 570 cm^{-1} are attributed to the vibrations of elongation and deformation of vibratory Zn-O.

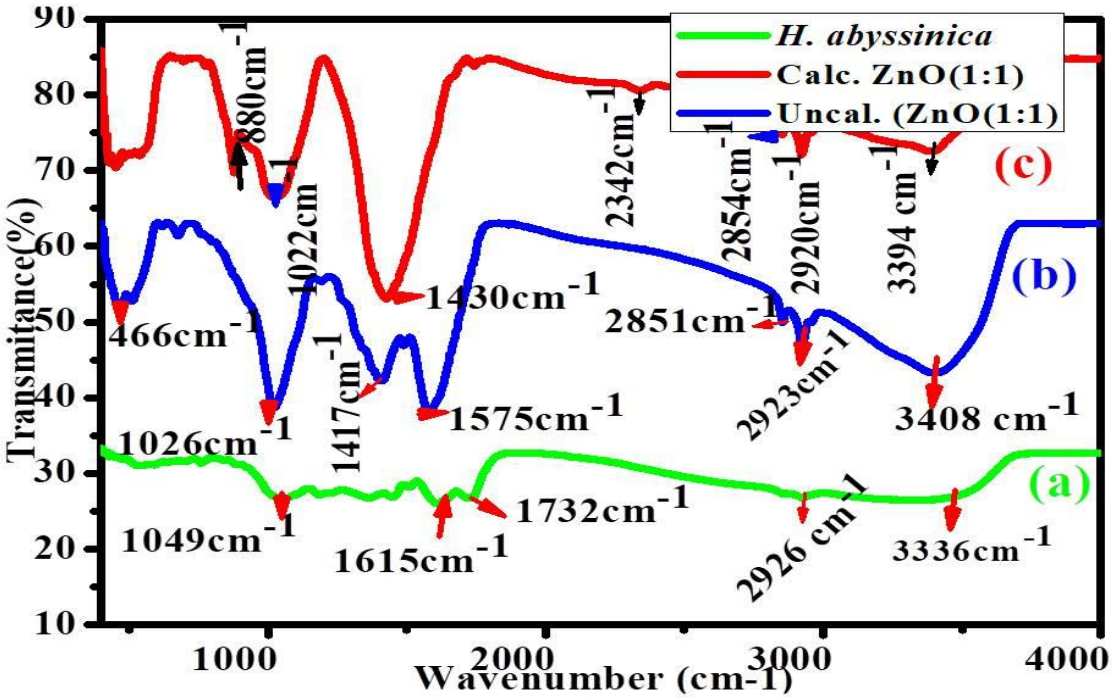

Figure 21: FT-IR result of *H. abyssinica* crude extract (a), before calcination ZnO (1:1) (b) and calcined ZnO (1:1) (c).

B. FT-IR Results of Purified Benonite and ZnO-benonite NCs

Figure 22 shows the FTIR spectra of purified bentonite (PB) (a), uncalcined and calcined ZB2 (1:1) (b & c). The FTIR spectrum of purified bentonite figure 22(a) indicates that montmorillonite is the dominant mineral phase in bentonite. The absorption band at 3557 cm^{-1} is due to stretching vibrations of structural OH groups of montmorillonite. The natural bentonite has characteristic montmorillonite with a single sharp band at 3557 cm^{-1} and a broad band at 3464 cm^{-1} of the OH stretching vibration of structural hydroxyl groups and water coordinated to octahedral Al^{3+} cations respectively. In the lower frequency region, montmorillonite had a strong band at 1020 cm^{-1} bonding to the Si–O stretching (in-plane) vibration of bentonite mineral. The absorption band at 1630 cm^{-1} was attributed to the OH deformation mode of water. The clay spectrum also contains a band in the region 700-800

cm^{-1} which indicated the presence of cristobalite/quartz. In addition the peaks at 461 and 518 $cm^{-1}$are due to the Si-O-Si vibrations and the silently group (Si-OH-Al) in the bentonite (Fisseha, 2017).

After coating of ZnO with bentonite, peaks appeared around 468 cm^{-1}(Si–O–Al), 516 cm^{-1} (Si–O–Mg), and another intense peak at 1020 and 1027 cm^{-1} due to Si-O stretching. An absorption band at 1620 and 1575 cm^{-1} shows, adsorbed water present in the clay and composites. The characteristic ZnO peak seen at 468 cm^{-1} was symmetric with Si-O-Al peak. The band observed in the region of 1434-1620 cm^{-1}in both composite reveals that the leaves extract and Zn^{2+} was successfully incorporated with the produced nanoclay (Chakraborty et al., 2019). From this FTIR spectra it is expected that calcination modifies the peaks intensity due to OH^- groups

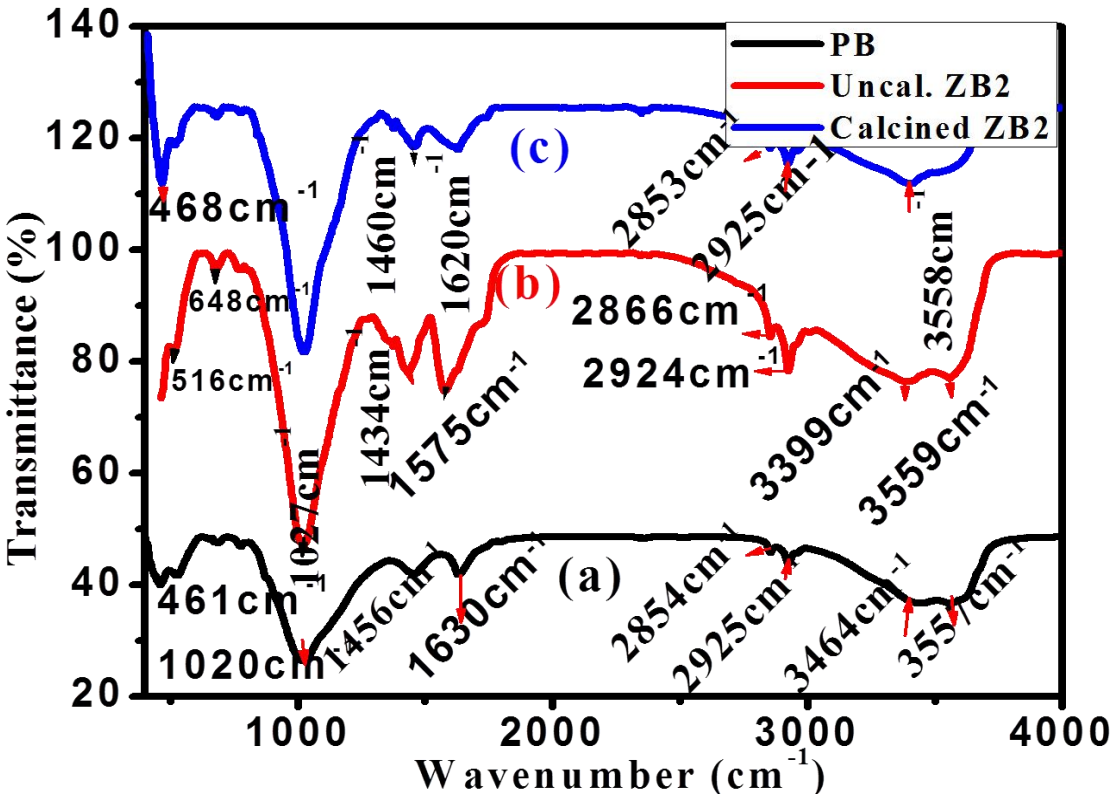

Figure 22: FT-IR Result of purified bentonite clay (PB), Uncalcined ZnO-bentonite (ZB2-1:1) and calcined ZnO-bentonite NCs (ZB2-1:1).

4.8. Antibacterial Activity Test

The biosynthesized ZnO NPs, ZnO-bentonite NCs, activated bentonite and *H.abyssinica* leaf extract were studied for the antibacterial activity against gram negative bacteria (*E.*

*coli)*and grams positive bacteria (*S. aureus)* bacteria. Ceftriaxone was taken as the standard (positive control) for all bacterial strains and DMSO was taken as negative control. For studying the antibacterial effect, four different concentrations (200, 150, 100 and 50 mg/ ml) of the samples have been taken as seen in Table 12.

Table 12: Antibacterial efficiency of *H. abyssinica* leaf crude extract, bentonite clay, ZnO NPs and ZnO-bentonite NCs at different concentration tested against *E. coli* and *S. aureus*

Sample	Diameter of Zone of inhibition observed at different concentration of samples (mm)							
	E.coli				*S. aureus*			
	200 mg/ ml	150 mg/ ml	100 mg/ ml	50 Mg/ ml	200 mg/ ml	150 Mg/ ml	100 mg/ ml	50 mg/ ml
ZOA	11±0.4	8.9±0.6	8±0.3	7.6±0.6	10±0.8	9.3±0.6	7.9±0.7	7.5±0.3
ceftriaxone	17.4±0.3				17.4±0.5			
ZOB	11±0.4	9.3±1.1	8.±0.6	7.7±0.3	9.7±0.4	9.1±0.5	8.4±0.9	7.3±0.7
ceftriaxone	17.2±0.2				17.6±1.5			
ZOC	10±0.4	8.8±0.6	8±0.2	7.2±0.2	10±0.6	8.6±0.6	8.1±0.1	7.3±0.9
ceftriaxone	17.6±0.1				17.4±0.5			
ZB2	13±0.8	11.5±1.9	8.6±1	8.7±0.1	12±0.3	11±0.9	8.7±1	7.5±0.7
ceftriaxone	17.1±0.2				17.3±0.8			
ZB1	13±0.5	11±1.6	8.7±1	7.5±0.9	11±0.4	11±0.8	9±0.4	7.6±1.1
ceftriaxone	17.0±0.4				17.6±0.6			
H.AP	7.9±0.3	7±0.1	6.7±0.3	6.8±0.2	8.5±0.3	6.9±0.2	7.1±0.4	6.7±0.7
ceftriaxone	17.3±0.3				17.4±1.1			
AB	6.3±0.2	6.2±0.1	6±0.1	6.1±0.4	6.6±0.5	6.5±0.1	6±0.1	6.1±1.3
ceftriaxone	17.8±0.5				17.6±0.2			
DMSO	6				6			

Where, ZOA is calcined ZnO NPs (1:1), ZOB is uncalcined ZnO NPs (1:1), ZOC is calcined ZnO NPs (1:2), ZB2 is ZnO-bentonite NCs (1:1), ZB1 is ZnO-bentonite NCs (2:1), H.AP is H. *Abyssinia* leaf crude extract and AB is activated bentonite.

A. Antibacterial Activity of H. *Abyssinia* leaf crude extract

Figure 23 (H.AP) shows the antibacterial activity of *H.abyssinica* leaf crude extract. *H. abyssinica* was traditionally known plant for de-worming intestinal parasites and treating infections. A leaf of crude extract was taken to test against two bacterial species (Table 12). The antibacterial activity of leaf crude extracts was found to be selective. The largest zones of inhibition were recorded with 200 mg/ ml concentration against *S. auras* (8.5 mm) followed by *E.coli* (7.9 mm) that could be attributed to the structural differences in the cell walls of bacteria. The lowest activity was determined with 50 mg/ ml against *S. aureus* (6.7 mm) followed by *E.coli* (6.73 mm) (Gulnaz and Savitha, 2013).

In general, the susceptibility of *S. aureus* and *E.coli* to the extract demonstrated the antibacterial activities in terms of growth inhibition of the test organisms. As the concentration of sample increases the mean inhibition zone also increases. As compared to standard drug the antibacterial activity of the *H. abyssinica* plant extracts on *S. aureus* and *E.coli* was 28.4 % and 36.7 %, respectively. The commercial standard drug (Ceftriaxone) showed the greatest inhibition effect against in all bacteria rather than the tested samples, the control (solvents) has no inhibition zone and was not observed any effect to the test solutions. In the case of both bacteria the growth of bacterial populations has decreased significantly at all concentration of plant extract relative to the positive control. The results are consistent with findings of other researchers Tadtong *et al*.and Wolde *et al.*; so that most plant extracts have inhibition effect on Gram positive bacteria and little effect on Gram negative bacteriaTadtong *et al*., 2014; Wolde *et al*., 2016).

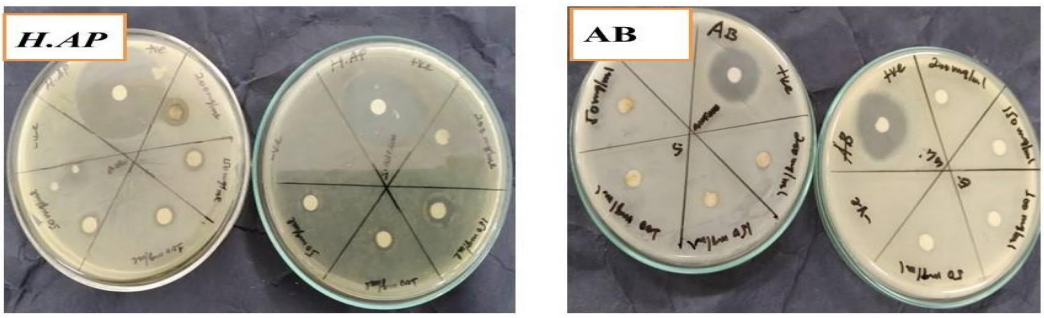

Figure 23: Antibacterial activity of *H. abyssinica* plant crude extracts (H.AP) and activated bentonite (AB).

B. Antibacterial Activity of Bentonite Nanoclay

Figure 24 (AB) shows the antibacterial activity of activated bentonite. Bentonite was traditionally known clay for healing and treating infections. The antibacterial activity of bentonite clay was found to be very less compared to positive control. The largest zones of inhibition were recorded with 200 mg/ ml concentration against *S. aureus* (6.6 mm) followed by *E.coli* (6.3 mm). The lowest activity was determined with 50 mg/ ml against *S. aureus* (6.13 mm) followed by *E.coli* (6.1 mm) as can be seen from Table 12. DMSO does not have any role in the zone of inhibition.

In general, as the concentration of sample increases the mean inhibition zone value increases. This might be due to the low concentration of bactericidal mineral present in clay. The presence of pyrite in bentonite in some extent may be important for bactericidal action and the bentonite may sequester toxic ions in the interlayer sites, which could be released upon rehydration in a clay poultice. Significantly concentrations of Al, P, Fe Cu, and Pb are associated with the whole bacteria killed by the bentonite leachate than in the living bacteria. Behroozian *et al.* reported that exchangeable metal ions and mineralogical composition of clay have been responsible for the activity of some antibacterial clay (Behroozian *et al*., 2020).

In contrast, the concentrations of Mg and Ca are much lower in the activated bentonite treated bacteria. This is due activation of bentonite with Na^+ which cause ion exchange between Na^+ and Ca^{2+} and Mg^{2+}, hence increase the basicity of clay (> 10). Also the high concentration of Al in the MMT leachate is of interest because the antibacterial clay leachates have extreme pH $\geq$ 10.

The process of transferring elements from a clay surface through water to a cell membrane involves numerous chemical reactions and the formation of rapidly reactive intermediates (radicals) that are affected by clay mineralogy and by surface complexation on the bacteria. It is expected that in the presence of water, pyrite produces reactive oxygen species (ROS) such as hydrogen peroxide and hydroxyl radicals that degrade nucleic acids in RNA and DNA via the fenton reaction. Park and Imlay showed that significant damage to cellular DNA occurs when hydrogen peroxide reacts with Fe^{2+} to form hydroxyl radicals in vivo. Penetration of Fe^{2+} into the cell will catalyse the fenton reaction (Park and Imlay, 2003).

Morrison *et al*. described the antimicrobial mechanism of natural clays. They opined that interlayer cation exchange, pyrite oxidation, and mineral dissolution of illite–smectite gave

soluble cations like Ca^{2+}, Al^{3+}, Fe^{3+}, and Fe^{2+} (Morrison *et al*., 2016). The generated Fe^{2+} and Al^{3+} attack the bacteria via oxidation, destroying the multiple cellular components. Also, the hydrogen peroxide released through the cell envelops and reacts with the intercellular Fe^{2+} to form radicals that react or oxidize the protein and DNA molecules, thus activating the ROS stress response. Figure 24 and 25 shows antibacterial activity of synthesized samples against *E.coli* and *S.aureus* bacterial strains as presented in table 12.

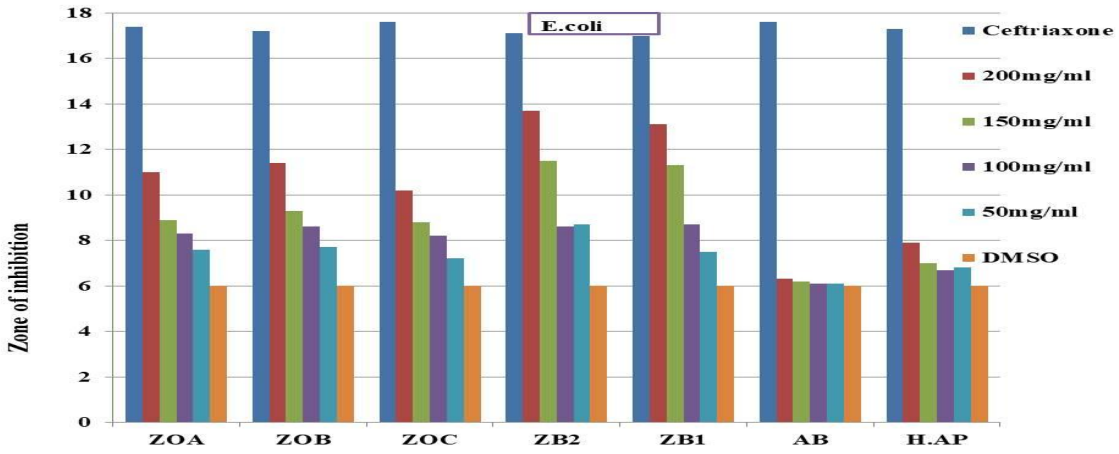

Figure 24: Diameter of Zone of inhibition of different sample at different concentration against *E. coli* strain.

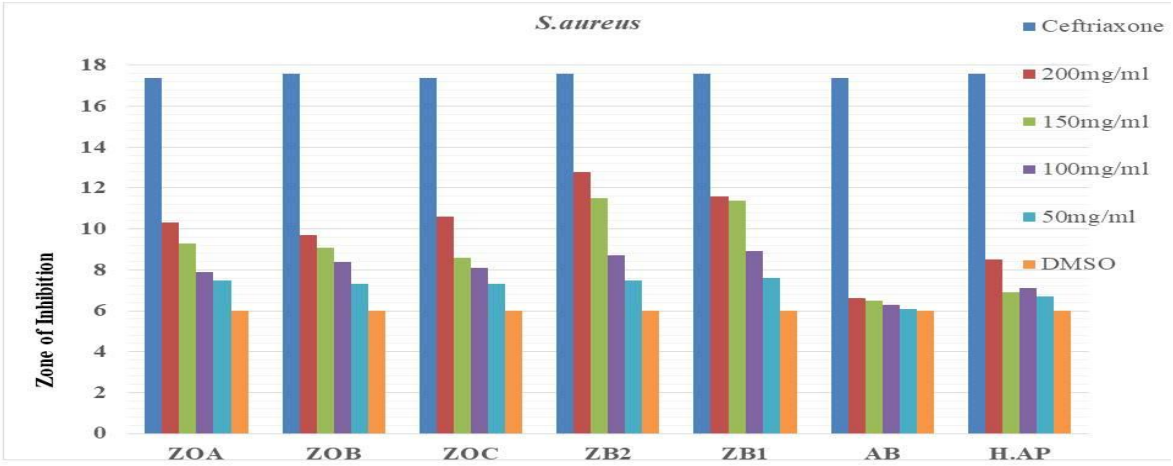

Figure 25: Diameter of Zone of inhibition of different sample at different concentration against *S. aureus* strain.

C. Antibacterial Activity of ZnO NPs

In the present study anti-bacterial activity of synthesized ZnO NPs was studied against two bacterial strains *E. coli and S. aureus.* The zone of Inhibition obtained at a different concentration of ZnO NPs is shown in the table 12.

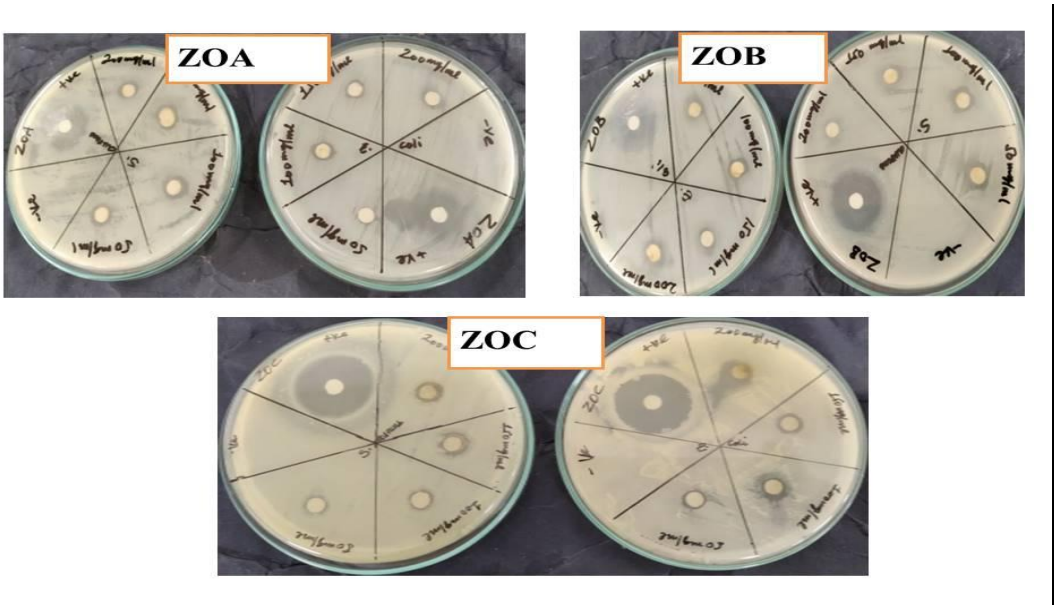

Figure 26: Antibacterial efficiency of calcined ZnO NPs-1:1(ZOA), uncalcined ZnO NPs-1:1(ZOB) and calcined ZnO Nps-1:2(ZOC) at different concentration.

The antibacterial activities of ZnO NPs in contact with bacteria are affected by particle sizes, concentration, their aggregates in colloidal solutions, chemical composition of dispersion media, storage time, morphologies and specific surface areas involved. Figure 26 showed that uncalcined ZnO NPs-1:1(ZOB) with 21.5 nm particle size shows the highest antibacterial activity than calcined ZnO NPs-1:1 (ZOA) with 21.67 nm particle size and ZnO NPs-1:2 (ZOC) with 23.06 nm particle size. The maximum zones of inhibition 11.4 mm were observed against the pathogen *E.coli* for uncalcined ZnO NPs-1:1 (ZOB) followed by 11.1 mm inhibition zone of calcined ZnO NPs-1:1 (ZOA) against *E.coli* and 10.6 mm inhibition zone of ZnO NPs-1:2 (ZOC) against S.*aureus*. The uncalcined ZnO NPs-1:1 (ZOB) in all concentration ranges showed a greater zone of inhibition against all bacterial strains compared to calcined ZnO NPs. This might be due to small crystalline size of uncalcined ZnO Nps-1:1(ZOB).

DMSO does not have any role in the zone of inhibition. In previous study; Raghupathi *et al*. investigated the antibacterial properties of ZnO NPs against both gram positive and gram negative microorganisms that are commonly found in environmental settings

(Raghupathi *et al*., 2011). Their demonstrations suggest that the antibacterial activity of ZnO NPs was inversely proportional to the size of the nanoparticles.

Figure 26 shows the antibacterial activity of the biosynthesized ZnO NPs. It's found that by increasing concentrations of ZnO NPs, growth inhibition was consistently improved due to a proper diffusion of nanoparticles in the agar medium (Wahab *et al*., 2010). It's observed from the present study that the inhibition zone of ZnO NPs was better at high ZnO NPs concentration than ZnO NPs at low concentration. At low concentration ZnO NPs has no significant effect on bacterial growth.

Stan *et al*. and Zakharova *et al*. observed the antibacterial activities of ZnO NPs synthesized by using plant extracts, such as *Allium sativum*, *Rosmarinus officinalis* and *Ocimum basilicum* (Stan *et al*., 2016; Zakharova *et al*., 2019). Their study results showed that green synthesized ZnO NPs exhibit strong levels of bactericidal activity against *S. auras*, *E. coli*, and *Salmonella typhimurium* bacterial strains.

Appierot *et al*. reported that the antimicrobial activity of the ZnO NPs depends on a size, *i.e*., decreasing ZnO NP sizes resulted in the greater antimicrobial activity(Appierot *et al*., 2009). The synthesized nanoparticles were smaller than bacteria pore, they could cross the cell membrane freely. The biosynthesized ZnO NPs samples which have the smallest size showed the highest radical scavenging activity compared to the larger size ZnO NPs.

The present study also shows antibacterial activity of ZnO NPS depend on types of bacteria. In general the antibacterial activity of ZOC, ZB1, H.AP and AB against *S.aureus* was greater than *E. coli*. But, the antibacterial activity of ZOB, ZOA and ZB2 samples against *E. coli* was greater than against *S.aureus.* Shu *et al*., report also indicates that bactericidal activity of ZnO NPs was greater on Gram-positive than Gram-negative bacteria. This is due to Gram-negative bacteria have an outer lipopolysaccharide membrane, and this makes the cell wall impermeable to antibacterial chemical substances. Gram-positive bacteria on the other hand are more susceptible having only an outer peptidoglycan layer which is not an effective permeability barrier. Therefore, the cell walls of Gram-negative bacteria are more complex in layout than the Gram-positive ones acting as a diffusion barrier and making them less susceptible to the antibacterial agents (Shu *et al*., 2017).

The detailed mechanism for the activity of ZnO is still under debate. For the ways of interactions of ZnO NPs with bacteria, scientists have suggested a few possible bactericidal

mechanisms. Some proposed that smaller NPs have greater surface reactivity and easier cell penetration that released Zn^{2+}. The release of Zn^{2+} from ZnO NPs is one of the main propositions in antibacterial mechanisms which are known to inhibit several bacterial cell activities including active transport, bacteria metabolism, and enzyme activity leading to bacterial cell death due to the toxicity properties of Zn^{2+}. As the present study investigation, Zn^{2+} might be bind to proteins and deactivate proteins, interact with microbial membrane and causing structural changes, and bind to electron donor groups in biological molecules containing sulphur, oxygen or nitrogen like nucleic acids and prevent microbial replication. Another possible mechanism for the antimicrobial activity of ZnO NPs is through the attachment of NPs to the bacteria cell membrane via electrostatic forces. This interaction may distort the membrane plasma structure and damage the bacterial cell integrity, resulting in the leakage of intracellular contents and ends with cell death (Maurya, 2020).

Several reports suggest that the action of ZnO on bacterial species is due to release of reactive oxygen species (ROS) species. The antibacterial activity of ZnO was attributed to reactions between ZnO surface and water, and the aqueous ZnO NPs suspensions were able to produce high levels of ROS. Generated ROS species, that is, the OH^-(hydroxyl radicals), O_2^{-2} (singlet oxygen), H_2O_2 (peroxide) and Zn^{2+} from ZnO nanoparticles bind to the negative surface of the cell membrane, leading to disruption of the cells followed by leakage of inner cellular material that causes cell death. Compared with O^{2-} and –OH, H_2O_2 is often considered the main harmful factor, because it can penetrate the bacteria easily due to relatively weaker electrostatic interaction between ions and bacteria (Sirelkhatim et al., 2015). The generation of hydrogen peroxide (H_2O_2) from the surface of ZnO is considered as an effective mean for the inhibition of bacterial growth according to some studies (Yamamoto *et al*., 2004).

It has been reported that ZnO can be activated by both UV and visible light and consequently, electron–hole pairs (e^-/h^+) can be created. The generation of H_2O_2 is explained as follows: the holes split the H_2O molecule from the suspension of ZnO into OH^- and H^+. Furthermore, dissolved oxygen molecules are converted to superoxide radical anions (O^{-2}) which react with hydrogen ion (H^+) to produce HO_2- radicals. The collision of these hydroxyl radicals with electrons will produce hydrogen peroxide anions HO^{-2}, which react with hydrogen to generate H_2O_2 molecules. The H_2O_2 molecules thus generated can penetrate the cell membrane and kill the bacteria (Padmavathy & Vijayaraghavan, 2008). .

D. Antibacterial Activity of ZnO-bentonite Nanocomposites

The antibacterial activity of the ZnO-bentonite NCs with different ZnO loading was performed to determine the proper mass ratio of ZnO. Figure 27 shows results of the antibacterial tests of composites of ZnO-bentonite. In the present study ZnO-bentonite NCs was taken to test the sensitivity against two bacterial species (Table 12). The antibacterial activity of ZnO-bentonite NCs was found to be selective. ZnO-bentonite NCs revealed more obvious inhibition on bacteria growth than that on equivalent doses of ZnO NPs. The largest zones of inhibition were recorded with 200 mg/ ml concentration of ZB2 against *E.coli* (13.7 mm) followed by 200 mg/ ml concentration of ZB1 against *E.coli* (13.1 mm). The lowest activity was determined with 50 mg/ ml concentration of ZB1 against *E.coli* (7.5 mm) followed by ZB2 against *S. auras* with little inhibition(7.5 mm) as can be seen from Table 12.

200 mg/ ml concentration was found to be the most active ZnO-bentonite NCs concentration for the tested bacteria. In general as concentration of sample increases the mean inhibition zone value increases. This might be due to the high concentration of bactericidal mineral present in composite. The antibacterial efficacy of high concentration ZB2 against *E.coli* was greater than that of *S. aureus and* antibacterial efficacy of high concentration ZB1against *S. aureus was greater than E.coli.* DMSO does not have any role in the zone of inhibition. The growth inhibition of bacteria was influenced by ZnO, and bentonite which showed very low cytotoxic effect. Bentonite clay and DMSO could facilitate the dispersion and stability of ZnO NPs and draw the ZnO-bentonite NCs in close contact with the bacterial membrane due their capping ability. ZnO NPs with higher dispersion may have increased surface area, causing more active sites to produce more ROS.

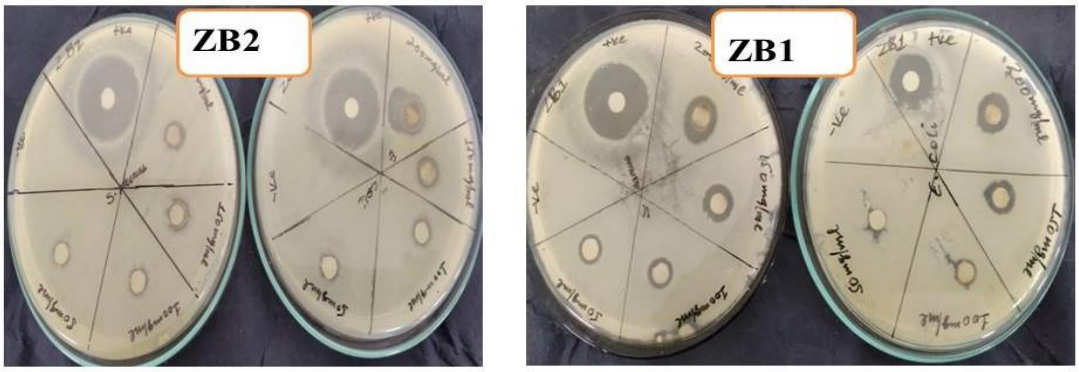

Figure 27: Antibacterial activity of ZnO-bentonite NCs (ZB2 (1:1) and ZB1 (2:1)).

ZB2 (1:1) shows the better antibacterial efficacy against both gram positive and gram negative bacteria than ZB1 (2:1). This might be due to the high dispersion of ZnO NPs in composite; with increased surface area, causing more active sites to produce more ROS. ZB1 (2:1) also shows better antibacterial activity next to ZB2 (1:1). This means by increasing number of ion exchange, the loading of Zn^{2+}increases; consequently. The increase in the amount of Zn^{2+} on the surface of bentonite increase the antibacterial efficacy of the composite (Shu *et al*., 2017). The incorporation of the anti-bacterial activities of ZnO NPs in nanocomposites will show a higher antibacterial activity.

In literature Pouraboulghasem *et al.* reported that enhanced antibacterial activity of the composites can be attributed to the chemical and physical properties of the nanoparticles with a large surface area of the clay. This implies that a great amount of ZnO is highly dispersed per unit area of the bentonite surfaces, thereby, maximizing antibacterial activity (Pouraboulghasem *et al*., 2016).

The antibacterial activity of ZnO-bentonite NCs is greater than the corresponding ZnO NPs due to enhancement of its physio-chemical properties.

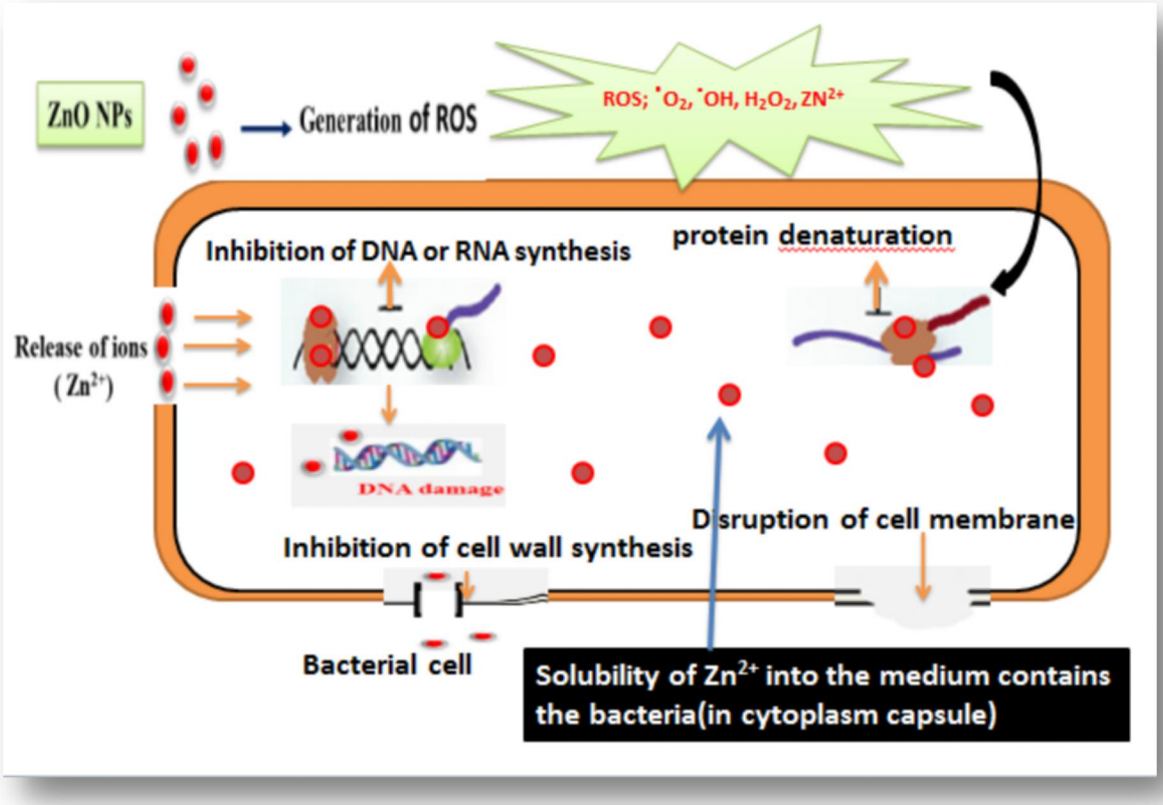

Figure 28: Mechanism of Antibacterial Activity of ZnO-NPs and ZnO-bentonite NCs (Chemingui *et al*., 2019).

Nanoparticles of smaller sizes can easily penetrate into bacterial cells and may release toxic metal ions upon dissolution. For instance, Wang *et al*. proposed that partial dissolution of nano-ZnO results in formation of surface defects giving an uneven surface texture due to rough edges and corners. This surface roughness was shown to be responsible for mechanical damage of the cell membrane of bacteria (Wang *et al*., 2007). The released toxic metal ions can linked to cytoplasm and can denature protein and alter enzyme function. In addition it binds to cell wall and cell membrane and cause mechanical damage and lipid peroxidation. This might be due to bacterial membranes and cell walls are typically of negative total charge. Electrostatic attractions can occur between bacterial surfaces and metal oxide nanoparticles.

5. CONCLUSION

In this study, ZnO NPs and ZnO-bentonite NCs were successfully synthesized using *H. abyssinica* leaf extract through a simple and green approach via the co-precipitation method. The biosynthesized NPs and NCs were characterized using techniques such as UV-Vis, DRS, TGA/DTA, XRD, SEM and FTIR. TGA analysis of biosynthesized ZnO NPs and ZnO-bentonite NCs showed thermal stability above 450 °C and 550 °C. The crystallinity of the both biosynthesized samples were proved from XRD analysis and the analysis showed all the diffraction peaks fit well with the hexagonal wurtzite structure. Furthermore, XRD analysis showed that the average crystal sizes of calc. ZnO (1:1), uncalc. ZnO (1:1), ZnO (1:2) and ZnO (0:100) synthesized from ratios by volume of plant extract were found to be 21.67 nm, 21.5 nm, 23.07 and 28.4 nm. XRD analysis also showed that the average crystal sizes of ZnO NPs in calc. ZnO-bentonite (2:1), (1:1) and ZnO(1:2) were found to be 21.78 nm, 13.33 nm and 8.48 nm. The optical band-gap energies were determined from UV-Vis-DRS spectra using the Kubelka munk function plot and found to be 3.12 for ZnO NPs (1:1) and 3.06 eV for ZnO NPs (1:2) respectively. The optical band-gap energies of ZnO-bentonite NCs (2:1) were 3.1 eV and 2.8 eV for ZnO-bentonite NC (1:1). The surface morphology of ZnO NPs and ZnO-bentonite NCs analysed from SEM characterization confirm that spherical shape of ZnO NPs and nano-sheet like shape of ZnO-bentonite NCs. The biosynthesized ZnO-bentonite NCs and ZnO NPs investigation showed better antibacterial agent against both *S. aureus* and *E. coli* bacteria. ZnO-bentonite NCs shows evident inhibition on bacteria growth with increased amount of ZnO loaded in nanocomposite than that of equivalent doses of ZnO NPs.

Generally, easy aggregation into big cluster of ZnO NPs at nanoscale in the solution could weaken the antibacterial effect. This drawn back of ZnO NPs were solved by hyperdization of ZnO NPs with activated bentonite, dispersibility of ZnO NPs in aqua can be improved by surface modification with activated bentonite, so ZnO-bentonite NCs can easily dispersible in aqueous solution, ZnO-bentonite NCs possessed larger specific surface area (small particle size), which can indeed facilitate the dispersion of ZnO nanoparticles; as a result ZnO NPs can be easily to be closer to the membrane of bacteria to hamper the normal function of bacteria and increase the local zinc concentration to inhibit the growth of bacteria.

6. RECOMMENDATION

ZnO-bentonite NCs and ZnO NPs have exhibited promising biomedical applications based on its anticancer, antibacterial, anti-diabetic, anti-inflammatory, as sunscreen, drug delivery, as well as bio-imaging activity. Due to inherent toxicity of ZnO NPs, ZnO-bentonite NCs and ZnO NPs possess strong inhibition effects against cancerous cell and bacteria, by inducing intracellular ROS generation and activating apoptotic signalling pathway, which makes ZnO NPs a potential candidate as anticancer and antibacterial agents. However, some critical issues of ZnO NPs still need to be further explored, which include the following:

- the limitations of ZnO NPs toxicity toward biological systems remain a controversial issue in recent researches
- Lack of insight into corresponding animals study about its anticancer, antibacterial, anti-inflammatory, and anti-diabetic activities.
- Detail mechanistic study of antibacterial function of nanoparticle may be elucidated.

Following studies focused on the above mentioned issues could further elucidate and comprehend the potential use of ZnO-bentonite NCs and ZnO NPs in biomedical diagnostic and therapeutic fields. I believe that nanomaterials would dramatically promote the development of medicine, ZnO/bentonite nanocomposites and ZnO nanoparticles are expected to make more exciting contributions in these fields.

7. REFERENCES

Abdullahi, S. L., and Audu, A. A. (2017). Comparative Analysis on Chemical Composition of Bentonite Clays Obtained from Ashaka and Tango Deposits in Gombe State , Nigeria. *ChemSearch Journal, 8*(2), 35-40.

Agarwal, H., Kumar, S. V., and Rajeshkumar, S. (2017). A review on green synthesis of zinc oxide nanoparticles – An eco-friendly approach. *Resource-Efficient Technologies*, *3*(4), 406-413.

Aguilar, J., Almeida-naranjo, C., Aldás, M. B., and Guerrero, V. H. (2020). Acid activation of bentonite clay for recycled automotive oil purification. *E3S Web of Conferences* 191, 03002.

Akram, M., Farooq, Q. H., Shafiq, M. I., and Awan, A. S. (2016). Synthesis and characterization of some important metal nanoparticles and their applications. *Sci. Int.(Lahore),* 28(4), 4049-4059.

Ammann, L. (2003). Cation exchange and adsorption on clays and clay minerals. 1-114.

Andrade, A. B., Ferreira, N. S., and Valerio, M. E. G. (2017). Particle size effects on structural and optical properties of BaF_2 nanoparticles. *RSC Advances*, *7*(43), 26839-26848.

Appendini, P., and Hotchkiss, J. H. (2002). Review of antimicrobial food packaging. *Innovative Food Science & Emerging Technologies*, *3(2)*, 113-126.

Appierot, G., Lipovsky, A., Dror, R., Perkas, N., Nitzan, Y., Lubart, R., and Gedanken, A. (2009). Enhanced antibacterial actiwity of nanocrystalline ZnO due to increased ROS-mediated cell injury. *Advanced Functional Materials*, *19*(6), 842-852.

Ashe, B. (2011). A Detail investigation to observe the effect of zinc oxide and Silver nanoparticles in biological system. *Master Thesis*, 1-228.

Assefa, B., Glatzel, G., and Buchmann, C. (2010). Ethnomedicinal uses of Hagenia abyssinica (Bruce) J . F . Gmel . among rural communities of Ethiopia. 6(1), 1-10.

Auwal, M. S., Saka, S., Mairiga, I. A., Sanda, K. A., Shuaibu, A., and Ibrahim, A. (2014). Preliminary phytochemical and elemental analysis of aqueous and fractionated pod extracts of Acacia nilotica (Thorn mimosa). *Veterinary Research Forum : An International Quarterly Journal*, *5*(2), 95-100.

Awwad, A.M., Albiss, B. and Ahmad, A. L. (2014). Green synthesis, characterization and optical properties of zinc oxide nanosheets using Olea europea leaf extract. A*dv.*

Materials Letters, 5(9), 520-524.

Azizi, S., Ahmad, M.B., Namvar,F and Mohamad, R(2014). Green biosynthesis and characterization of zinc oxide nanoparticles using brown marine macro-alga Sargassum muticum aqueous extract, *Mater. Lett* 116 (2014): 275–277.

Baek, Y.W and An, Y.J (2011). Microbial toxicity of metal oxide nanoparticles (CuO, NiO, ZnO, and Sb_2O_3) to *Escherichia coli, Bacillus subtilis,* and *Streptococcus aureus. Sci. Total Environ*. 409, 1603-1608.

Bagabas, A., Alshammari, A., Aboud, M. F. and Kosslick, H. (2013). Room-temperature synthesis of zinc oxide nanoparticles in different media and their application in cyanide photodegradation. *Nanoscale Research Letters*, 8(1), 1-10.

Baruah, S., and Dutta, J. (2009). Hydrothermal growth of ZnO nanostructures. *Science and Technology of Advanced Materials*, *10*(1), 013001.

Basnet, P., Chanu, T.I., Samanta, D., and Chatterjee, S. (2018). A review on bio-synthesized zinc oxide nanoparticles using plant extracts as reductants and stabilizing agents. *Journal of Photochemistry and Photobiology. B: Biology*, *183*, 201-221.

Bauer, A. W., Kirby, W. M., Scherris, J. C and Truck, M.(1966). Antibiotic susceptibility testing by a standardized single disc method. *Am. J. Clin. Pathol*. 45 149-158.

Behroozian, S., Svensson, S.L., Li, L.Y. and Davies, J.E.(2020). Broad Spectrum Anti-microbial and Anti-biofilm Activity of a Natural Clay Mineral from British Columbia, Canada. *American Society for Microboilogy, 11*(5), 1-14.

Belachew, N., and Bekele, G. (2020). Synergy of magnetite intercalated bentonite for enhanced adsorption of congo red dye. *Silicon*, *12*(3), 603-612.

Bisht, G., Rayamajhi, S., Biplab, K.C., Paudel, S. N., Karna, D. and Shrestha, B. G. (2016). Synthesis, Characterization and Study of in Vitro Cytotoxicity of ZnO-Fe_3O_4 Magnetic NanoComposite in Human Breast Cancer Cell Line (MDA-MB-231) and Mouse Fibroblast (NIH 3T3). *Nanoscale Research Letters*, 11(1), 1-11.

Bujdak, J., Janek, M., Madejová, J. and Komadel, P.(2001). The interaction of Methylene blue with reduced-charge smectites. *Clays and Clay Minerals*, 49(3), 244-254.

Bukit, N., Frida, E., and Harahap, M. H. (2013). Preparation Natural Bentonite in Nano Particle Material as Filler Nanocomposite High Density Poliethylene (Hdpe). *Chemistry and Materials Research*, *3*(13), 10-21.

Calabria, J. A., Amaral, D. N.D., Ladeira, A. C. Q., Cota, S. D. and. Silva, T. S.(2013). Determination of the cation exchange capacity of bentonite exposed to hyperalkaline fluid.

Chakraborty, T., Chakraborty, A., Shukla, M., and Chattopadhyay, T. (2019). ZnO–Bentonite nanocomposite: an efficient catalyst for discharge of dyes, phenol and Cr(VI) from water. *Journal of Coordination Chemistry*, *72*(1), 53-68.

Chemingui, H., Missaoui, T., Mzali, J. C., Yildiz, T., Konyar, M., Smiri, M.and Yatmaz, H. C. (2019). Facile green synthesis of Zinc oxide nanoparticles (ZnO NPs): Antibacterial and photocatalytic activities. *Materials Research Express*, *6*(10), 1050b4.

Dasai, T.P., Pathakoti, K and Hwang, H.M (2013). Determination of the mechanism of photoinduced toxicity of selected metal oxide nanoparticles (ZnO, CuO, Co_3O_4 and TiO_2) to E. coli bacteria. *J. Environ. Sci.* 25, 882-888.

Dardir, F. M., Mohamed, A. S., Abukhadra, M. R., Ahmed, E. A., and Soliman, M. F. (2018). Cosmetic and pharmaceutical qualifications of Egyptian bentonite and its suitability as drug carrier for Praziquantel drug. *European Journal of Pharmaceutical Sciences,* 115, 320-329.

Demissie, M. G., Sabir, F. K., Edossa, G. D., and Gonfa, B. A. (2020). Synthesis of Zinc Oxide Nanoparticles Using Leaf Extract of Lippia adoensis (Koseret) and Evaluation of Its Antibacterial Activity. *Journal of Chemistry*, 2020.

Desai, A. V. and Haque, M. A. (2007). Mechanical properties of ZnO nanowires. *Sensors and Actuators, A: Physical*, *134*(1), 169-176.

Desta, B. (1995). Ethiopian traditional herbal drugs. Part I: Studies on the toxicity and therapeutic activity of local taenicidal medications. *Journal of Ethnopharmacology*, *45*(1), 27-33.

Dobrucka, R., and Długaszewska, J. (2016). Biosynthesis and antibacterial activity of ZnO nanoparticles using Trifolium pratense flower extract. *Saudi Journal of Biological Sciences*, *23*(4), 517-523.

Dusenkova, I., Kusiņa, I., Mālers, J., and Bērziņa-Cimdiņa, L. (2015). Application of Latvian illite clays in cosmetic products with sun protection ability. *Environment. Technology. Resources*. *Proceedings of the International Scientific and Practical Conference*, *1*, 28-32.

Eren, E., Afsin, B. and Onal, Y. (2013). Removal of lead ions by acid activated and manganese oxide-coated bentonite. *Journal of Hazardous Materials*, *161*(2-3), 677-685.

Espinosa, H. D., Bernal, R. A., and Minary-Jolandan, M. (2012). A review of mechanical and electromechanical properties of piezoelectric nanowires. *Advanced Materials*,

24(34), 4656-4675.

Evangeline, Y. S., Vinod, S. and Manju, A.K.(2009). Permeability Variation of Sodium Activated Bentonites. In *Indian Geotechnical Conference,* 43-46.

Farias, A. F. F., Souza, A. G. D., Pontes, L. F. B. L., Santos, I. M. G. and Longo, E.(2011). ZnO-motmorillonite Nanocomposite Synthesis by hydrothermal microwave method. *49*(2010), 6719.

Fernandez, L., Garro, N., El Haskouri, J., Prez-Cabero, M., Alvarez-Rodríguez, J., Latorre, J.and Amoros, P. (2008). Mesosynthesis of ZnO-SiO_2 porous nanocomposites with low-defect ZnO nanometric domains. *Nanotechnology*, *19*(22), 225603.

Fessi, H. P., Puisieux, F., Devissaguet, J. P., Ammoury, N., and Benita, S. (1989). Formation of Nanocapsule by interfacial polymer deposition following solvent displacement. *International journal of pharmaceutics*, *55*(1), R1-R4.

Foroughi, M. M., Pardakhty, A., and Ranjbar, M. (2017). Simple Microwave Synthesis of CdO/Clay Nanocomposites and Investigation its Application for Degradation of MB. *Journal of Cluster Science*, *28*(3), 1685-1692.

Garshasbi, N., Ghorbanpour, M., Nouri, A. and Lotfiman, S. (2017). Preparations of zinc oxide-nanoclay hybrids by alkaline ion exchange method. *Brazilian Journal of Chemical Engineering* 34(04), 1055 – 1063.

Getie, S., Belay, A., Chandra, A. R., and Belay, Z. (2017). Synthesis and characterizations of zinc oxide nanoparticles for antibacterial applications. *J. Nanomed Nanotechno., S*, *8*(004).

Ghorbanpour, M., Mazloumi, M., Nouri, A. and lotfiman, S.(2017). Silver-doped Nanoclay with Antibacterial Activity. *Journal of Ultrafine Grained and Nanostructured Materials, 50*(2), 124-131.

Ghoshal, T., Biswas, S., Paul, M., and De, S. K. (2009). Synthesis of ZnO nanoparticles by solvothermal method and their ammonia sensing properties. *Journal of Nanoscience and Nanotechnology*, *9*(10), 5973-5980.

Gong, Z., Liao, L., and Wang, X. (2016). A simple method for physical purification of bentonite. *Applied Clay Science, 119*, 294-300.

Gulnaz, A.R. and Savitha, G. (2013). Phytochemical Evaluation of Leaf and Stem Extracts of Siddha Medicinal Plant: Sida Cordata. *Journal of Evolution of Medical and Dental Sciences*, *2*(15), 1-8.

Hakimi, B., Ghorbanpour, M., and Feizi, A. (2018a). A Comparative Study between Photocatalytic activity of ZnO / bentonite Composites Prepared by Precipitation ,

Liquid-state Ion Exchange and Solid-state Ion Exchange Methods. *J. of Water and Environ. Nanotechnol., 3*(3), 273-278.

Hakimi, B., Ghorbanpour, M., and Feizi, A. (2018b). ZnO / bentonite Nanocomposites Prepared with Solid-state Ion Exchange as Photocatalysts. *Journal of Ultrafine Grained and Nanostructured Materials*, *51*(2), 139-146.

Haneef, M.D., and Abdo, J. (2012). Growth of ZnO nanorods in clay matrix to ensure uniform dispersion in drilling fluids. *Technical Proceedings of the 2012 NSTI Nanotechnology Conference and Expo, NSTI-Nanotech*, *1*, 652-655.

Hang, P.T. and Brindley, G.W. (1970). Methylene Blue Absorption by Clay Minerals: Determination of Surface Areas and Cation Exchange Capacities (Clay-Organic Studies XVIII). *Clays and Clay Minerals*, 18, 203-212.

Hayakawa, T., Minase, M., Fujita, K., and Ogawa, M.(2016). Modified method for bentonite purification and characterization; a case study using bentonite from Tsunagi mine , Niigata , Japan. *Clays and Clay Minerals*, 64(3), 275–282.

Henrique, P., Camargo, C., Satyanarayana, K. G., and Wypych, F. (2009). Synthesis , Structure , Properties and New Application Opportunities of Nanocomposites. *Materials Research*, *12*(1), 1-39.

Higgs, N. B. (1988). Methylene blue adsorption as a rapid and economical method for detecting smectite. *Geo-technical Testing Journal*, *11*(1), 68-71.

Honarmand, M., Golmohammadi, M.,and Naeimi, A. (2020). Green synthesis of SnO_2 - bentonite nanocomposites for the efficient photodegradation of methylene blue and eriochrome black-T. *Materials Chemistry and Physics*, *241*(2020), 122-416.

Iravani, S. (2011). Green synthesis of metal nanoparticles using plants. *Green Chemistry*, *13*(10), 2638-2650.

Ismaeel, S. H., Mabrouk, M. S., Ali, A. A. and Elwalead, K. A. (2017). Synthesis and Characterization of Bentonite Nanocomposites from Egyptian Bentonite Clay. *Journal of Nanotechnology and Allied Sciences*, *1*(1), 16-29.

Jamdagni, P., Khatri, P., and Rana, J. S. (2018). Green synthesis of zinc oxide nanoparticles using flower extract of Nyctanthes arbor-tristis and their antifungal activity. *Journal of King Saud University - Science*, *30*(2), 168-175.

Ji, S., and Ye, C. (2008). Synthesis, growth mechanism, and applications of zinc oxide nanomaterials. *Journal of Materials Science and Technolog*. 24(4), 457.

Jiang, J., Pi, J., and Cai, J. (2018). The Advancing of Zinc Oxide Nanoparticles for Biomedical Applications. *Bioinorganic Chemistry and Applications*, 2018.

Jiang, Y., Zhang, L., Wen, D., and Ding, Y. (2016). Role of physical and chemical interactions in the antibacterial behavior of ZnO nanoparticles against E. coli. *Materials Science and Engineering: C*, *69*, 1361-1366.

Kahsay, M. H. (2021). Synthesis and characterization of ZnO nanoparticles using aqueous extract of Becium grandiflorum for antimicrobial activity and adsorption of methylene blue. *Applied Water Science*, *11*(2), 1-12.

Kaur, S., and Kaur, P. (2019). Nanoparticles Characterization and Applications: An Overview. *Indo Global Journal of Pharmaceutical Sciences*, *9*(2), 146-146.

Komine, H., and Ogata, N. (2011). Experimental Study on Swelling Characteristics of Compacted Bentonite. *Canadian Geotechnical Journal*, *31*, 478-490.

Krishnan, B., and Mahalingam, S. (2017). Synthesis and Characterization of Mn_3O_4 / BC Nanocomposite and Its Antimicrobial Activity. *Journal of Inorganic and Organometallic Polymers and Materials*, *27*(1), 275-284.

Kutlakova, K.M., Tokarsky, J., and Peikertova, P. (2015). Functional and eco-friendly nanocomposite kaolinite/ZnO with high photocatalytic activity. *Applied Catalysis B: Environmental*, *162*, 392-400.

Li, Y., Zhang, W., Niu , J.and Chen, Y. (2012). Mechanism of photogenerated reactive oxygen species and correlation with the antibacterial properties of engineered metal-oxide nanoparticles. *ACS nano.* 6(6):5164-73.

Lu, P. J., Huang, S. C., Chen, Y. P., Chiueh, L. C., and Shih, D. Y. C. (2015). Analysis of titanium dioxide and zinc oxide nanoparticles in cosmetics. *Journal of Food and Drug Analysis*, *23*(3), 587-594.

Madathil, A. N.P., Vanaja, K. A., and Jayaraj, M. K. (2007). Synthesis of ZnO nanoparticles by hydrothermal method. *Nanophotonic Materials IV*, *6639*(1), 277-786.

Manzoor, U., Tuz Zahra, F., Rafique, S., Moin, M. T. and Mujahid, M. (2015). Effect of synthesis temperature, nucleation time, and postsynthesis heat treatment of ZnO nanoparticles and its sensing properties. *Journal of Nanomaterials*, 2015.

Maurya, P. K. and Dua, K. (Eds). (2020). Role of Oxidative Stress in Pathophysiology of Diseases.Springer.

Meruvu, H., Vangalapati, M., Chippada, S.C.and Bammidi, S. R. (2011). Synthesis and characterization of zinc oxide nanoparticles and its antimicrobial activity against bacillus subtilis and escherichia coli. *Rasayan journal* chem., *4*(1), 217-222.

Meshram, S., Limaye, R., Ghodke, S., Nigam, S., Sonawane, S., and Chikate, R. (2011). Continuous flow photocatalytic reactor using ZnO-bentonite nanocomposite for

degradation of phenol. *Chemical Engineering Journal*, *172*(2–3), 1008-1015.

Motshekga, S. C., Ray, S. S., Onyango, M. S., and Momba, M. N. (2013). Microwave-assisted synthesis, characterization and antibacterial activity of Ag/ZnO nanoparticles supported bentonite clay. *Journal of Hazardous Materials*, *262*, 439-446.

Mueen, R., Lerch, M., Cheng, Z., and Konstantinov, K. (2020). Na-doped ZnO UV filters with reduced photocatalytic activity for sunscreen applications. *Journal of Materials Science*, 55 (7), 2772-2786.

Murthy, H. C. A., Desalegn, T. and Kassa, M. (2020). Synthesis of Green Copper Nanoparticles Using Medicinal Plant Hagenia abyssinica (Brace) JF. Gmel. Leaf Extract: Antimicrobial Properties. *Journal of Nanomaterials*, *2020*, 1-12.

Mustapha, S., Ndamitso, M. M., Abdulkareem, A. S., Tijani, J. O., Shuaib, D. T., Ajala, A. O., and Mohammed, A. K. (2020). Application of TiO_2 and ZnO nanoparticles immobilized on clay in wastewater treatment: a review. In *Applied Water Science* 10(1), 1-36.

Nagarajan, P. and Rajagopalan, V. (2008). Enhanced bioactivity of ZnO nanoparticles: an antimicrobial study. *Sci. Technol. Adv. Mater*, *9*(03500410.1088), 1468-6996.

Narayanan, G. N., Ganesh, R. S., andKarthigeyan, A. (2016). Effect of annealing temperature on structural, optical and electrical properties of hydrothermal assisted zinc oxide nanorods. *Thin Solid Films*, *598*(3), 39-45.

Nayak, P. S., and Singh, B. K. (2007). *Instrumental characterization of clay by XRF , XRD and FTIR*. *Bull. Mater. Sci., 30*(3), 235-238.

Nizamani, A. A., Ismail, A. R., Junin, R., Dayo, A. Q., Tunio, A. H., Ibupoto, Z. H., and Sidek, M. A. M. (2017). Synthesis of titania-bentonite nanocomposite and its applications in water-based drilling fluids. *Chemical Engineering Transactions*, *56*, 949-954.

Oliveira, C. I. R., Rocha, M. C. G., Silva, A. L. N., and Bertolino, L. C. (2016). *Characterization of bentonite clays from Cubati , Paraíba (Northeast of Brazil)*. *Journal of Ceramics*, *62*, 272-277.

Oliveira, F. S.D., Varajão, A. F. D.C., Varajão, C. A. C., and Boulangé, B. (2013). A comparison of properties of clay minerals in isalteritic and in degraded facies. *Clay Minerals*, *48*(5), 697-711.

Oloyed, O.I. (2005). Chemical profile of unripe pulp of Carica pagaya. *Pakistan Journal of Nutrition*, 4: 379-381.

Osuntokun, J., Onwudiwe, D. C., and Ebenso, E. E. (2019). Green synthesis of ZnO

nanoparticles using aqueous Brassica oleracea L . var . italica and the photocatalytic activity.*Green Chemistry Letters and Reviews 12(4)*, 444-457

Ozgur, Ü., Alivov, Y. I., Teke, A., Reshchikov, M.A., Doğan, S., Avrutin, V., Cho, S.J., Morkoç, H., and Liu, C., (2005). A comprehensive review of ZnO materials and devices. *Journal of Applied Physics,* 98(4), *11*.

Pharmacopeia, U. S. (2007). National Formulary 25: In *Rockville, MD: US Pharmacopeial Convention* (p. 1654).

Pourabolghasem, H., Ghorbanpour, M.,and Shayegh, R. (2016). Antibacterial Activity of Copper-doped Montmorillonite Nanocomposites Prepared by Alkaline Ion Exchange Method. *Journal of Physical Science, 27*(2), 1-12.

Pouraboulghasem, H., Ghorbanpour, M., Shayegh, R., and Lotfiman, S. (2016). Synthesis , characterization and antimicrobial activity of alkaline ion-exchanged ZnO / bentonite nanocomposites. *J. Cent. South Univ.,* 23, 787-792.

Ruiz-Hitzky, E., Aranda, P., Akkari, M., Khaorapapong, N., and Ogawa, M. (2019). Photoactive nanoarchitectures based on clays incorporating TiO_2 and ZnO nanoparticles. *Beilstein Journal of Nanotechnology*, *10*, 1140-1156.

Salam, H., Sivaraj, R., and Venckatesh, R. (2014). Green synthesis and characterization of zinc oxide nanoparticles from Ocimum basilicum L. var. purpurascens Benth.-Lamiaceae leaf extract. *Materials Letters*, *131*, 16-18.

Samat, N.A. and Nor, R.M. (2013). Sol–gel synthesis of zinc oxide nanoparticles using Citrus aurantifolia extracts. *Journal of Ceramic International,* 39, 545–548.

Sasikala, S. P., Nibila, T. A., Babitha, K. B., Mohamed, A. A. P., and Solaiappan, A. (2019). Competitive photo-degradation performance of ZnO modified bentonite clay in water containing both organic and inorganic contaminants. *Sustainable Environment Research*, *29*(1), 1-12.

Seabra, A. B., and Durán, N. (2015). Nanotoxicology of metal oxide nanoparticles. *Journal of Metals*, *5*(2), 934-975.

Shah, L. A., Khattak, N. S., Valenzuela, M., Manan, A., and Díaz, F. V. (2013). Preparation and characterization of purified Na-activated bentonite from Karak (Pakistan) for pharmaceutical use. *Clay Minerals*, *48*(4), 595-603.

Sharifia, S., Behzadib, S., Laurentc, S., Forrest, M. L., Stroevee, P and Mahmoudib, M. (2016). Toxicity of nanomaterials. *Physiology & Behavior*, *176*(1), 139-148.

Sharma, D., Rajput, J., Kaith, B. S., Kaur, M. and Sharma, S. (2010). Synthesis of ZnO nanoparticles and study of their antibacterial and antifungal properties. *Thin Solid*

Films, 519(3), 1224-1229.

Shu, Z., Zhang, Y., Yang, Q., and Yang, H. (2017). Halloysite Nanotubes Supported Ag and ZnO Nanoparticles with Synergistically Enhanced Antibacterial Activity. *Nanoscale Research Letters*, *12*(1), 0-6.

Sirelkhatim, A., Mahmud, S., Seeni, A., Kaus, N. H. M., Ann, L. C., Bakhori, S. K. M., Hasan, H., and Mohamad, D. (2015). Review on zinc oxide nanoparticles: Antibacterial activity and toxicity mechanism. *Nano-Micro Letters*, *7*(3), 219-242.

Sivaraj, R., Abdul salam, H. and Venckatesh, R. (2014). Green synthesis and characterization of zinc oxide nanoparticles from Ocimum basilicum L . var . purpurascens Benth . -Lamiaceae leaf extract. *Materials Letters*, *131*, 16-18.

Smijs, T.G. and Pavel, S. (2011). Titanium dioxide and zinc oxide nanoparticles in sunscreens : focus on their safety and effectiveness. *Nanotechnology, Science and Applications,* (4), 95-112.

Stan, M., Popa, A., Toloman, D., Silipas, T. D., and Vodnar, D. C. (2016). Antibacterial and antioxidant activities of ZnO nanoparticles synthesized using extracts of Allium sativum, Rosmarinus officinalis and Ocimum basilicum. *Acta Metallurgica Sinica (English Letters)*, *29*(3), 228-236.

Stankic, S., Suman, S., Haque, F., and Vidic, J. (2016). Pure and multi metal oxide nanoparticles: Synthesis, antibacterial and cytotoxic properties. *Journal of Nanobiotechnology*, *14*(1), 1-20.

Sundrarajan, M., Ambika, S., and Bharathi, K. (2015). Plant-extract mediated synthesis of ZnO nanoparticles using Pongamia pinnata and their activity against pathogenic bacteria. *Advanced Powder Technology*, *26*(5), 1294-1299.

Suresh, D., Shobharani, R. M., Nethravathi, P. C., Kumar, M. A. P., Nagabhushana, H., and Sharma, S. C. (2015). Spectrochimica Acta Part A: Artocarpus gomezianus aided green synthesis of ZnO nanoparticles : Luminescence , photocatalytic and antioxidant properties Intensity (au). *Molecular and biomolecular spectroscopy*, *141*, 128-134.

Suresh, J., Pradheesh, G., Alexramani, V., Sundrarajan, M., and Hong, S. I. (2018). Green synthesis and characterization of zinc oxide nanoparticle using insulin plant (*Costus pictus D. Don*) and investigation of its antimicrobial as well as anticancer activities. *Advances in Natural Sciences: Nanoscience and Nanotechnology*, *9*(1).

Ta, U. J. I. (2016). Modified method for bentonite purification and characterization ; a case study using bentonite from tsunagi mine , niigata , japan. *64*(3), 275-282.

Tadtong, S., Watthanachaiyingcharoen, R., & Kamkaen, N. (2014). Antimicrobial

constituents and synergism effect of the essential oils from Cymbopogon citratus and Alpinia galanga. *Natural Product Communications*, *9*(2), 277-280.

Talam, S., Karumuri, S. R., and Gunnam, N. (2012). Synthesis, Characterization, and Spectroscopic Properties of ZnO Nanoparticles. *ISRN Nanotechnology*, 2012, 1-6.

Tan, S. Z., Zhang, K. H., Zhang, I. L., Xie, Y. S., and Liu, Y. L. (2008). Preparation and characterization of the antibacterial zn^{2+} and Ce^{3+} loaded montmorillonites. *Chinese Journal of Chemistry*, *26*(5), 865-869.

Toor, M., Jin, B., Dai, S. and Vimonses, V. (2015). Activating natural bentonite as a cost-effective adsorbent for removal of Congo-red in wastewater. *Journal of Industrial and Engineering Chemistry*, *21*, 653-661.

Trimaille, T., Chaix, C., Delair, T., Pichot, C., Teixeira, H., Dubernet, C. and Couvreur, P. (2001). Nano capsule production by Interfacial deposition of functionalized copolymers onto nanoemulsions produced througth the solvent displacement method. *Colloid and Polymer Science*, *279*(8), 784-792.

Tripathi,R.M., Bhadwal, A.S., Gupta,R.K., Singh, P., Shrivastav, A and Shrivas,B.R (2014). ZnO nanoflowers: novel biogenic synthesis and enhanced photocatalytic activity, J. Photochem. Photobiol. B Biol 141 (2014): 288–295

Tsuzuki, T., He, R., Wang, J., Sun, L., Wang, X., & Hocking, R. (2012). Reduction of the photocatalytic activity of ZnO nanoparticles for UV protection applications. *International Journal of Nanotechnology*, *9*(10–12), 1017-1029.

Unnithan, R. R. (2017). Characterization of Na_2CO_3 activated Calcium Bentonite and its application as a GCL. *Journal of Engineering Research & Technology, 5*(08), 3-6.

Upadhyaya, H.,Shome, S., Sarma, R., Tewari, S., Bhattacharya, M. K. and Panda, S. K.(2018). Green Synthesis, Characterization and Antibacterial Activity of ZnO Nanoparticles. *American Journal of Plant Sciences*, (9), 1279-1291

Vaishnav, J., Subha, V., Kirubanandan, S., Arulmozhi, M., and Renganathan, S. (2017). Green Synthesis of Zinc Oxide Nanoparticles By Celosia Argentea and Its Characterization. *Journal of Optoelectronics and Biomedical Materials*, *9*(1), 59–71.

Vasuki, K. and Manimekalai, R. (2019). NIR light active ternary modified ZnO nanocomposites for combined cancer therapy. *Journal of Heliyon*, *5(11)*, e02729.

Vishwakarma, K. (2013). Green synthesis of zno nanoparticles using abrus precatorius seeds extract and their characterization. (Doctorial Dissertation).

Wahab, R., Kim, Y. S., Mishra, A., Yun, S. I. and Shin, H. S. (2010). Formation of ZnO Micro-Flowers Prepared via Solution Process and their Antibacterial Activity.

Nanoscale Research Letters, *5*(10), 1675–1681.

Wang, J., Tsuzuki, T., Sun, L., and Wang, X. (2009). Reducing the photocatalytic activity of zinc oxide quantum dots by surface modification. In *Journal of the American Ceramic Society*, 92(9), 2083–2088.

Wang, X., Yang, F., Yang, W. and Yang, X.(2007). A study on the antibacterial activity of one-dimensional ZnO nanowire arrays: effects of the orientation and plane surface. *Chem Commun.*;42:4419–21.

Williams, L. B., Metge, D. W., Eberl, D. D., Harvey, R. W., Turner, A. G., Prapaipong, P., and Poret-peterson, A. T. (2011). *What Makes a Natural Clay Antibacterial ?* 3768–3773.

Wojnarowicz, J., Chudoba, T., and Lojkowski, W. (2020). A review of microwave synthesis of zinc oxide nanomaterials: Reactants, process parameters and morphoslogies. *Nanomaterials*, *10*(6).

Wolde, T., Bizuayehu, B., Hailemariam, T., and Tiruha, K. (2016). Phytochemical Analysis and Antimicrobial Activity of Hagenia Abyssinica Phytochemical Analysis and Antimicrobial Activity of Hagenia Abyssinica. *Journal of Pharmacy and Pharmacology , 3(8), 1-9*

Xu, H., Zhang, D., Xu, A., Wu, F., and Cao, R. (2015). Quantum Sized Zinc Oxide Immobilized on Bentonite Clay and Degradation of C.I. Acid Red 35 in Aqueous under Ultraviolet Light. *International Journal of Photoenergy*, 2015.

Yamamoto, O., Komatsu, M., Sawai, J., and Nakagawa, Z. E. (2004). Effect of lattice constant of zinc oxide on antibacterial characteristics. *Journal of Materials Science: Materials in Medicine*, *15*(8), 847-851.

Yuvakkumar, R., Suresh, J., Saravanakumar, B., Nathanaeld, A. J. and Honga, S.I. Rajendran, (2015). Rambutan peels promoted biomimetic synthesis of bioinspired zinc oxide nanochains for biomedical applications. Spectrochim. Biomol. Spectrosc. 137, 250-258.

Zak, A. K., Hashim, A. M., and Darroudi, M. (2014). Optical properties of ZnO/$BaCO_3$ nanocomposites in UV and visible regions. *Nanoscale Research Letters*, *9*(1), 1-6.

Zakharova, O., Kolesnikov, E., Vishnyakova, E., Strekalova, N., and Gusev, A. (2019). Antibacterial activity of ZnO nanoparticles: Dependence on particle size, dispersion media and storage time. *IOP Conference Series: Earth and Environmental Science*, *226*(1), 012-062.

Zhang, L., Jiang, Y., Ding, Y., Daskalakis, N., Jeuken, L. and Povey, M. (2010).

Mechanistic investigation into antibacterial behaviour of suspensions of ZnO nanoparticles against E. coli. *Journal of Nanoparticle Research*, 12(5), 1625-1636.

Zhang, Z. Y., and Xiong, H. M. (2015). Photoluminescent ZnO nanoparticles and their biological applications. *Materials*, *8*(6), 3101-3127.